Supplementary information

Controlling optoelectronic properties and aggregation of planar dipoles through symmetry-preserving modifications

José García-Calvo*[a,b] María Modino-Montes,[a] Ignacio Romero-Muñiz,[a] Tomás Torres,*[a,b,c]

[a]*Department of Organic Chemistry, Facultad de Ciencias, Universidad de Madrid Autónoma Cantoblanco, 28049-Madrid, Spain*

[b]*Institute for Advanced Research in Chemical Sciences (IAdChem), Universidad Autónoma de Madrid, Campus de Cantoblanco, 28049 Madrid, Spain*

[c]*IMDEA-Nanociencia, c/Faraday 9, Campus de Cantoblanco, 28049 Madrid, Spain*

jose.garciac@uam.es

tomas.torres@uam.es

Table of contents

1. Materials and methods

Chemicals, including reagents and solvents, were acquired from different suppliers; Merck-Sigma Aldrich, BLD-pharmaceuticals, TCI, and Across. These chemicals were used directly without any additional purification steps. Reaction progress was tracked using thin layer chromatography (TLC) on aluminum sheets coated with a 0.2 mm layer of silica gel 60 F254 (E. Merck). The synthesized products were purified and separated via column chromatography, employing silica gel with a particle size of 230–400 mesh (0.040-0.063 mm, Merck).

Mass Spectrometry (MS) and High-Resolution Mass Spectrometry (HRMS) spectra were recorded employing Electrospray Ionization (ESI Positive TOF_MS) mass spectra using a MAXIS II spectrometer, or Matrix Assisted Laser Desorption/Ionization-Time of Flight (MALDI-TOF) using a Bruker Ultraflex III TOF/TOF spectrometer, with a nitrogen laser operating at 337 nm, or with a NdYAG laser operating at 335 nm. The different matrixes employed are indicated for each spectrum. Mass spectrometry data are expressed in m/z units. All MS experiments were carried out at the "Servicio Interdepartamental de Investigación" (SIdI) of the Universidad Autónoma de Madrid.

^{1}H NMR and ^{13}C NMR were recorded on Bruker XRD-300 (300 MHz) and/or Bruker XRD-500 (500 MHz) instruments at room temperature (25 °C) and are reported as chemical shifts (δ) in ppm relative to TMS (δ = 0). Spin multiplicities are reported as a singlet (s), doublet (d), triplet (t) and quartet (q) with coupling constants (*J*) given in Hz, or multiplet (m). Broad peaks are marked as br. ^{1}H and ^{13}C resonances were assigned with the aid of additional information from 1D and 2D NMR spectra (H,H-NOESY, H,H-COSY, DEPT 135, HSQC and HMBC). Deuterated solvents employed are indicated in each spectrum.

Cyclic voltametry (CV) and differential pulse voltammetry (DPV) in solution were measured with an Autolab equipment, using carbon electrode (work electrode), Ag/Ag^{+} electrode (reference electrode) and Pt electrode (counter-electrode). Ferrocene was employed as reference. E is given in V, vs Fc/Fc^{+}.

UV-vis spectra in solution were recorded on a JASCO-V660 UV-vis spectrophotometer using spectroscopic grade solvents and 10×10mm quartz cuvettes with a Jasco Peltier ETCS-761 temperature controller incorporated, or in a double beam UV-Vis-NIR Varian Cary 6000i spectrophotometer (Varian, Palo Alto, CA, USA). Fluorescence spectra in solution were recorded with a JASCO FP-8600 spectrophotometer using spectroscopic grade solvents and quartz cuvettes (1cm) with a Jasco Peltier ETCS-761 temperature controller incorporated, or in a Spex Fluoromax-4 spectrofluorometer (Horiba Jobin-Yvon, Edison, NJ, USA) equipped with a stirrer and a temperature controller. All Fluorescence spectra were corrected for lamp intensity fluctuations, background, and

the wavelength-dependent response function of the detector. Photoluminescence measurements in powder samples were performed at room temperature in an Edinburgh Instrument FS5 spectrometer equipped with a 150 W CW Ozone-free xenon arc lamp, and a photomultiplier detector (spectral coverage 250-800 nm). Fluorescence lifetime measurements (τ_F) in solution were performed with an Edinburgh Instrument FLS980 by performing Time-Correlated Single Photon Counting (TCSPC) in the measurement range. The excitation source light was a picosecond pulsed laser (470-478 nm).

The single crystal structure was resolved using Rigaku XtaLAB Synergy-S diffractometer equipped with a HyPix-6000HE Hybrid Photon Counting detector and Cu microfocus sealed X-ray sources. The crystal was mounted in cryoloop with Paratone-N oil. The data were collected at 150.00(10) K. The structures were solved using Olex2 software where XT1 structure solution program using Intrinsic Phasing and the XL2 refinement package using Least Squares minimization were employed in solving and refining the structures, respectively. Mercury (CCDC software) was used as the crystal structure visualization software for the images presented in the manuscript.

Abbreviations: dimethyl sulfoxide (DMSO), 4,4′-Di-tert-butyl-2,2′-dipyridyl (dtbpy), methylcyclohexane (MCH), microwave (MW), perylene derivatives (PD), perylene dianhydride (PDA), perylene monoimide (PMI), perylene diimide (PDI).

2. Synthesis and characterization

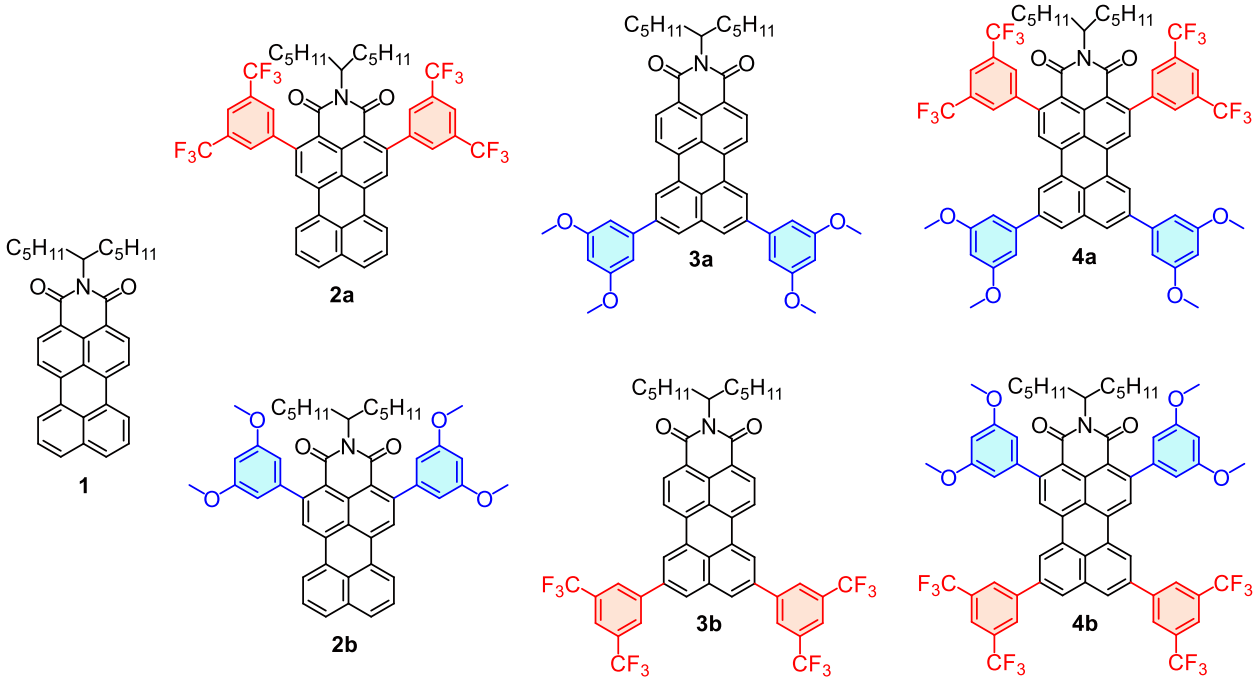

Fig. S1 Structures of the PMI derivatives studied in this work.

2.1.General procedure for the Suzuki coupling reactions

A 25 mL Schlenk containing PMI, $Pd_2(dba)_3$ (0.2 eq), SPhos (0.4 eq) and the corresponding aryl halyde (4 eq) were put under Ar atmosphere. The reagents were mixed with toluene/water (4:1) and stirred at 110 ºC for 36 h. The reaction was evaporated *in vacuo*, redissolved in CH_2Cl_2 (20 mL) and washed with water (2×20 mL) and brine (20 mL) then, dried with $MgSO_4$, filtered and concentrated again *in vacuo*. The crude was purified by SiO_2 column chromatography in mixtures CH_2Cl_2/heptane → CH_2Cl_2 to obtain the product.

2.2. Synthesis of *ortho*-PMIs 2a and 2b

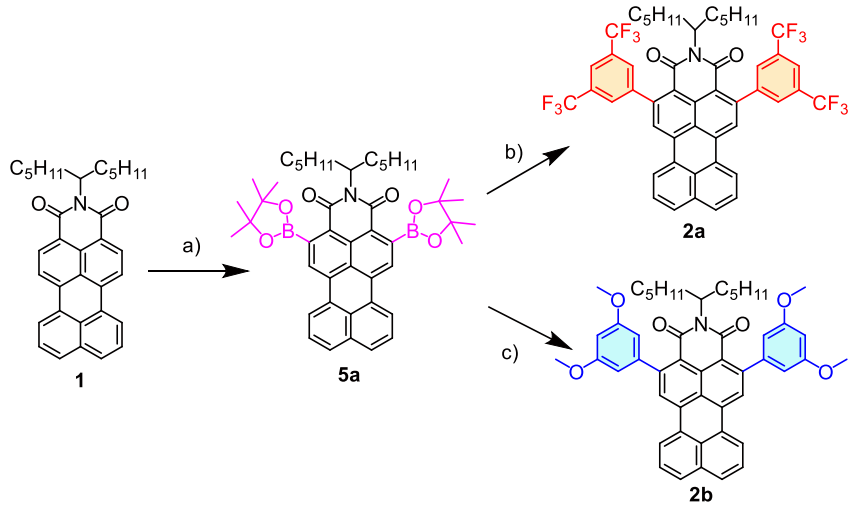

Scheme S1 Synthetic route for the PMI derivatives **2a** and **2b**. a) B_2Pin_2 (8 eq.), $[Ir(OMe)(COD)]_2$ (0.05 eq) and $P(C_6F_5)_3$ (0.1 eq), 20 mM solutions, dioxane, 140 ºC 72 h, 72%; b) 1-bromo-3,5-bis(trifluoromethyl)benzene (4 eq), K_2CO_3 (10 eq), $Pd_2(dba)_3$ (0.2 eq), SPhos (0.4 eq), toluene/water (4:1), 110 ºC, 36 h, 61%; c) 1-bromo-3,5-dimethoxybenzene (4 eq), K_2CO_3 (10 eq), $Pd_2(dba)_3$ (0.2 eq), SPhos (0.4 eq), toluene/water (4:1), 110 ºC, 36 h, 70%.

Compound 5a. The compound was synthesized following the previously reported procedure.[S1]

Compound 2a. Following the general procedure (2.1.), PMI **5a** (60 mg, 0.08 mmol), $Pd_2(dba)_3$ (16 mg, 0.02 mmol), SPhos (15 mg, 0.04 mmol), K_2CO_3 (105 mg, 0.76 mmol) and 1-bromo-3,5-bis(trifluoromethyl)benzene (97 mg, 165 µl, 0.33 mmol) were mixed. Compound **2a** was isolated as a red powder (45 mg, yield 61%). **^{1}H NMR** (300 MHz, $CDCl_3$): 8.47 (d, $^3J_{H\text{-}H}$ = 7.8 Hz, 2H), 8.22 (s, 2H), 8.05 – 7.92 (m, 4H), 7.90 (s, 4H), 7.66 (t, $^3J_{H\text{-}H}$ = 7.8 Hz, 2H), 4.90 (dd, $^3J_{H\text{-}H}$ = 9.6, 5.6 Hz, 1H), 2.11 – 1.92 (m, 2H), 1.63 (m, , 2H), 1.24 (m,12H), 0.89 – 0.75 (m, 6H). **^{13}C NMR** (75 MHz, $CDCl_3$): 163.3 (C), 144.9 (C), 136.5 (C), 134.4 (C), 132.4 (C), 131.9 (C), 131.8 (CH), 131.7 (C), 131.5 (C),

131.0 (C), 129.0 (C), 128.5 (CH), 128.0 (C), 127.4 (CH), 126.8 (C), 125.4 (C), 124.6 (CH), 124.4 (CH), 121.8 (C), 121.6 (CH), 55.1 (CH), 32.1 (CH_2), 31.7 (CH_2), 26.8 (CH_2), 22.6 (CH_2), 14.1 (CH_3). **^{19}F NMR** (282 MHz, $CDCl_3$): -62.60. **HRMS** (APCI$^+$): m/z = calcd 900.2705 $[M+H]^+$, measured 900.2714 $[M+H]^+$.

Compound 2b. Following the general procedure (2.1.), PMI **5** (60 mg, 0.08 mmol), $Pd_2(dba)_3$ (16 mg, 0.02 mmol), SPhos (15 mg, 0.04 mmol), K_2CO_3 (105 mg, 0.8 mmol) and 1-bromo-3,5-dimethoxybenzene (72 mg, 0.33 mmol) were mixed. Compound **2b** was obtained as a dark red powder (43 mg, yield 70%). **^{1}H NMR** (300 MHz, $CDCl_3$): 8.40 (d, $^3J_{H-H}$ = 7.6 Hz, 2H), 8.24 (s, 2H), 7.88 (d, $^3J_{H-H}$ = 7.6 Hz, 2H), 7.59 (t, $^3J_{H-H}$ = 7.6 Hz, 2H), 6.60 – 6.56 (m, , 6H), 4.99 (dd, $^3J_{H-H}$ = 9.4, 5.8 Hz, 1H), 3.85 (s, 12H), 2.22 – 1.97 (m, 2H), 1.77 – 1.59 (m, 2H), 1.27 – 1.21 (m, 12H), 0.89 – 0.78 (m, 6H). **^{13}C NMR** (75 MHz, $CDCl_3$): 160.8 (C=O), 145.3 (C), 135.3 (C), 134.4 (C), 131.6 (C), 130.8 (CH), 129.2 (C), 128.2 (C), 127.2 (CH), 125.8, 124.7 (CH), 123.8 (CH), 106.5 (CH), 99.7 (CH), 55.5 (CH_3), 54.7 (CH), 32.3 (CH_2), 32.0 (CH_2), 26.9 (CH_2), 22.8 (CH_2), 14.2 (CH_3). **HRMS** (APCI$^+$): m/z = calcd 748.3633 $[M+H]^+$, measured 748.3627 $[M+H]^+$.

2.3. Synthesis of *ortho*-PMIs 3a and 3b

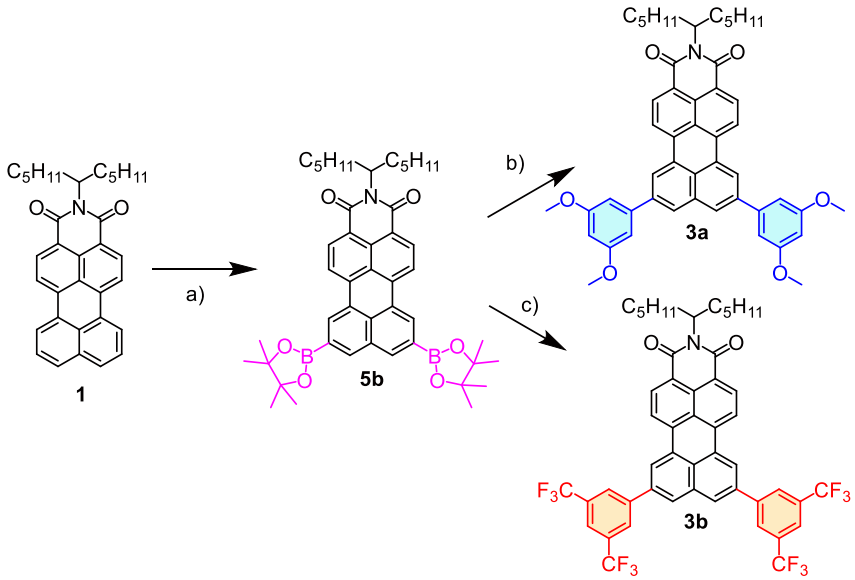

Scheme S2 Synthetic route for the PMI derivatives **3a** and **3b**. a) B_2Pin_2 (8 eq), $[Ir(OMe)(COD)]_2$ (0.05 eq) and dtbpy (0.1 eq), 20 mM solution, THF, 110 ºC (MW), 1h, 85%; b) 1-bromo-3,5-dimethoxybenzene (4 eq), K_2CO_3 (10 eq), $Pd_2(dba)_3$ (0.2 eq), SPhos (0.4 eq), toluene/water (4:1), 36 h, 110 ºC, 51%; c) 1-bromo-3,5-bis(trifluoromethyl)benzene (4 eq), K_2CO_3 (10 eq), $Pd_2(dba)_3$ (0.2 eq), SPhos (0.4 eq), toluene/water (4:1), 36 h, 110 ºC, 65%.

Compound 5b. The compound was synthesized following the previously reported procedures.[S1]

Compound 3a. Following the general procedure (2.1.), PMI **6** (120 mg, 0.16 mmol), $Pd_2(dba)_3$ (32 mg, 0.03 mmol), SPhos (30 mg, 0.07 mmol), K_2CO_3 (210 mg, 1.44 mmol) and 1-bromo-3,5-dimethoxybenzene (144 mg, 0.66 mmol) were mixed. Compound **3a** was obtained as a dark red powder (102 mg, yield 83%). **^{1}H NMR** (300 MHz, $CDCl_3$): 8.58 – 8.47 (m, 4H), 8.39 (d, $^3J_{H\text{-}H}$ = 8.3 Hz, 2H), 7.99 (s, 2H), 6.88 (d, $^4J_{H\text{-}H}$ = 2.3 Hz, 4H), 6.56 (t, $^4J_{H\text{-}H}$ = 2.3 Hz, 2H), 5.26 – 5.15 (m, 1H), 3.93 (s, 12H), 2.25 (m, 2H), 1.99 – 1.77 (m, 2H), 1.34 – 1.25 (m, 12H), 0.93 – 0.72 (m, 6H). **^{13}C NMR** (75 MHz, $CDCl_3$): 165.2 (C), 161.5 (C), 142.4 (C), 140.3 (C), 136.7 (C), 135.0 (C), 130.1 (C), 129.7 (C), 128.8 (CH), 126.9 (C), 126.6 (C), 123.1 (CH), 120.5 (CH), 105.9 (CH), 99.9 (CH), 55.7 (CH_3), 54.6 (CH), 32.5 (CH_2), 32.0 (CH_2), 26.9 (CH_2), 22.7 (CH_2), 14.2 (CH_3). **HRMS** (APCI$^+$): m/z = calcd. 748.3633 $[M]^+$, measured 748.3620 $[M]^+$.

Compound 3b. Following the general procedure (2.1.), PMI **6** (120 mg, 0.16 mmol), $Pd_2(dba)_3$ (32 mg, 0.03 mmol), SPhos (30 mg, 0.07 mmol), K_2CO_3 (210 mg, 1.44 mmol) and 3,5-trifluoromethyl-1-bromobenzene (194 mg, 330 µl, 0.66 mmol) were mixed. Compound **3b** was obtained as a red powder (96 mg, yield 65%). **^{1}H NMR** (300 MHz, $CDCl_3$): 8.72 – 8.51 (m, 6H), 8.29 – 8.14 (m, 6H), 8.01 (s, 2H), 5.21 (dd, $^3J_{H\text{-}H}$ = 9.0, 5.9 Hz, 1H), 2.30 – 2.20 (m, 2H), 1.95 – 1.82 (m, 2H), 1.35 – 1.22 (m, 12H), 0.87 – 0.80 (m, 6H). **^{13}C NMR** (75 MHz, $CDCl_3$): 142.4 (C), 138.1 (C), 135.7 (C), 135.2 (C), 132.8 (q, $^1J_{C\text{-}F}$ = 33.3 Hz, C-F), 131.4 (CH), 131.0 (C), 130.1 (C), 129.2 (CH), 127.7 (CH), 127.0 (C), 125.2 (C), 122.7 (CH), 122.1 (CH), 121.6 (C), 121.3 (CH), 54.8 (CH), 32.5 (CH_2), 31.9 (CH_2), 26.8 (CH_2), 22.7 (CH_2), 14.2 (CH_3). **^{19}F NMR** (282 MHz, $CDCl_3$): -62.67. **HRMS** (APCI$^+$): m/z = calcd. 900.2705 $[M+H]^+$, measured 900.2699 $[M+H]^+$.

2.4. Synthesis of *ortho*-PMIs 4a and 4b

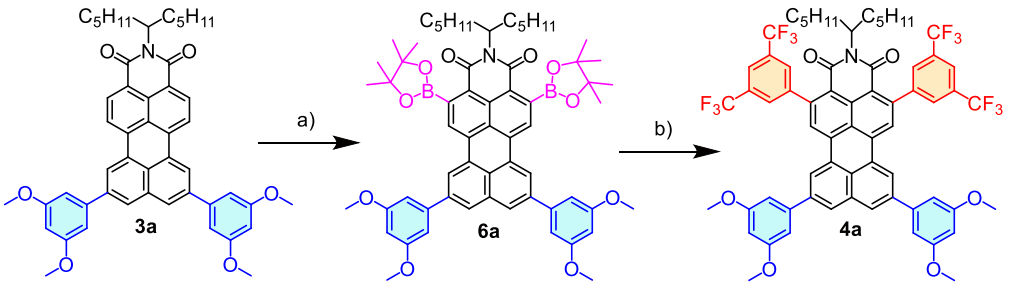

Scheme S3 Synthetic route of the PMI derivative **4a.** a) B_2Pin_2 (8 eq), $[Ir(OMe)(COD)]_2$ (0.1 eq) and $P(C_6F_5)_3$ (0.2 eq), 20 mM solution, dioxane, 140 ºC 72 h, 79%; b) 1-bromo-3,5-

bis(trifluoromethyl)benzene (4 eq), K_2CO_3 (10 eq), $Pd_2(dba)_3$ (0.2 eq), SPhos (0.4 eq), toluene/water (4:1), 36 h, 110 ºC, 61%.

Compound 6a. In a 50 mL Schlenk, **3a** (70 mg, 0.09 mmol), B_2pin_2 (190 mg, 0.75 mmol), $[Ir(OMe)(cod)]_2$ (7 mg, 0.01 mmol) and $P(C_6F_5)_3$ (11 mg, 0.02 mmol) were put under Ar atmosphere and dissolved in dry dioxane (5 mL). The orange mixture was stirred under reflux (140 ºC) with a condenser for 72 h. The reaction was cooled down to rt and the solvent was evaporated *in vacuo*. The resulting oil was redissolved in CH_2Cl_2 (10 mL) and precipitated with a mixture of MeOH/EtOH (4:1 mL). After evaporating the CH_2Cl_2 at reduced pressure, the suspended red solid was filtered and washed with further MeOH (3 x 5 ml) affording **6a** as a red powder (74 mg, 79%). **^{1}H NMR** (300 MHz, $CDCl_3$): 8.58 (s, 2H), 8.42 (s, 2H), 8.05 (s, 2H), 6.90 (d, $^4J_{H\text{-}H}$ = 2.3 Hz, 4H), 6.57 (t, $^4J_{H\text{-}H}$ = 2.3 Hz, 2H), 5.07 (dd, $^3J_{H\text{-}H}$ = 8.9, 5.9 Hz, 1H), 3.92 (s, 12H), 2.28 – 2.14 (m, 2H), 1.83 (m, 2H), 1.55 (s, 24H), 1.33 – 1.23 (m, 12H), 0.90 – 0.83 (m, 6H). **^{13}C NMR** (75 MHz, $CDCl_3$): 166.2 (C), 161.4 (C), 143.1 (C), 140.6 (C), 135.3 (C), 135.1 (C), 130.0 (C), 128.9 (CH), 123.5 (CH), 123.2 (CH), 106.1 (CH), 99.9 (CH), 84.5, 55.7 (CH_3), 54.6 (CH), 32.4 (CH_2), 31.9 (CH_2), 26.7 (CH_2), 25.3 (CH_3), 22.7 (CH_2), 14.2 (CH_3).

Compound 4a. Following the general procedure (2.1.), PMI **6a** (60 mg, 0.07 mmol), $Pd_2(dba)_3$ (13 mg, 0.01 mmol), SPhos (12 mg, 0.03 mmol), K_2CO_3 (22 mg, 0.64 mmol) and 3,5-trifluoromethyl-1-bromobenzene (82 mg, 140 µl, 0.30 mmol) were mixed. Compound **4a** was obtained as a dark red powder (50 mg, yield 61%). **^{1}H NMR** (300 MHz, $CDCl_3$): 8.58 (s, 2H), 8.29 (s, 2H), 8.16 (s, 2H), 8.00 (s, 2H), 7.89 (s, 4H), 6.88 (d, $^4J_{H\text{-}H}$ = 2.3 Hz, 4H), 6.57 (t, $^4J_{H\text{-}H}$ = 2.3 Hz, 2H), 4.88 (dd, $^3J_{H\text{-}H}$ = 9.3, 4.5 Hz, 1H), 2.09 – 1.91 (m, 2H), 1.73 – 1.57 (m, 2H), 1.22 (s, 12H), 0.87 – 0.75 (m, 6H). **^{13}C NMR** (76 MHz, $CDCl_3$): 161.6 (C), 144.8 (C), 142.3 (C), 140.9 (C), 136.2 (C), 135.0 (C), 131.8 (q, $^1J_{C\text{-}F}$ = 33.3 Hz, C-F), 131.7 (C), 129.8 (CH), 128.9 (C), 128.4 (CH), 127.0 (C), 126.6 (C), 125.4 (C), 124.6 (CH), 124.0 (CH), 121.8 (CH), 106.2 (CH), 99.7 (CH), 55.7 (CH_3), 55.1, 32.1 (CH_2), 31.7 (CH_2), 26.8 (CH_2), 22.6 (CH_2), 14.1 (CH_3). **^{19}F NMR** (282 MHz, $CDCl_3$): -62.57. **HRMS** (APCI$^+$): m/z = calcd. 1172.3754 $[M\text{-}H]^+$, measured 1172.3748 $[M\text{-}H]^+$.

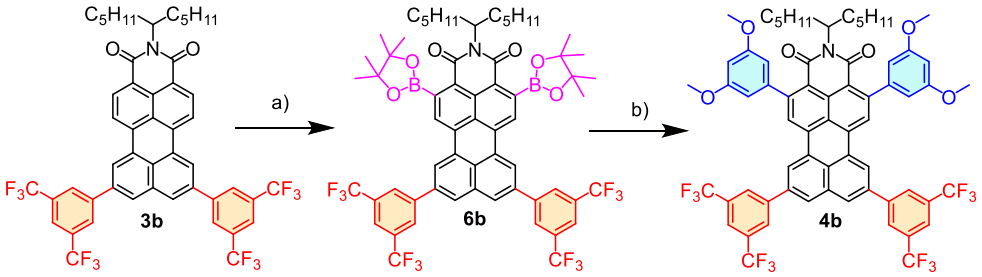

Scheme S4 Synthetic route of the PMI derivative **4b.** a) B_2Pin_2 (8 eq), $[Ir(OMe)(COD)]_2$ (0.1 eq) and $P(C_6F_5)_3$ (0.2 eq), 20 mM solution, dioxane, 140 ºC 72 h, 77%; b) 1-bromo-3,5-dimethoxybenzene (4 eq), K_2CO_3 (10 eq), $Pd_2(dba)_3$ (0.2 eq), SPhos (0.4 eq), toluene/water (4:1), 36 h, 110 ºC, 77%.

Compound 6b. In a 50 mL Schlenk, **3a** (70 mg, 0.08 mmol), B_2pin_2 (157 mg, 0.62 mmol), $[Ir(OMe)(cod)]_2$ (7 mg, 0.01 mmol) and $P(C_6F_5)_3$ (11 mg, 0.02 mmol) were put under Ar atmosphere and dissolved in dry dioxane (5 mL). The orange mixture was stirred under reflux (140 ºC) with a condenser for 72 h. The reaction was cooled down to rt and the solvent was evaporated *in vacuo*. The resulting oil was redissolved in CH_2Cl_2 (10 mL) and precipitated with a mixture of MeOH/EtOH (4:1 mL). After evaporating the CH_2Cl_2 at reduced pressure, the suspended red solid was filtered and washed with further MeOH (3 x 5 ml) affording the product **6b** as a red powder (70 mg, 77%). **^{1}H NMR** (300 MHz, $CDCl_3$): 8.62 (s, 2H), 8.46 (s, 2H), 8.23 (s, 4H), 8.17 (s, 2H), 8.00 (s, 2H), 5.13 – 5.00 (m, 1H), 2.26 – 2.14 (m, 2H), 1.91 – 1.79 (m, 2H), 1.55 (s, 24H), 1.34 – 1.24 (m, 12H), 0.90 – 0.83 (m, 6H). **^{13}C NMR** (76 MHz, $CDCl_3$): 165.0 (C), 142.7 (C), 138.0 (C), 135.2 (C), 134.3 (C), 133.0 (C), 132.5 (C), 131.0 (C), 129.1 (CH), 128.5 (C), 127.8 (C), 127.1 (CH), 125.3, 124.0 (CH), 122.8 (CH), 122.0 (CH), 121.7 (C), 84.7 (C), 54.8 (CH), 32.4 (CH_2), 31.9 (CH_2), 26.7 (CH_2), 25.2 (CH_3), 22.7 (CH_2), 14.2 (CH_3).

Compound 4b. Following the general procedure (2.1.), PMI **6b** (60 mg, 0.05 mmol), $Pd_2(dba)_3$ (9 mg, 0.01 mmol), SPhos (8 mg, 0.02 mmol), K_2CO_3 (29 mg, 0.21 mmol) and 1-bromo-3,5-dimethoxybenzene (45 mg, 0.21 mmol) were mixed. Compound **4b** was obtained as a red powder (49 mg, yield 70%). **^{1}H NMR** (300 MHz, $CDCl_3$): 8.58 (s, 2H), 8.39 (s, 2H), 8.26 – 8.10 (m, 6H), 8.00 (s, 2H), 6.70 – 6.48 (m, 6H), 4.99 (dd, $^3J_{H\text{-}H}$ = 9.4, 5.7 Hz, 1H), 3.86 (s, 12H), 2.10 (m, 2H), 1.79 – 1.59 (m, 2H), 1.25 (m, 12H), 0.91 – 0.75 (m, 6H). **^{13}C NMR** (75 MHz, $CDCl_3$): 160.9 (C), 144.8 (C), 142.5 (C), 138.4 (C), 135.1 (C), 134.0 (C), 132.7 (q, $^1J_{C\text{-}F}$ = 33.3 Hz, C-F), 131.5 (C), 130.7 (C), 129.5 (CH), 127.9 (CH), 127.7 (C), 126.0 (C), 125.4 (CH), 125.2 (C), 122.8 (CH), 122.1 (CH), 121.6, 106.6 (CH), 99.6 (CH), 55.5 (CH), 54.9 (CH), 32.3 (CH_2), 32.0 (CH_2), 26.9 (CH_2), 22.8 (CH_2), 14.2 (CH_3). **^{19}F NMR** (282 MHz, $CDCl_3$): -62.60. **HRMS** ($APCI^+$): m/z = calcd. 1172.3754 $[M+H]^+$, measured 1172.3747 $[M+H]^+$.

3. Computational studies

The structures of compounds **2a**, **2b**, **3a**, **3b**, **4a** and **4b** were optimized by DFT using the B3LYP[S2] functional at the 6-31G(d,p) level, with chloroform as solvent. Analytical harmonic frequencies were computed at the same level of theory. All the calculations were carried out by the methods implemented in Gaussian 16 package.[S3] The imide substituent was changed from 6-undecanyl imide to isopropyl imide in order to reduce the time and simplify the calculations.

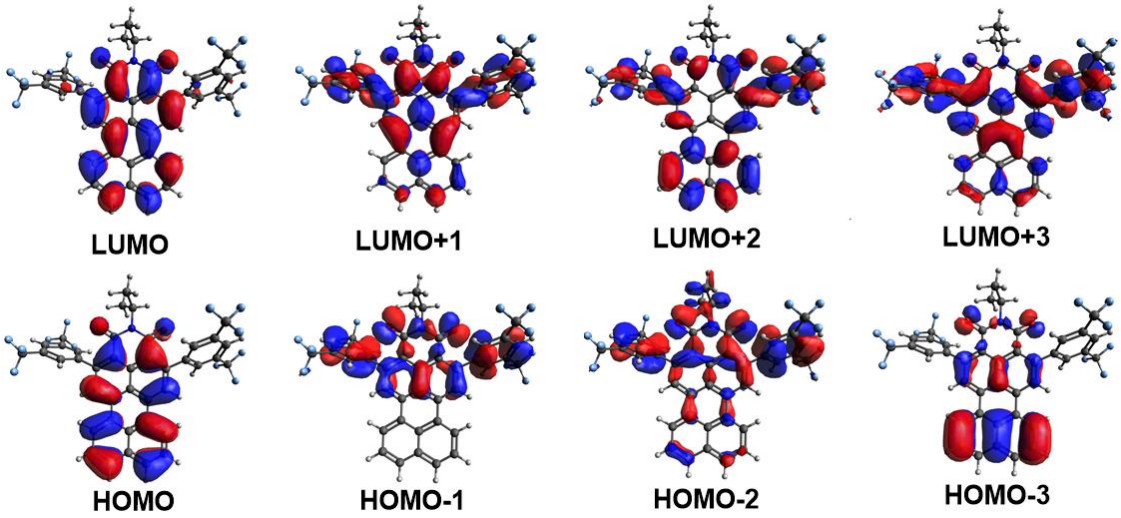

Fig. S2 Kohn–Sham orbital representations of the H-3 to L+3 levels of **2a**.

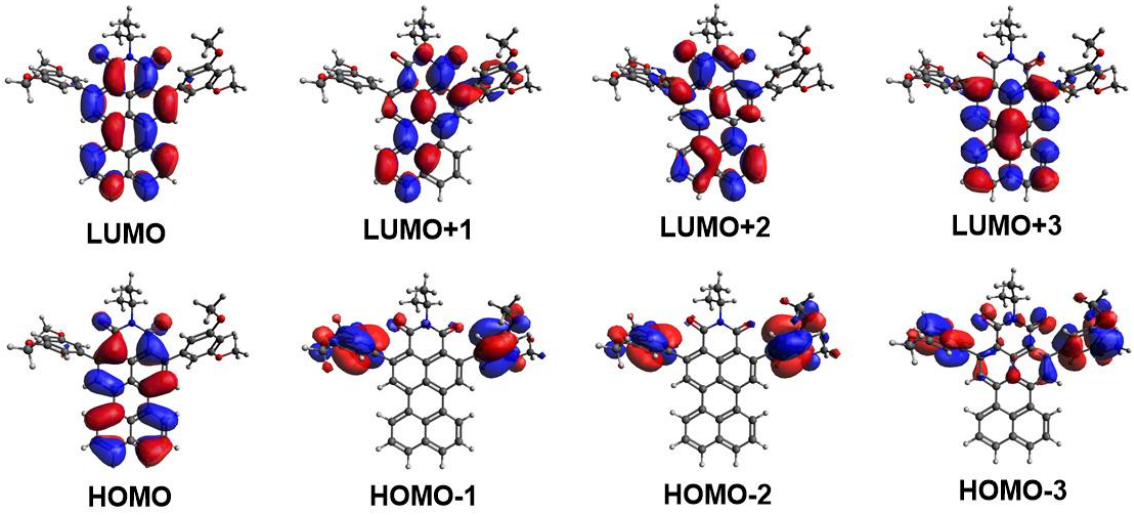

Fig. S3 Kohn–Sham orbital representations of the H-3 to L+3 levels of **2b**.

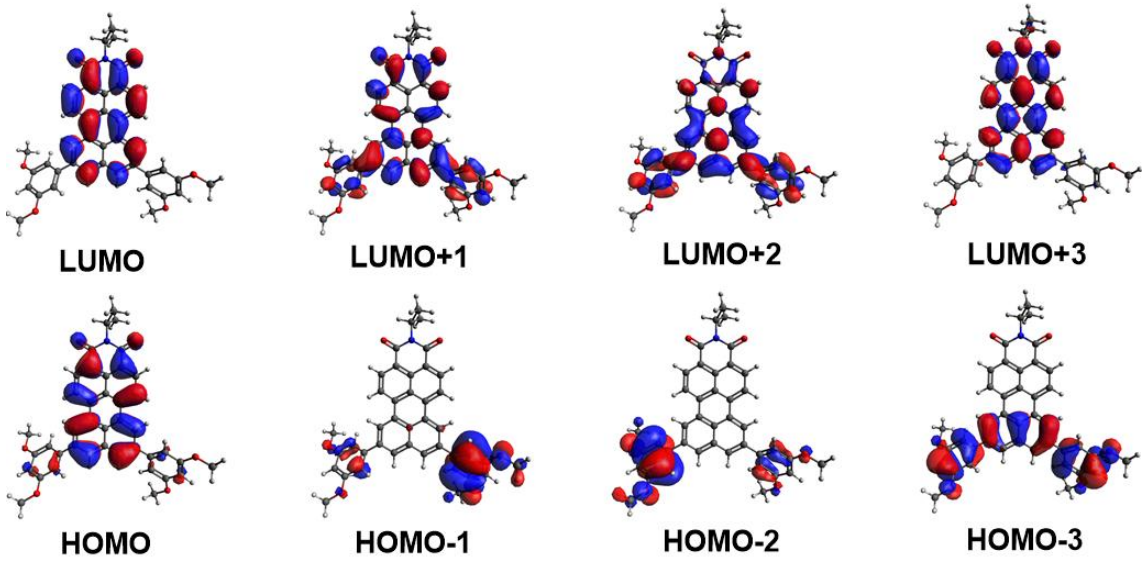

Fig. S4 Kohn–Sham orbital representations of the H-3 to L+3 levels of **3a**.

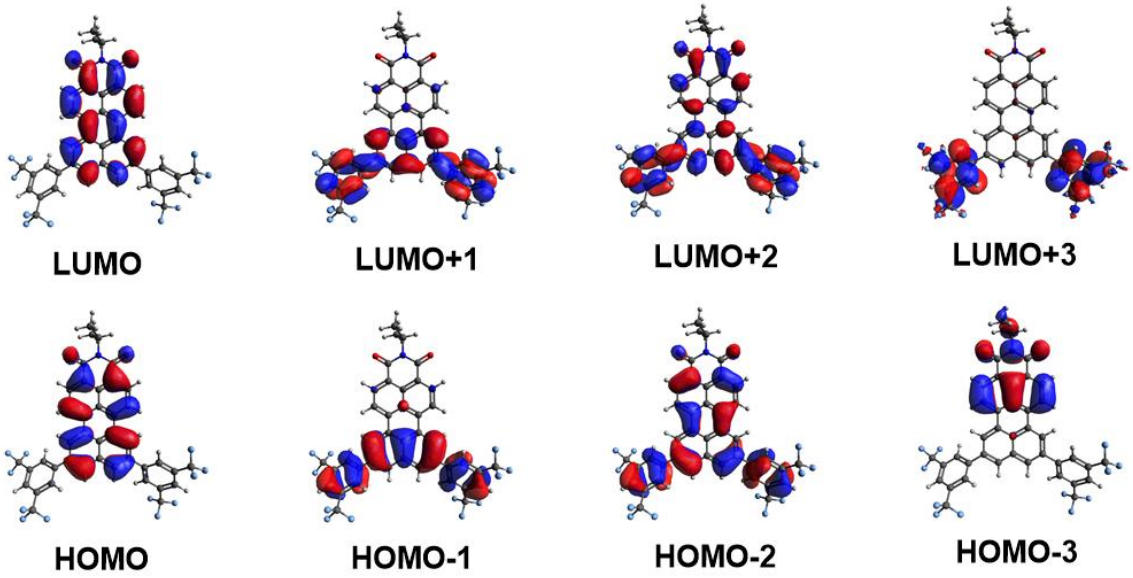

Fig. S5 Kohn–Sham orbital representations of the H-3 to L+3 levels of **3b**.

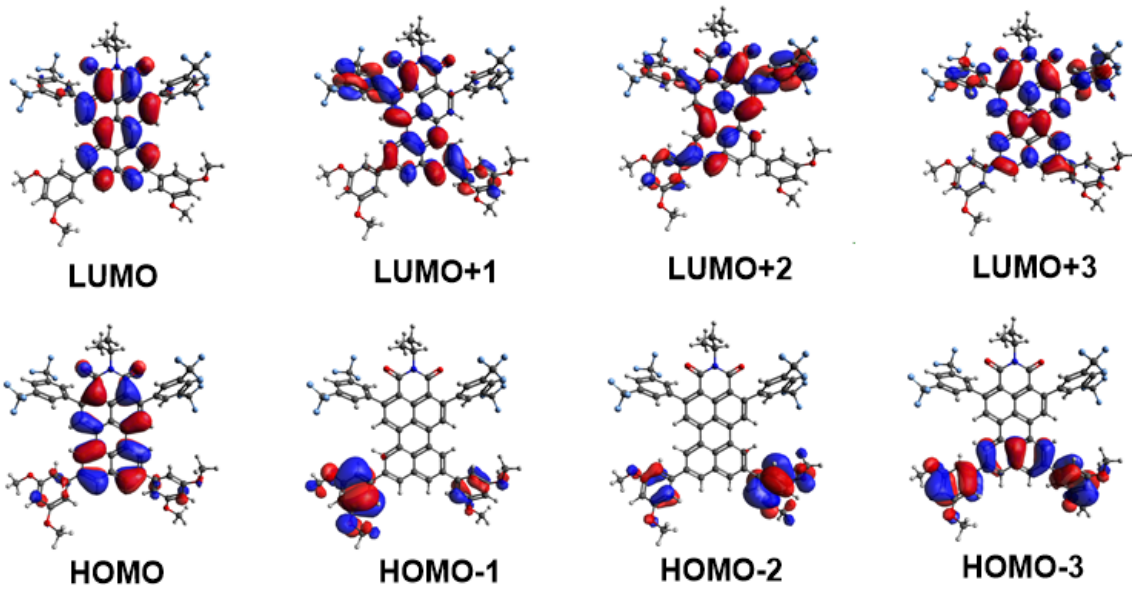

Fig. S6 Kohn–Sham orbital representations of the H-3 to L+3 levels of **4a.**

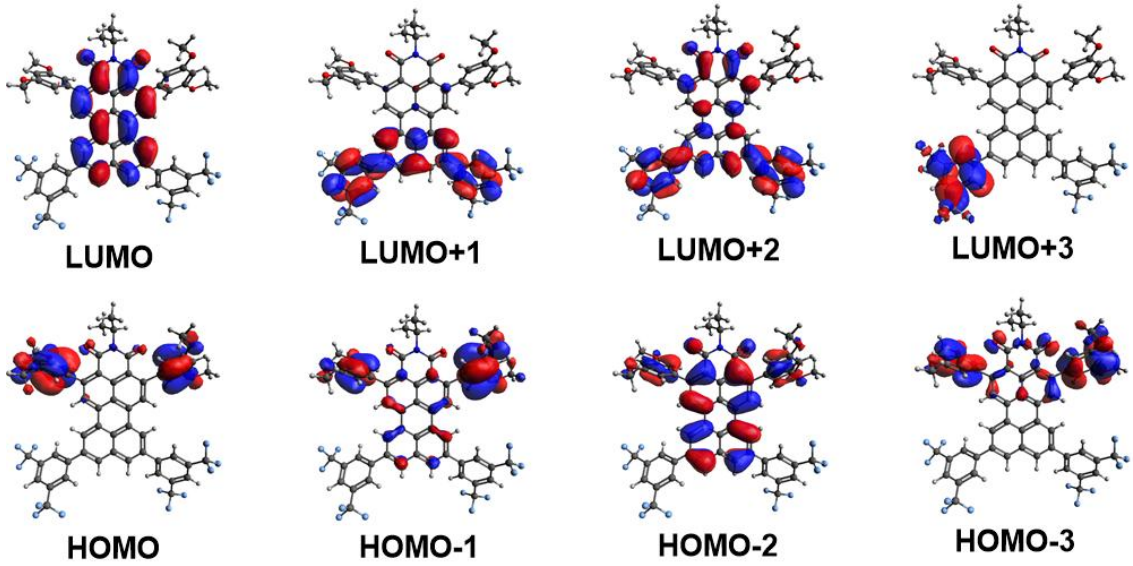

Fig. S7 Kohn–Sham orbital representations of the H-3 to L+3 levels of **4b.**

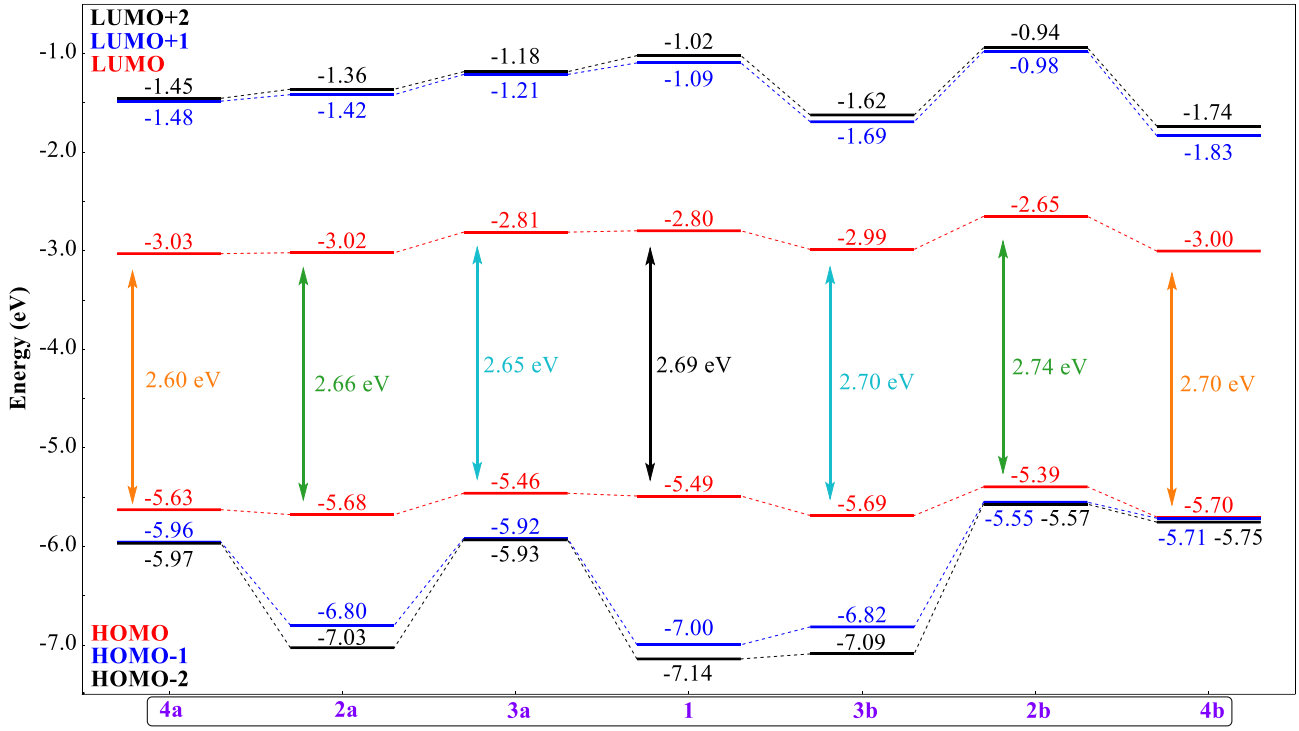

Fig. S8 HOMO-LUMO levels and their DFT calculated energy for compounds **1**, **2a**, **2b**, **3a**, **3b**, **4a** and **4b**.

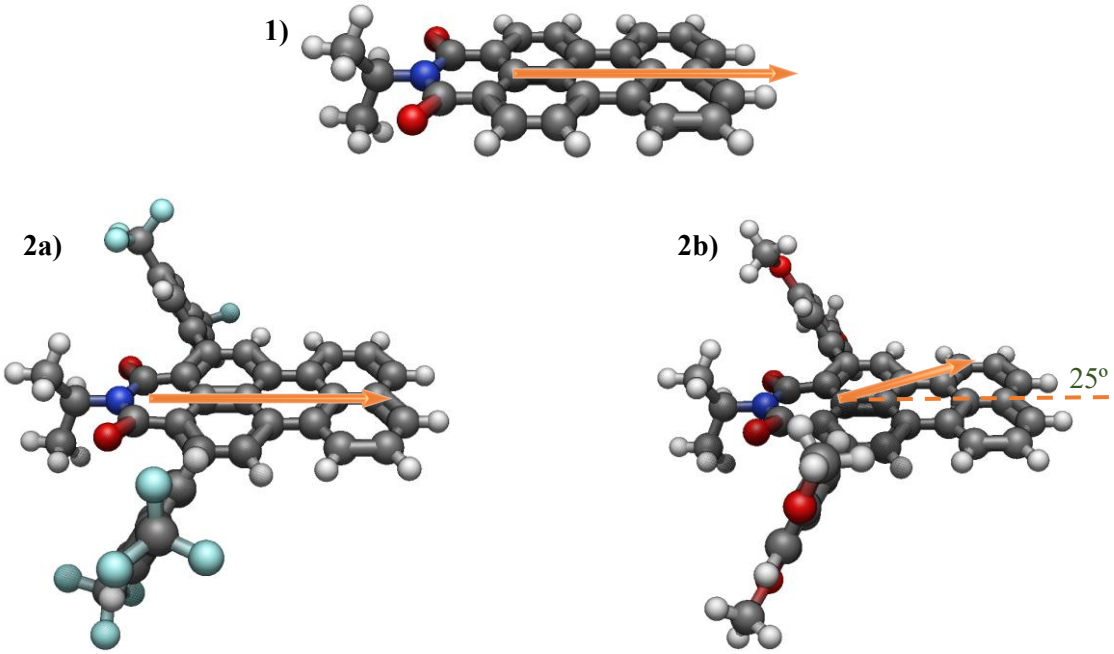

Fig. S9 Vectors representing the value and the direction of dipole moment in the PMI derivatives **1**, **2a** and **2b**.

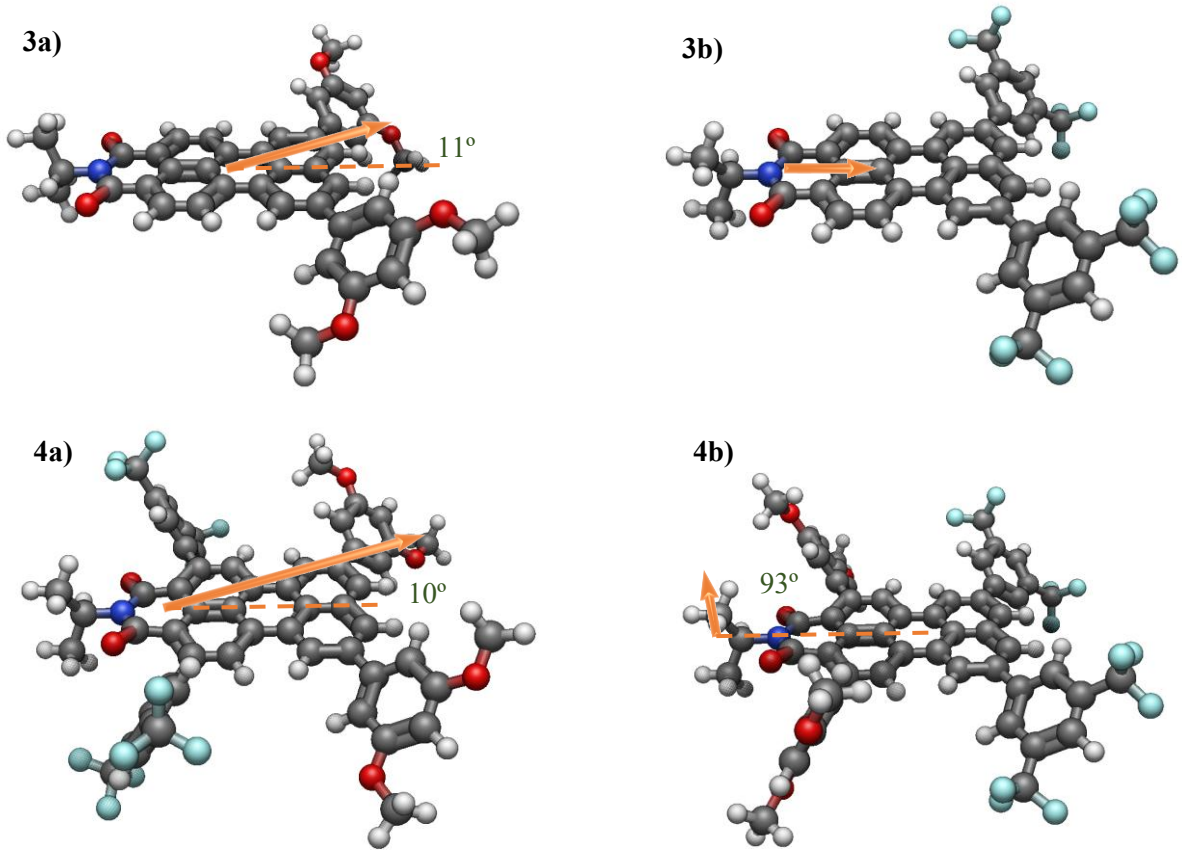

Fig. S10 Vectors representing the value and the direction of dipole moment in the PMI derivatives **3a**, **3b**, **4a** and **4b**.

4. Electrochemistry studies in dissolved samples

Electrochemical measurements employing cyclic voltammetry (CV) and differential pulse voltammetry (DPV) were conducted on a glassy carbon working electrode under an argon atmosphere. Compounds were dissolved in CH_2Cl_2 with tetrabutylammonium hexafluorophosphate ($(n\text{-Bu})_4NPF_6$, 0.1 M) as the supporting electrolyte.

Concentrated solutions of **1**, **2a**, **2b**, **3a**, **3b**, **4a** and **4b** were subjected to electrochemical analysis across a range of applied potentials. The observed reversible electrochemical events were referenced to the ferrocene/ferrocenium (Fc/Fc^+) redox couple. The potential sweep rate for CV measurements was maintained at 100 mV s^{-1}, and all solutions were deoxygenated by purging with argon for a 30 seconds prior to electrochemical measurements. The values for the oxidation and reduction potentials were taken from the DPV and corrected according to literature[S4] (Fig. S13), in the same manner than for other publications that measured PDIs or perylene derivatives.

$$E_{HOMO} = -(E_{oxi} + 4.8)\ eV \qquad E_{LUMO} = -(E_{red} + 4.8)\ eV \qquad \text{(Eq. S1)}$$

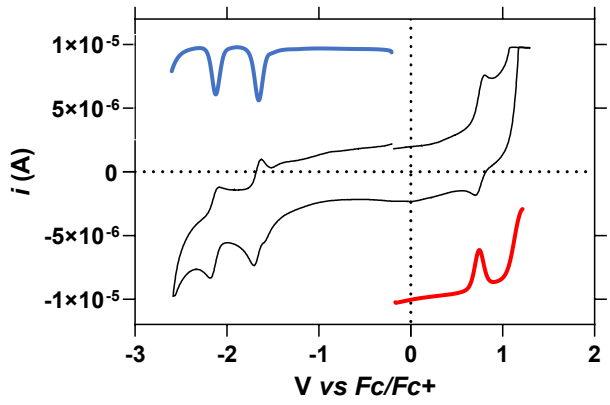

Fig. S11 Cyclic voltamogram of compound **1** in CH_2Cl_2, $(n\text{-Bu})_4NPF_6$ (0.1 M), referenced to Fc/Fc^+. Reduction DPV (blue) and oxidation DPV (red).

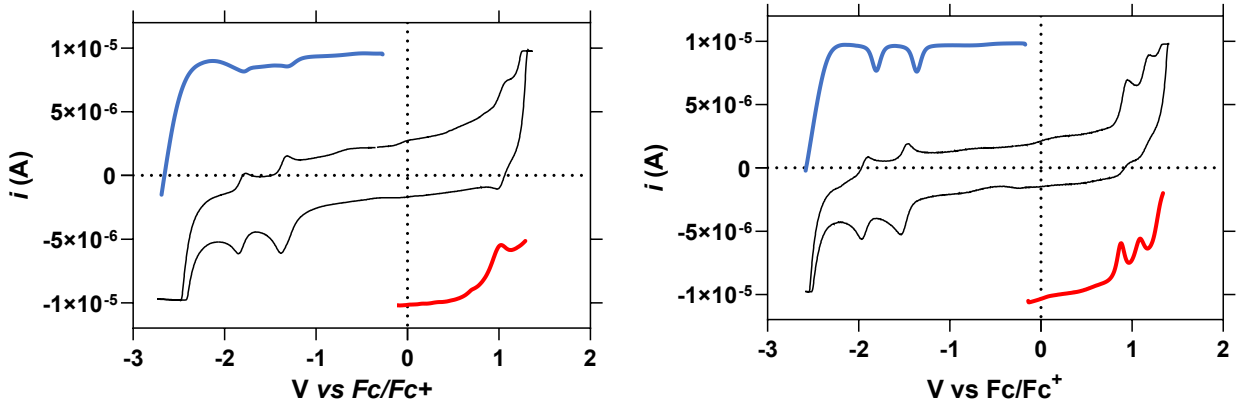

Fig. S12 Cyclic voltamogram of compounds **2a** (left) and **2b** (right) in CH_2Cl_2, $(n\text{-Bu})_4NPF_6$ (0.1 M), referenced to Fc/Fc^+. Reduction DPV (blue) and oxidation DPV (red).

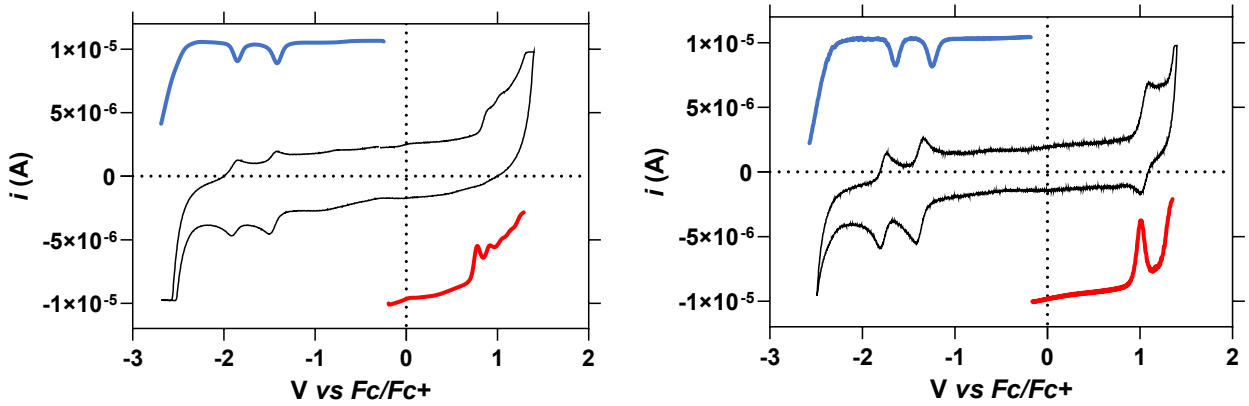

Fig. S13 Cyclic voltamogram of compounds **3a** (left) and **3b** (right) in CH_2Cl_2, $(n\text{-Bu})_4NPF_6$ (0.1 M), referenced to Fc/Fc^+. Reduction DPV (blue) and oxidation DPV (red).

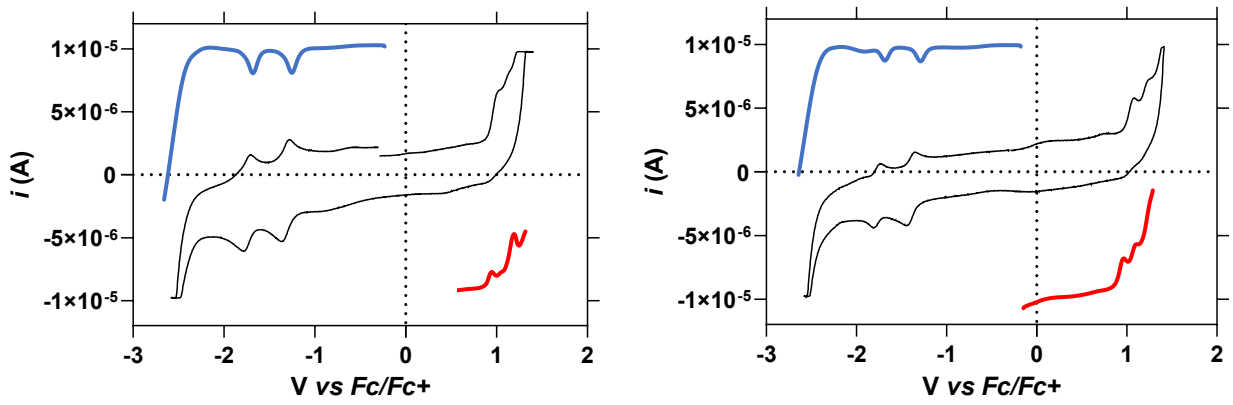

Fig. S14 Cyclic voltamogram of compounds **4a** (left) and **4b** (right) in CH_2Cl_2, $(n\text{-Bu})_4NPF_6$ (0.1 M), referenced to Fc/Fc^+. Reduction DPV (blue) and oxidation DPV (red).

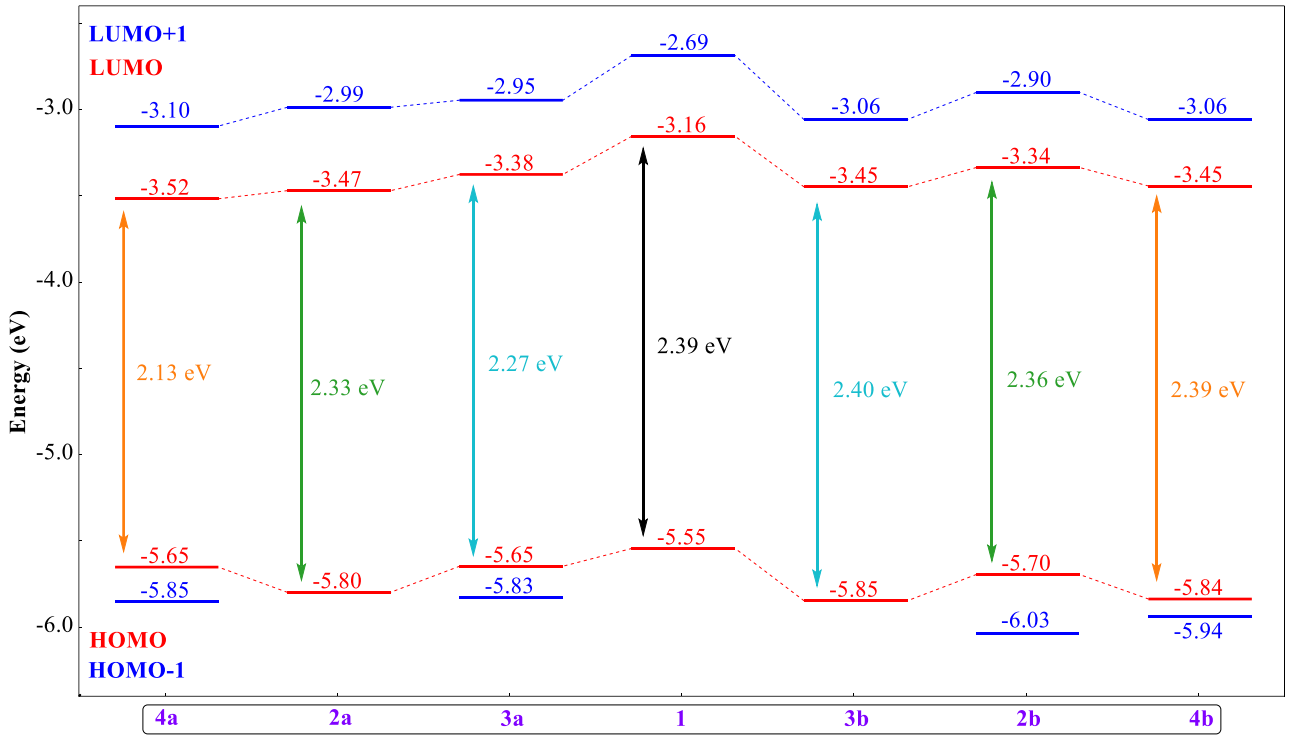

Fig. S15 HOMO-LUMO levels and energy calculated from transformed electrochemistry results, for compounds **1**, **2a**, **2b**, **3a**, **3b**, **4a** and **4b**.

5. Optoelectronic measurements in dissolved samples

The absorption and fluorescence emission spectra of **1**, **2a**, **2b**, **3a**, **3b**, **4a** and **4b** (λ_{ex} = 460 or 480 nm) were recorded at 25 ºC (c = 5 μM).

Fluorescence quantum yields were calculated for solutions with absorbance < 0.1. They were evaluated by comparison with the standard of Rhodamine 6G (EtOH, Φ_R = 95%, λ_{ex} = 480 nm), using equation (S2):

$$\Phi = \Phi_R \frac{Int}{Int_R}\left(\frac{A_R}{A}\right)\frac{n^2}{n_R^2} \qquad \text{(Eq. S2)}$$

where Φ_R is the quantum yield of the standards, Int is the area of the emission intensity of the sample, Int_R is the area of the emission intensity of the standard, A is the absorbance, A_R is the absorbance of the standard, n is the refractive index of the sample and n_R is the refractive index of the standard.

5.1. Absorption and fluorescence results

Absorption and fluorescence spectra were measured in DMSO, THF, $CHCl_3$, toluene and MCH.

From the previously optimized structures, TD-DFT calculations were carried out at the CAM-B3LYP/6-31+G(d,p) level of theory, with chloroform as solvent.

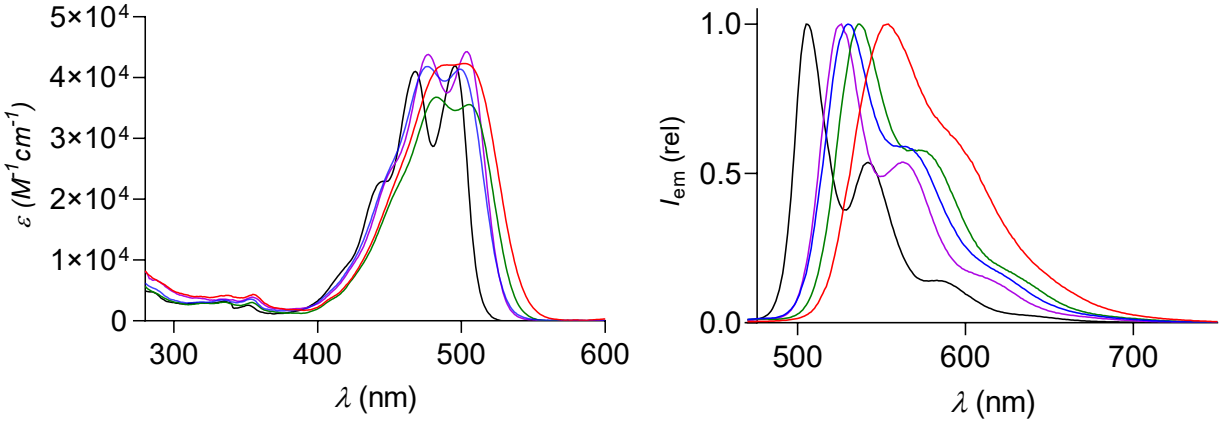

Fig. S16 Absorbance (left) and fluorescence emission (right) of **1** (λ_{ex} = 460 nm, 5 μM) in DMSO (red), THF (blue), $CHCl_3$ (green), toluene (purple) and MCH (black).

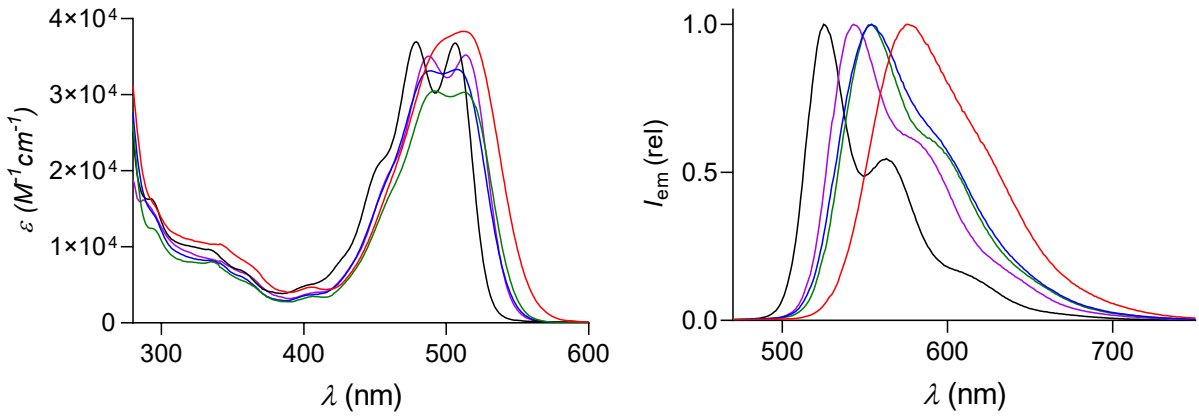

Fig. S17 Absorbance (left) and fluorescence emission (right) of **2a** (λ_{ex} = 460 nm, 5 μM) in DMSO (red), THF (blue), $CHCl_3$ (green), toluene (purple) and MCH (black).

Table S1 Selected transition properties of **2a** calculated at CAM-B3LYP/6-31+G(d,p) level of theory.

Wavelength (nm)[a]	**Osc. Strength**[b]	**Major contributions**[c]
455.8	0.8032	H->L (98%)
328.7	0.1006	H-1->L (68%)
300.2	0.0697	H-4->L (19%), H-3->L (31%), H->L+1 (16%)
274.1	0.1588	H->L+3 (55%)
251.1	0.1287	H-9->L (10%), H-7->L (62%)
242.0	0.6235	H-11->L (24%)

[a]Wavelength associated to the transition. [b]Oscillator strength. [c]MOs involved in the transitions (H = HOMO and L= LUMO).

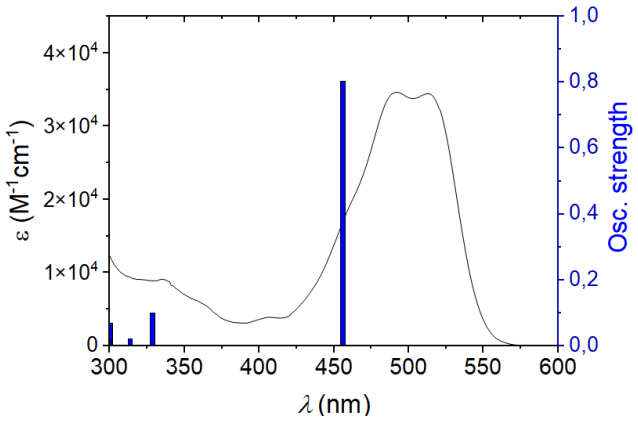

Fig. S18 Molar extinction coefficient spectra vs calculated oscillator strength and their contribution (blue bars, from Table S1) at different wavelengths for compound **2a**.

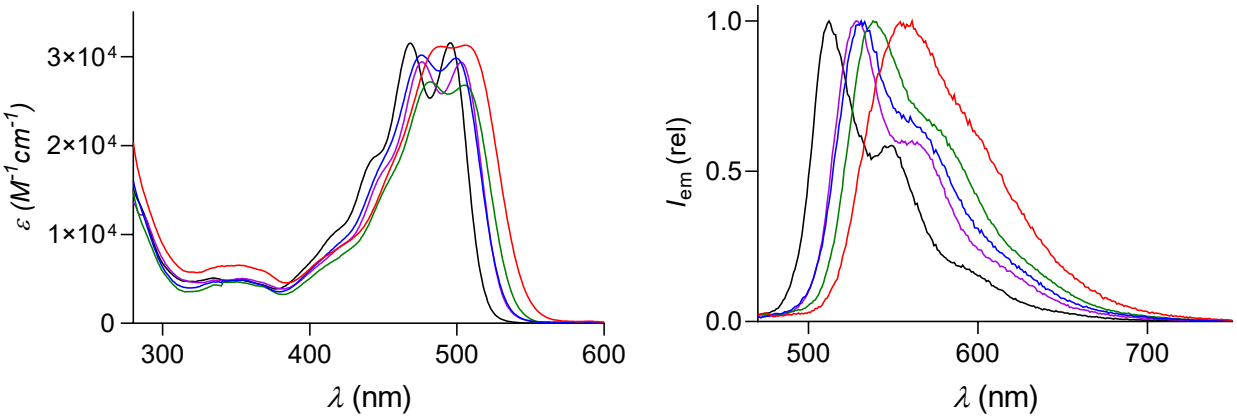

Fig. S19 Absorbance (left) and fluorescence emission (right) of **2b** (λ_{ex} = 480 nm, 5 µM) in DMSO (red), THF (blue), $CHCl_3$ (green), toluene (purple) and MCH (black).

Table S2 Selected transition properties of **2b** calculated at CAM-B3LYP/6-31+G(d,p) level of theory.

Wavelength (nm)[a]	**Osc. Strength**[b]	**Major contributions**[c]
445.2	0.8022	H->L (98%)
344.4	0.1064	H-3->L (25%), H-1->L (53%)
327.8	0.0554	H-3->L (40%), H-1->L (34%)
297.7	0.0598	H-6->L (34%), H->L+1 (24%)
273.7	0.081	H-8->L (35%), H->L+1 (24%), H->L+3 (16%)

[a]Wavelength associated to the transition. [b]Oscillator strength. [c]MOs involved in the transitions (H = HOMO and L= LUMO).

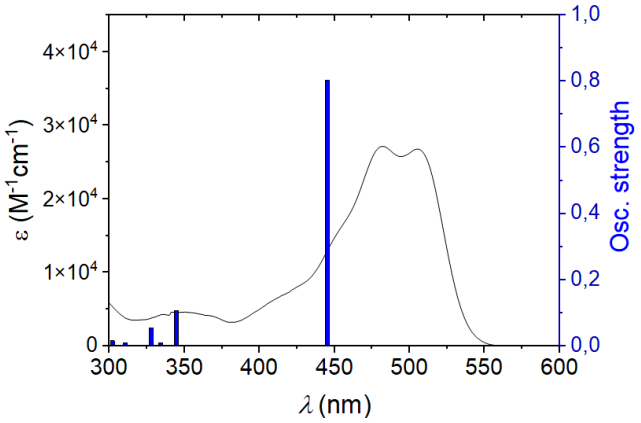

Fig. S20 Molar extinction coefficient spectra vs calculated oscillator strength and their contribution (blue bars, from Table S2) at different wavelengths for compound **2b**.

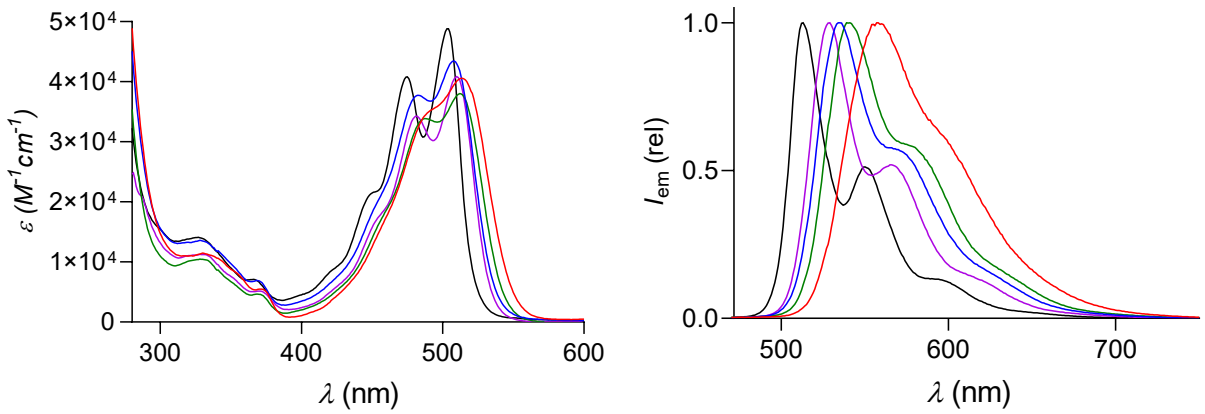

Fig. S21 Absorbance (left) and fluorescence emission (right) of **3a** (λ_{ex} = 460 nm, 5 µM) in DMSO (red), THF (blue), $CHCl_3$ (green), toluene (purple) and MCH (black).

Table S3 Selected transition properties of **3a** calculated at CAM-B3LYP/6-31+G(d,p) level of theory.

Wavelength (nm)[a]	**Osc. Strength**[b]	**Major contributions**[c]
452.5	0.870	H->L (97%)
308.5	0.102	H-5->L (29%), H->L+1 (16%), H->L+4 (15%)
295.1	0.054	H-4->L (60%)
280.2	0.348	H-8->L (16%), H->L+1 (29%), H->L+3 (27%)
255.5	0.062	H-1->L+1 (38%)
255.2	0.059	H-2->L+1 (18%), H-2->L+2 (26%)
254.0	0.233	H-10->L (25%), H-5->L (20%), H->L+4 (30%)

[a]Wavelength associated to the transition. [b]Oscillator strength. [c]MOs involved in the transitions (H = HOMO and L= LUMO).

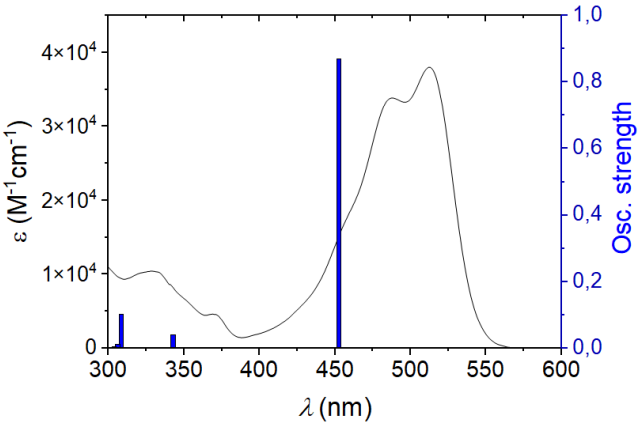

Fig. S22 Molar extinction coefficient spectra vs calculated oscillator strength and their contribution (blue bars, from Table S3) at different wavelengths for compound **3a**.

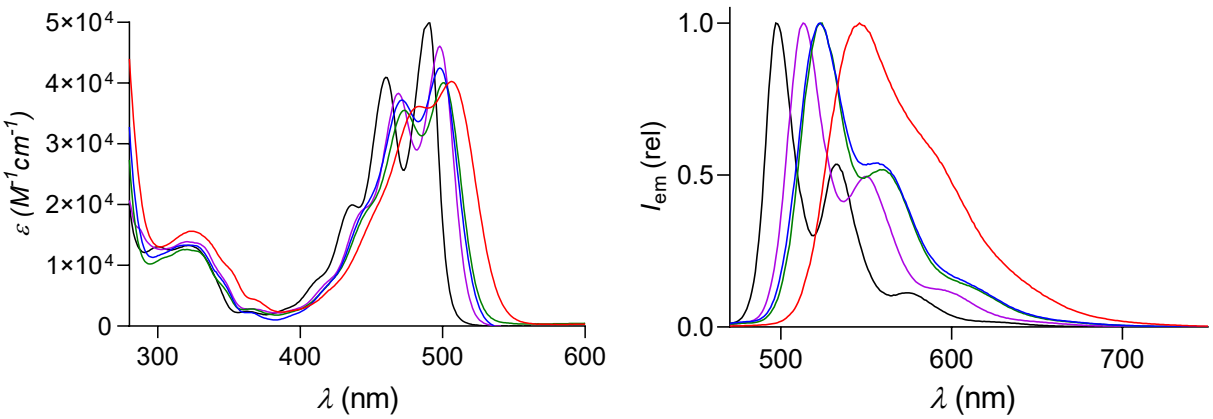

Fig. S23 Absorbance (left) and fluorescence emission (right) of **3b** (λ_{ex} = 460 nm, 5 µM) in DMSO (red), THF (blue), $CHCl_3$ (green), toluene (purple) and MCH (black).

Table S4 Selected transition properties of **3b** calculated at CAM-B3LYP/6-31+G(d,p) level of theory.

Wavelength (nm)[a]	**Osc. Strength**[b]	**Major contributions**[c]
446.4	0.865	H->L (98%)
307.1	0.079	H-3->L (65%), H->L+6 (16%)
303.8	0.064	H-4->L (23%), H->L+1 (35%), H->L+5 (18%)
288.5	0.073	H-2->L (36%), H->L+2 (50%)
278.9	0.462	H-4->L (22%), H->L+1 (24%), H->L+5 (24%)
253.4	0.335	H-6->L (46%), H->L+6 (24%)
238.2	1.029	H-6->L (40%), H->L+6 (38%)
235.9	0.439	H-2->L+2 (15%), H-1->L+1 (52%), H->L+7 (21%)

[a]Wavelength associated to the transition. [b]Oscillator strength. [c]MOs involved in the transitions (H = HOMO and L= LUMO).

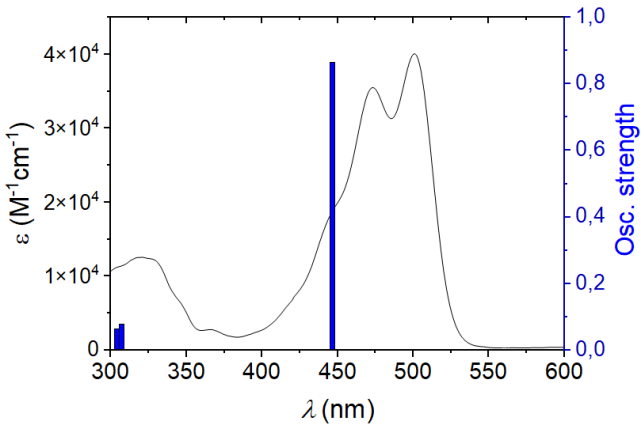

Fig. S24 Molar extinction coefficient spectra vs calculated oscillator strength and their contribution (blue bars, from Table S4) at different wavelengths for compound **3b**.

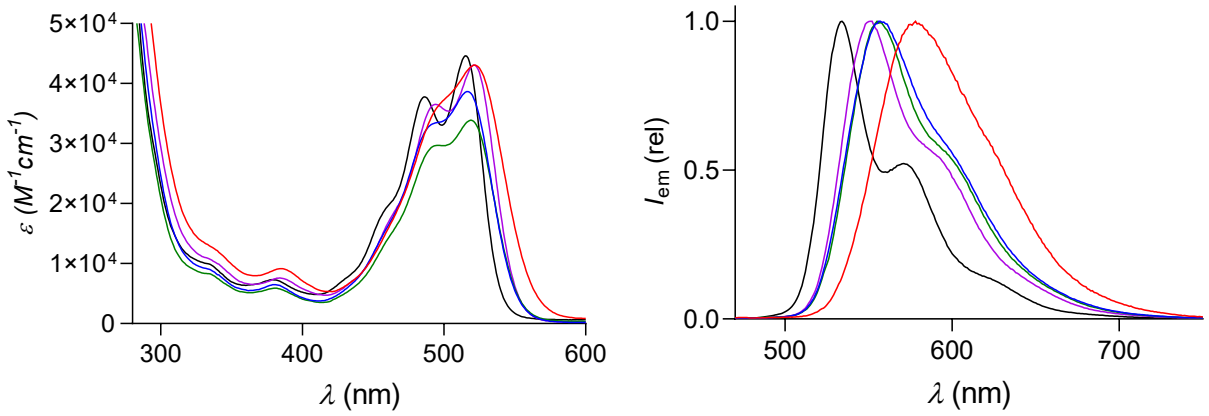

Fig. S25 Absorbance (left) and fluorescence emission (right) of **4a** (λ_{ex} = 460 nm, 5 µM) in DMSO (red), THF (blue), $CHCl_3$ (green), toluene (purple) and MCH (black).

Table S5 Selected transition properties of **4a** calculated at CAM-B3LYP/6-31+G(d,p) level of theory.

Wavelength (nm)[a]	**Osc. Strength**[b]	**Major contributions**[c]
460.3	0.844	H->L (96%)
326.9	0.202	H-5->L (66%)
283.1	0.107	H-9->L (23%), H->L+3 (28%)
264.5	0.612	H->L+4 (16%)
262.7	0.079	H-10->L (28%), H-6->L (27%)
257.3	0.066	H-2->L+1 (22%)

[a]Wavelength associated to the transition. [b]Oscillator strength. [c]MOs involved in the transitions (H = HOMO and L= LUMO).

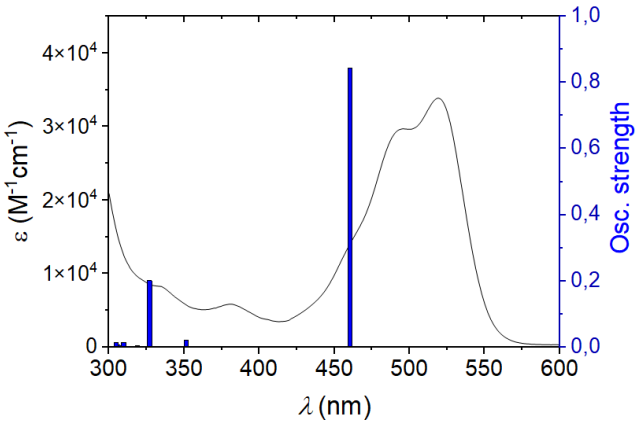

Fig. S26 Molar extinction coefficient spectra vs calculated oscillator strength and their contribution (blue bars, from Table S5) at different wavelengths for compound **4a**.

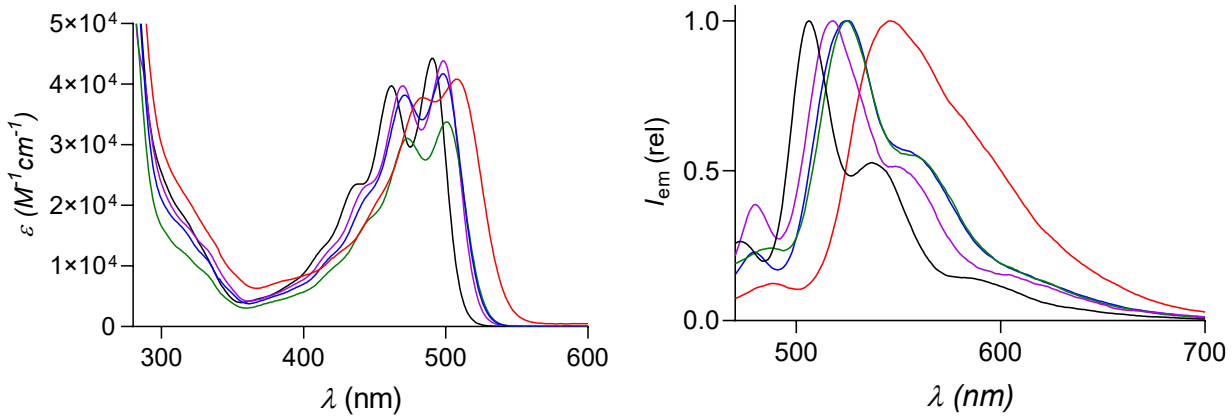

Fig. S27 Absorbance (left) and fluorescence emission (right) of **4b** (λ_{ex} = 460 nm, 5 µM) in DMSO (red), THF (blue), $CHCl_3$ (green), toluene (purple) and MCH (black).

Table S6 Selected transition properties of **4b** calculated at CAM-B3LYP/6-31+G(d,p) level of theory.

Wavelength (nm)[a]	**Osc. Strength**[b]	**Major contributions**[c]
442.9	0.836	H->L (98%)
354.0	0.084	H-3->L (19%), H-1->L (62%)
327.0	0.052	H-5->L (43%), H->L+1 (21%)
303.9	0.071	H-8->L (15%), H->L+1 (31%), H->L+5 (20%)
278.9	0.326	H-8->L (18%), H->L+1 (22%), H->L+5 (19%)
273.6	0.103	H-8->L (32%), H->L+5 (24%)
254.9	0.490	H-10->L (34%), H->L+6 (21%)

[a]Wavelength associated to the transition. [b]Oscillator strength. [c]MOs involved in the transitions (H = HOMO and L= LUMO).

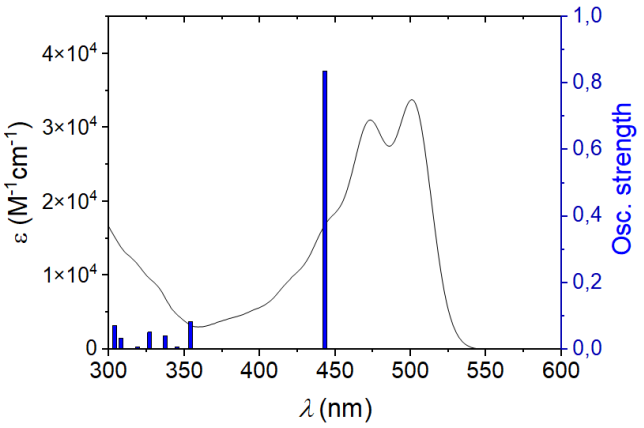

Fig. S28 Molar extinction coefficient spectra vs calculated oscillator strength and their contribution (blue bars, from Table S6) at different wavelengths for compound **4b**.

5.2.Fluorescence lifetimes

The fluorescence lifetimes (τ_F) of **1**, **2a**, **2b**, **3a**, **3b**, **4a** and **4b** were recorded in chloroform at 25 ºC (c = 5 µM) with a 475 nm laser as excitation source.

Table S7 Fluorescence lifetime data of compounds **1**, **2a**, **2b**, **3a**, **3b**, **4a** and **4b** in chloroform (10^{-5}M).

Compound	λ_{em} (nm) [a]	τ_F (ns) [b]	χ^2 [c]	k_r ($\times10^{-9}$ s^{-1}) [d]	k_{nr} ($\times10^{-9}$ s^{-1}) [e]
1	530	5.062	1.05	0.156	0.042
2a	555	5.56	0.97	0.140	0.040
2b[f]	535	4.37	1.22	0.009	0.220
3a	535	4.912	1.08	0.159	0.045
3b	520	4.604	1.06	0.187	0.030
4a	560	5.387	1.07	0.126	0.059
4b[f]	520	4.166	1.33	0.001	0.239

[a]Wavelength of emission for the photo-counting. [b]Calculated fluorescence lifetime. [c]Chi square error. [d]Radiative fluorescence emission relaxation constant. [e]Non-radiative fluorescence emission relaxation constant. [f] response had to be determine by tail fitting due to the low fluorescence quantum yield (see Fig. S31 and S35), higher error and lower reproducibility are associated to these compounds.

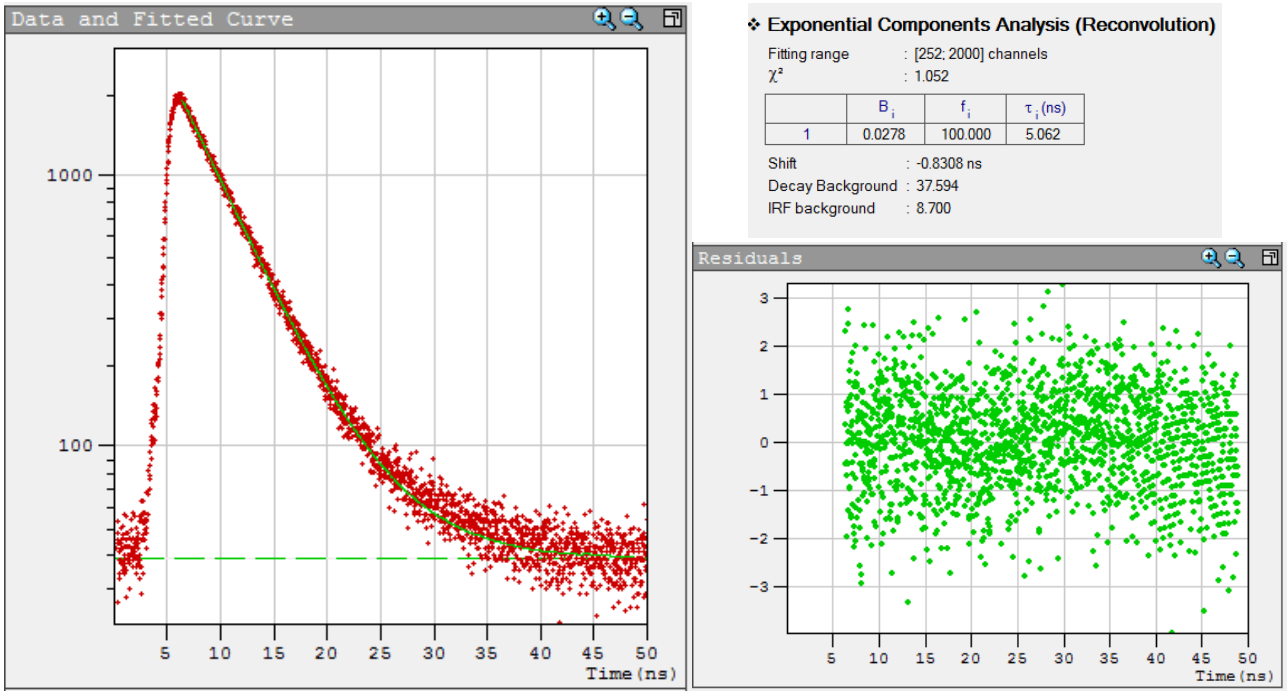

Fig. S29 Emission decay fitting (left) and calculated parameters and residuals (right) of **1**.

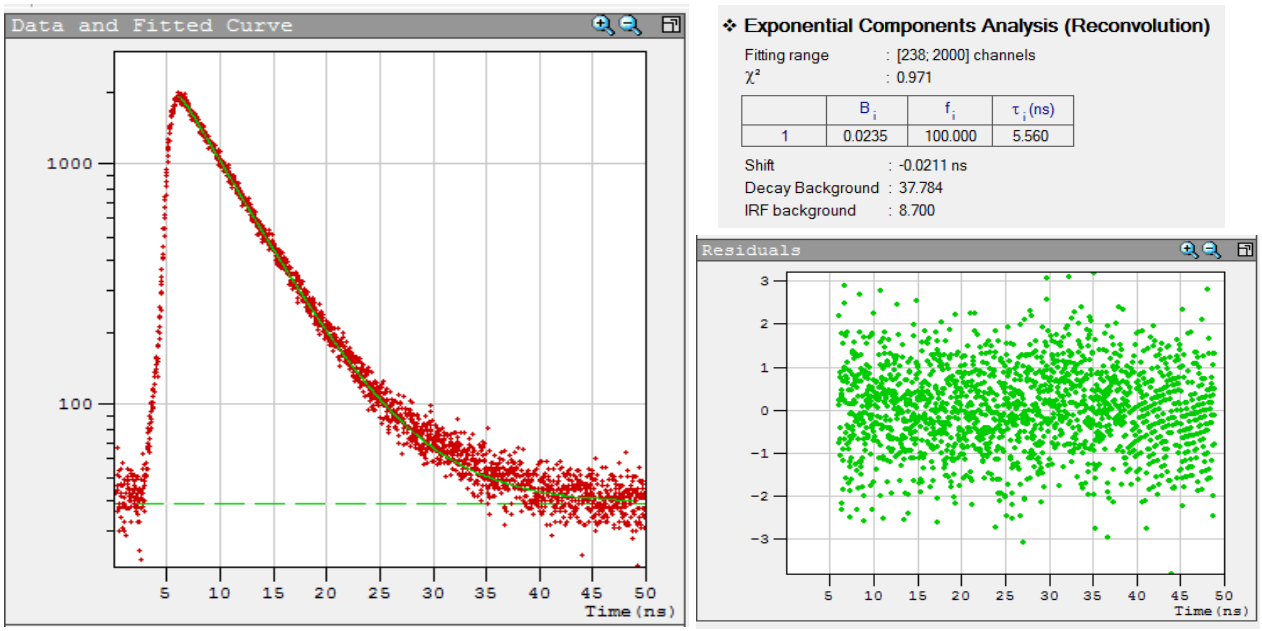

Fig. S30 Emission decay fitting (left) and calculated parameters and residuals (right) of **2a**.

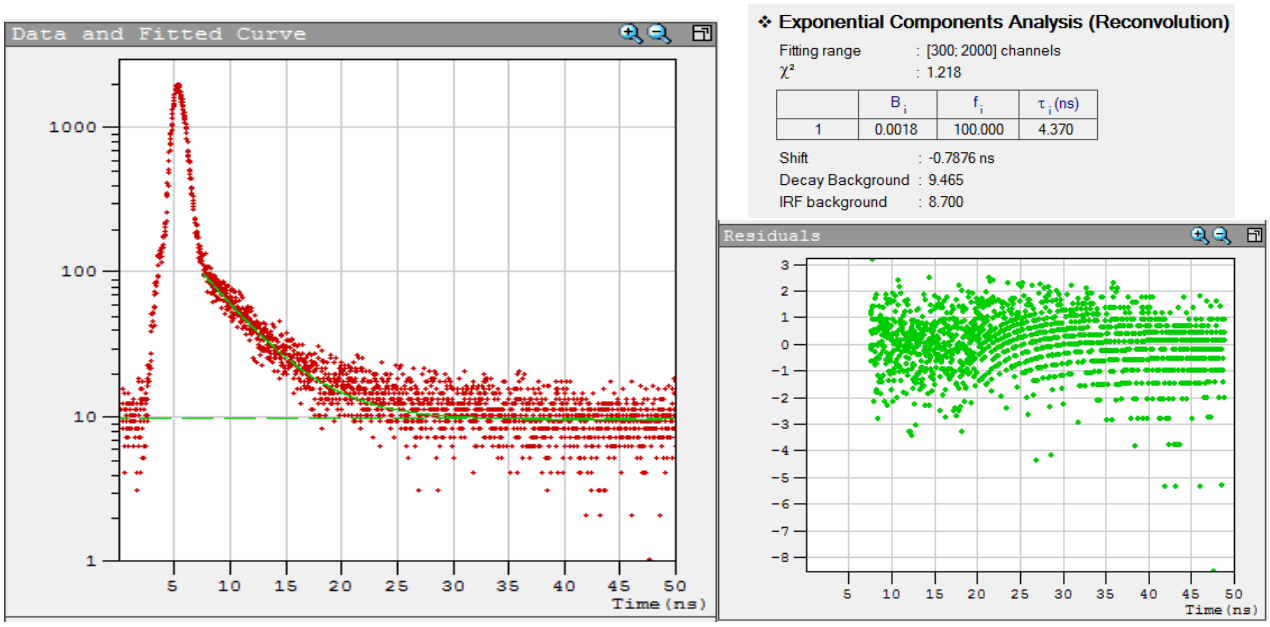

Fig. S31 Emission decay fitting (left), calculated parameters and residuals (right) of **2b**.3

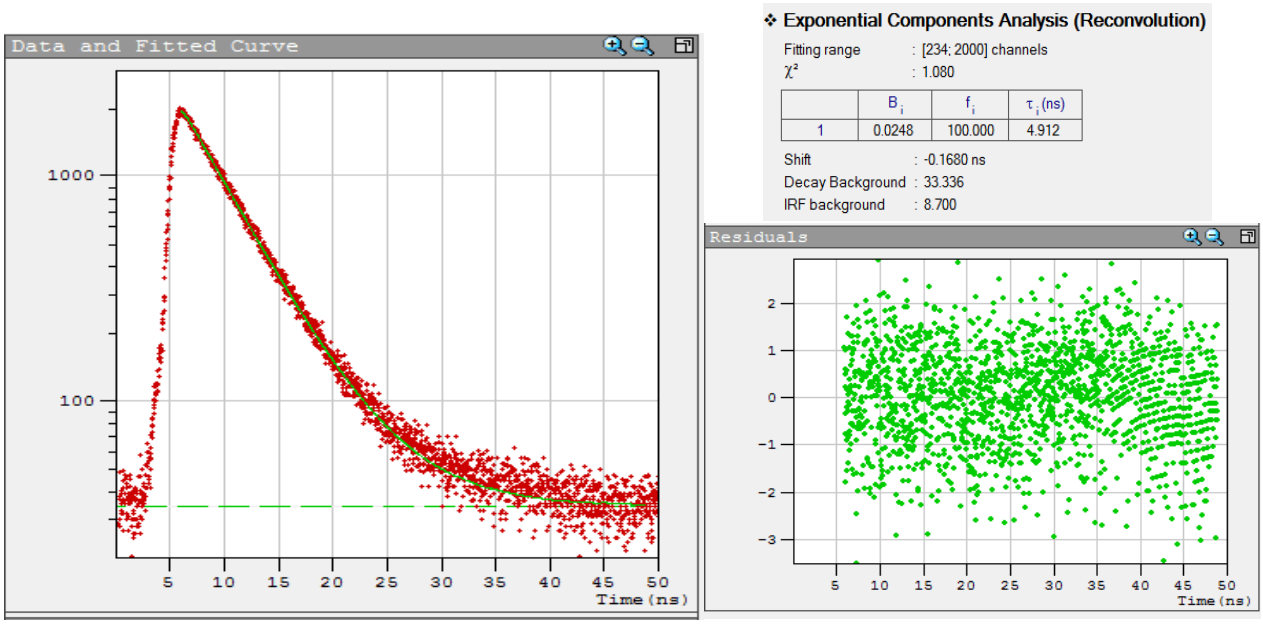

Fig. S32 Emission decay fitting (left), calculated parameters and residuals (right) of **3a**.

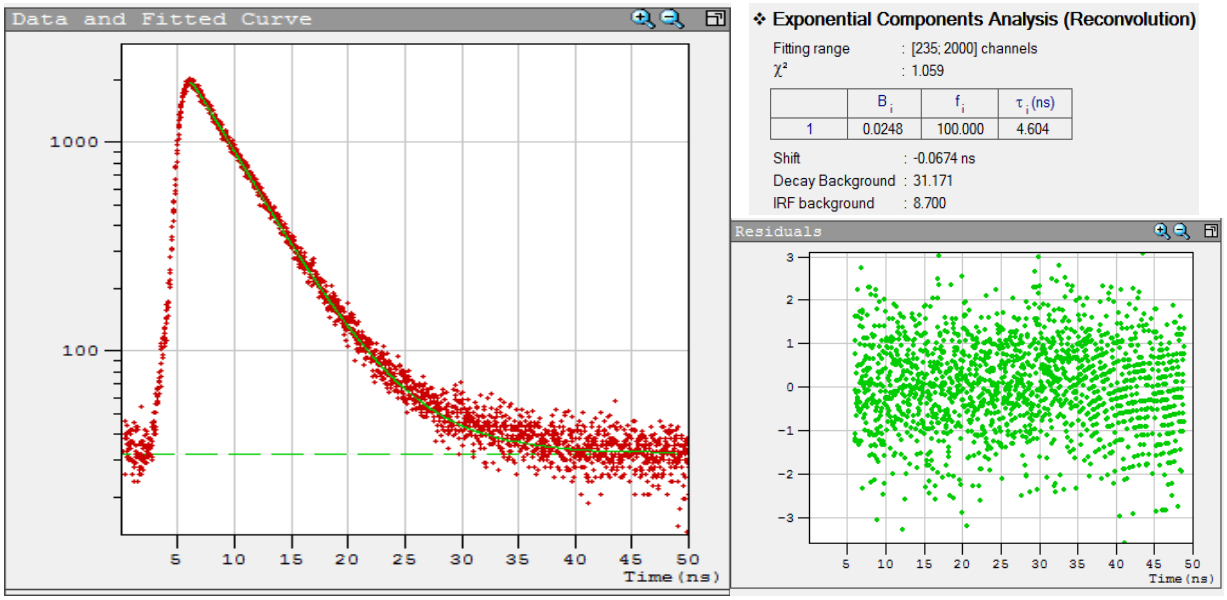

Fig. S33 Emission decay fitting (left), calculated parameters and residuals (right) of **3b**.

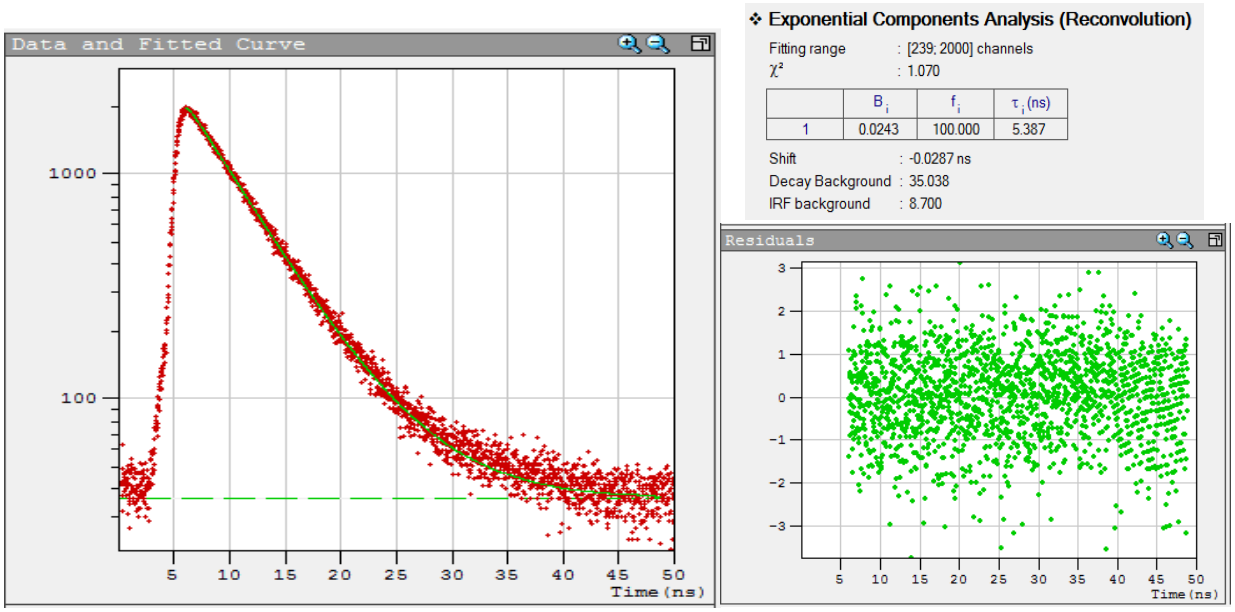

Fig. S34 Emission decay fitting (left), calculated parameters and residuals (right) of **4a**.

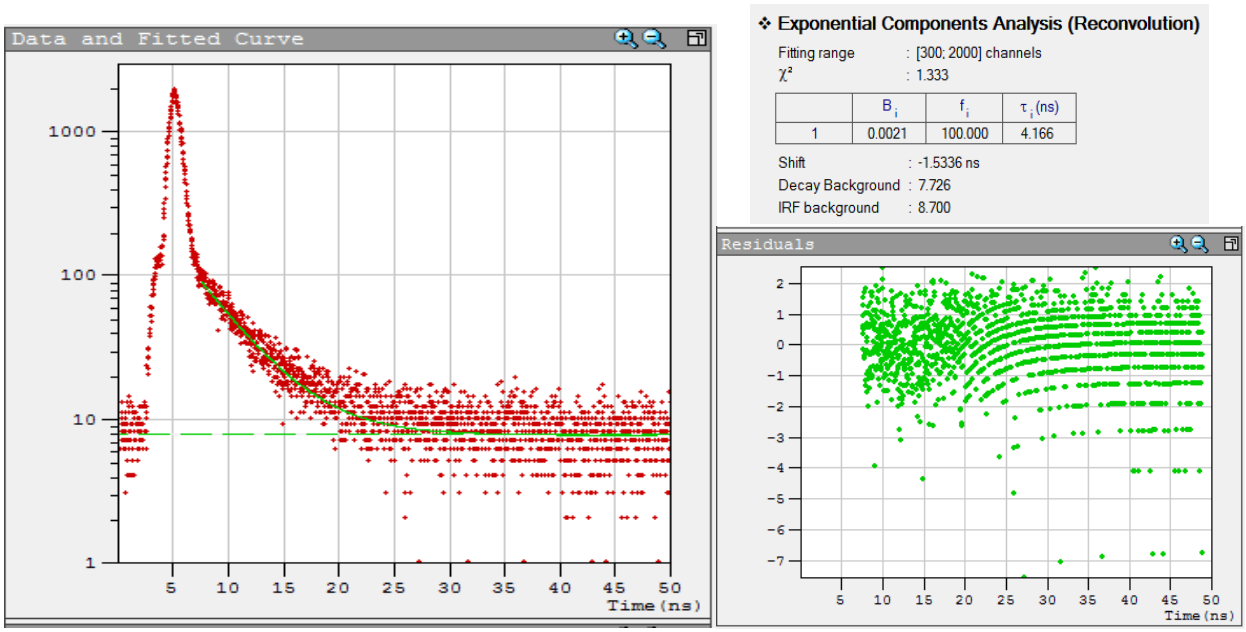

Fig. S35 Emission decay fitting (left), calculated parameters and residuals (right) of **4b**.

5.3. Aggregation studies in solution

PMI 1 was dissolved in $CHCl_3$ or THF and diluted in 2 mL of the corresponding mixture of solvents to evaluate aggregation.

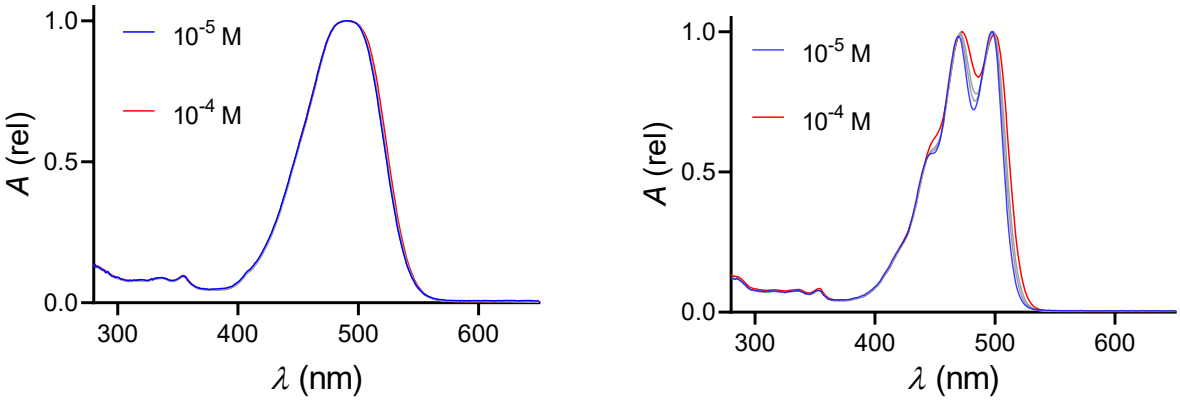

Fig. S36 Normalized absorption spectra of **1** in a) MeOH/$CHCl_3$ solution (99:1) and b) MCH/$CHCl_3$ (99:1) increasing concentration from 10^{-5} M to 10^{-4} M.

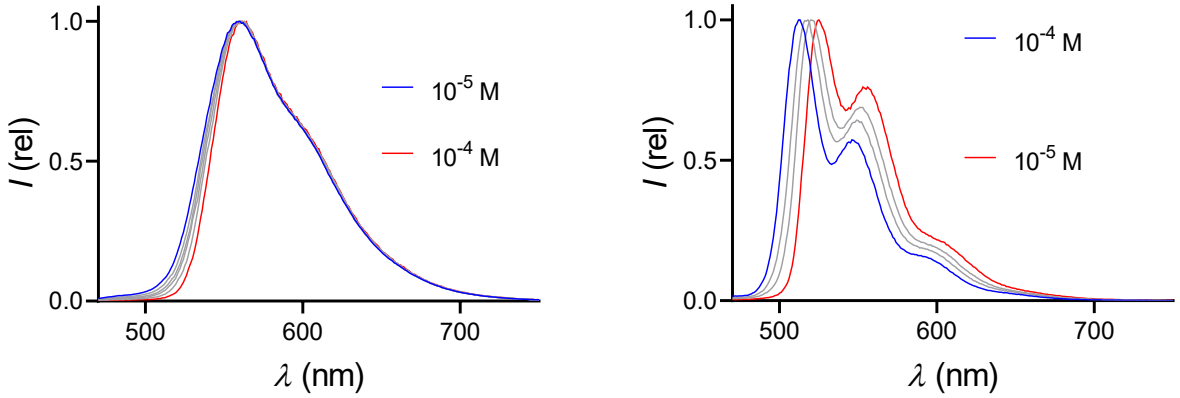

Fig. S37 Normalized fluorescence spectra (λ_{ex} = 460 nm) of **1** in a) MeOH/$CHCl_3$ solution (99:1) and b) MCH/$CHCl_3$ (99:1) increasing concentration from 10^{-5} M to 10^{-4} M.

Compounds **1**, **2a**, **2b**, **3a**, **3b**, **4a** and **4b** were measured by diluting a concentrated solution in THF (1 mM) in THF/Water mixtures from 100% to 1% THF (Water % = 99%, 90%, 80%, 70%, 60%, 50%, 40%, 30%, 20%, 10% and 0%).

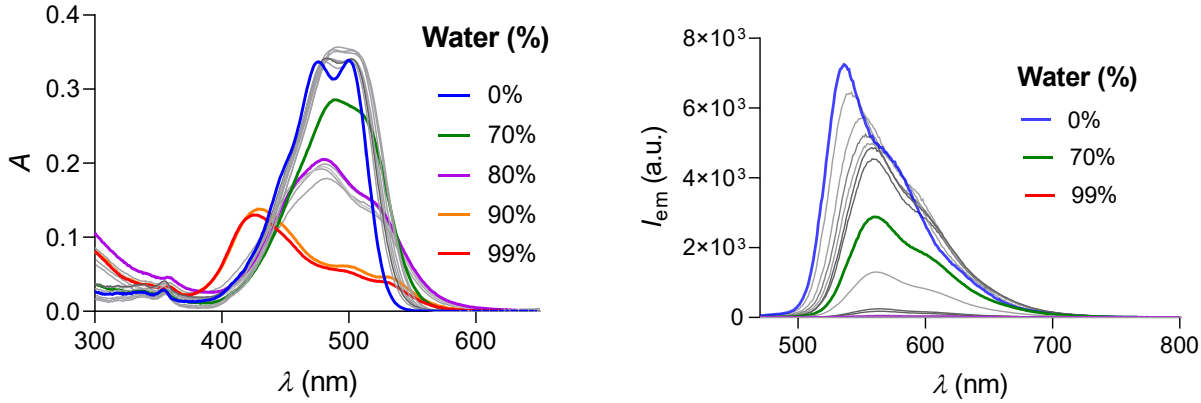

Fig. S38 Absorption spectra (left) and emission spectra (right) of **1** (10^{-5} M) after increasing the percentage of water from 0 to 99%.

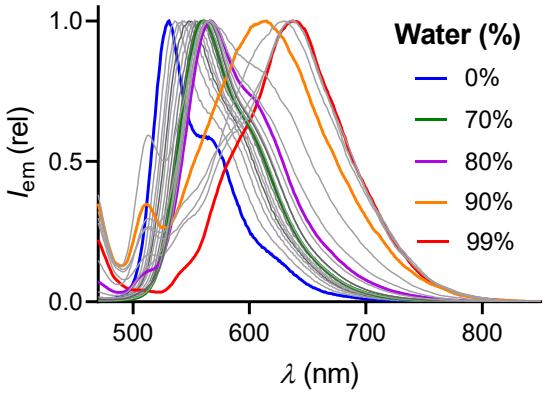

Fig. S39 Normalized fluorescence spectra (λ_{ex} = 460 nm) of **1** (10^{-5} M) after increasing the percentage of water from 0 to 99%.

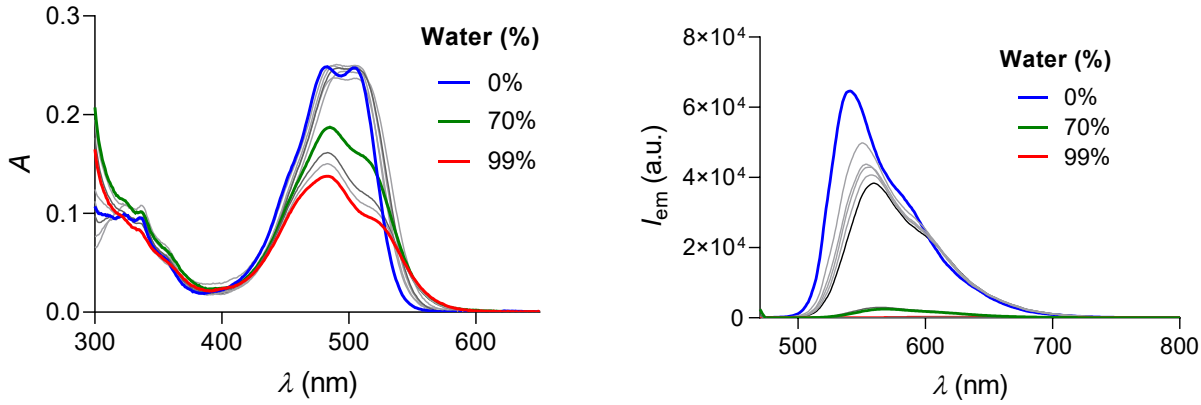

Fig. S40 Absorption spectra (left) and emission spectra (right) of **2a** (10^{-5} M) after increasing the percentage of water from 0 to 99%.

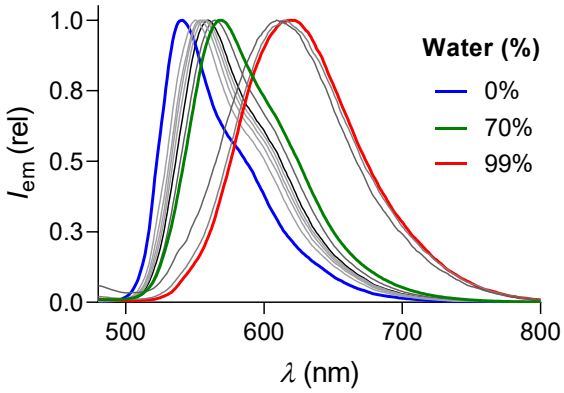

Fig. S41 Normalized fluorescence spectra (λ_{ex} = 460 nm) of **2a** (10^{-5} M) after increasing the percentage of water from 0 to 99%.

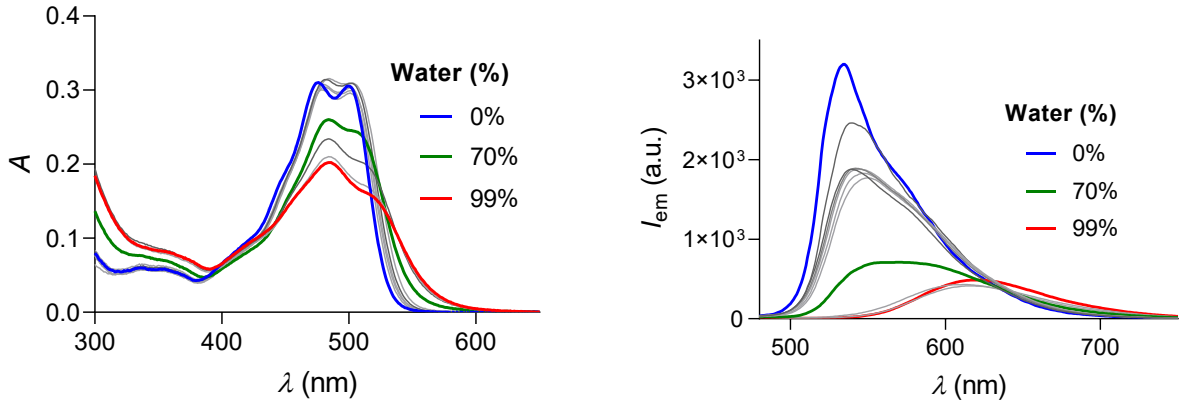

Fig. S42 Absorption spectra (left) and emission spectra (right) of **2b** (10^{-5} M) after increasing the percentage of water from 0 to 99%.

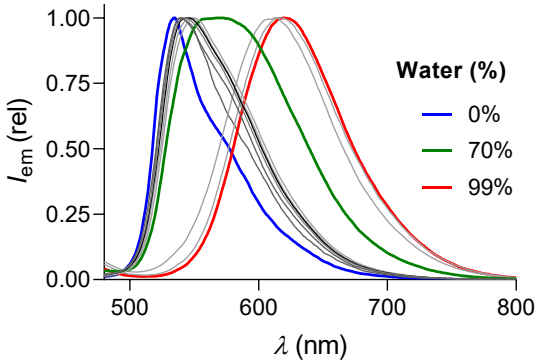

Fig. S43 Normalized fluorescence spectra (λ_{ex} = 460 nm) of **2b** (10^{-5} M) after increasing the percentage of water from 0 to 99%.

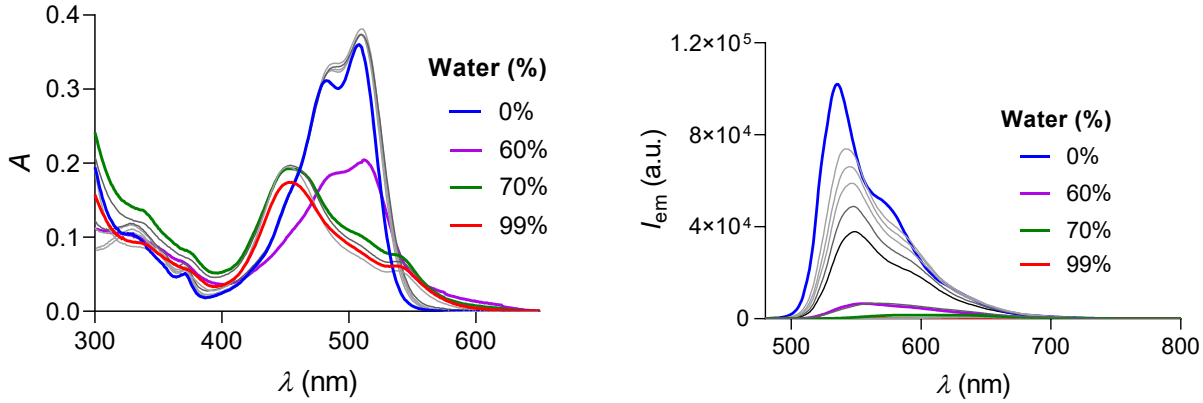

Fig. S44 Absorption spectra (left) and emission spectra (right) of **3a** (10^{-5} M) after increasing the percentage of water from 0 to 99%.

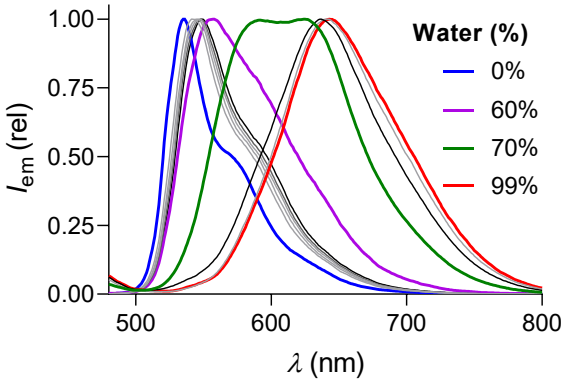

Fig. S45 Normalized fluorescence spectra (λ_{ex} = 460 nm) of **3a** (10^{-5} M) after increasing the percentage of water from 0 to 99%.

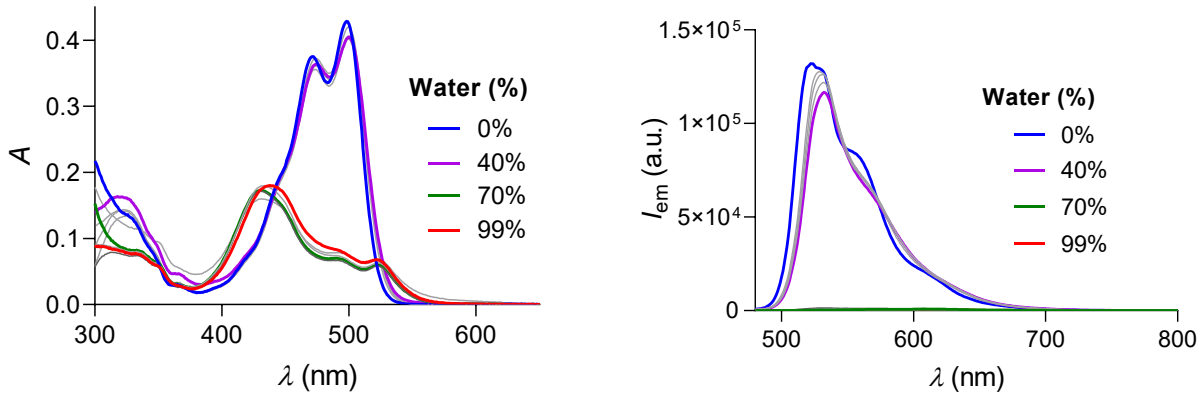

Fig. S46 Absorption spectra (left) and emission spectra (right) of **3b** (10^{-5} M) after increasing the percentage of water from 0 to 99%.

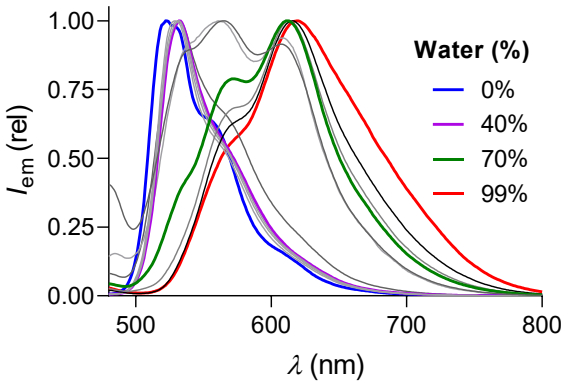

Fig. S47 Normalized fluorescence spectra (λ_{ex} = 460 nm) of **3b** (10^{-5} M) after increasing the percentage of water from 0 to 99%.

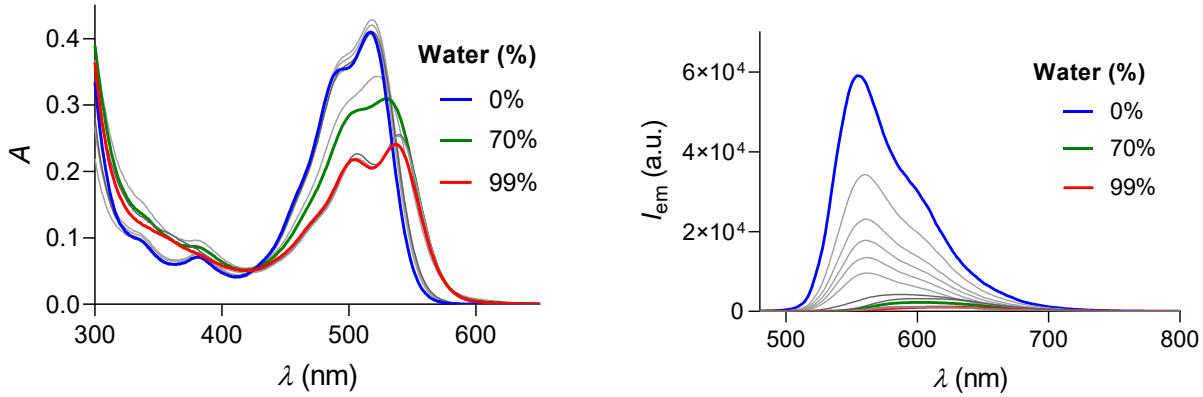

Fig. S48 Absorption spectra (left) and emission spectra (right) of **4a** (10^{-5} M) after increasing the percentage of water from 0 to 99%.

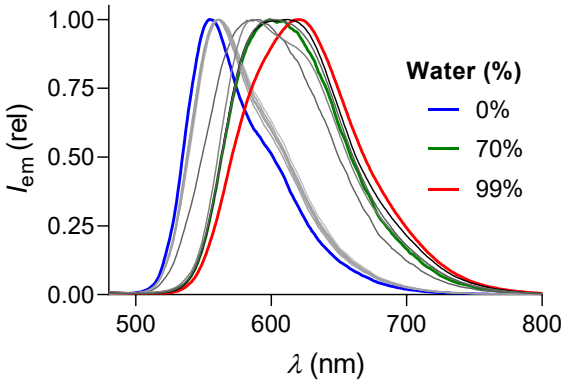

Fig. S49 Normalized fluorescence spectra (λ_{ex} = 460 nm) of **4a** (10^{-5} M) after increasing the percentage of water from 0 to 99%.

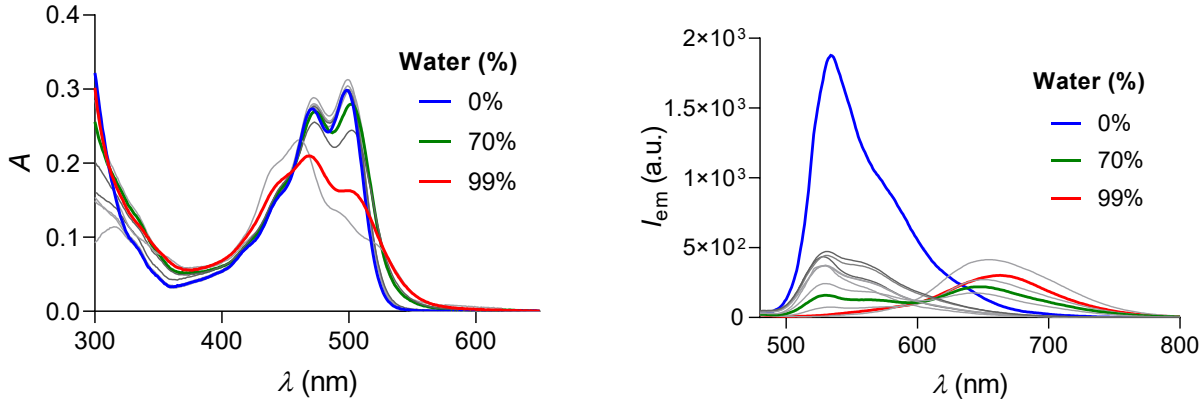

Fig. S50 Absorption spectra (left) and emission spectra (right) of **4b** (10^{-5} M) after increasing the percentage of water from 0 to 99%.

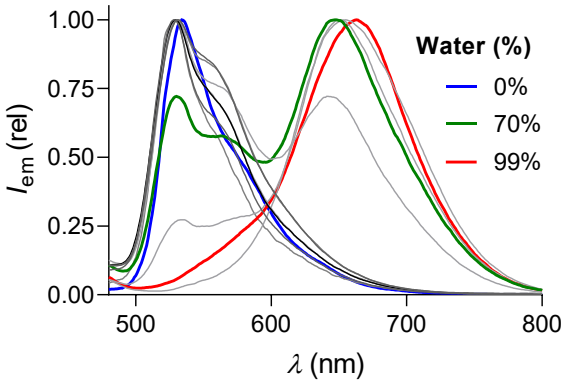

Fig. S51 Normalized fluorescence spectra (λ_{ex} = 460 nm) of **4b** (10^{-5} M) after increasing the percentage of water from 0 to 99%.

6. Solid state optical properties

Excitation and emission spectra were registered for solid samples of **1**, **2a**, **2b**, **3a**, **3b**, **4a** and **4b**. They were registered with the proper angle (97º) to avoid the scattering. Photoluminescence quantum yields were also calculated for the samples by direct acquisition in an integration sphere, by comparison with the background by using equation 3.

$$\eta_{QE} = I_S/(E_R - E_S) \qquad \text{(Eq. 3)}$$

where I_S represents the luminescence emission spectrum of the sample, E_R is the spectrum of the excitation light from the empty integrated sphere (without the sample), and E_S is the excitation spectrum for exciting the sample.

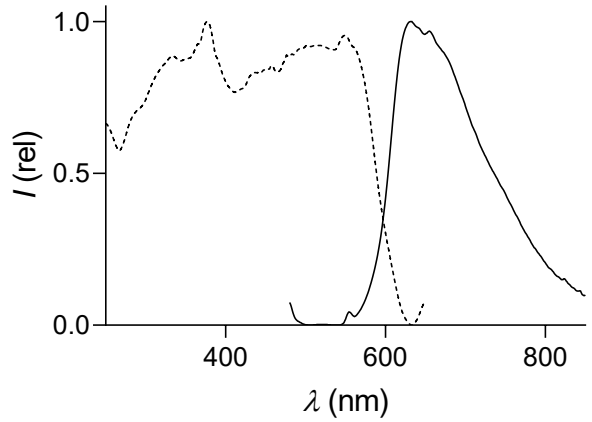

Fig. S52 Excitation (dashed) and fluorescence emission (plain) spectra of **1** (λ_{ex} = 450 nm, λ_{em} = 675 nm) powder.

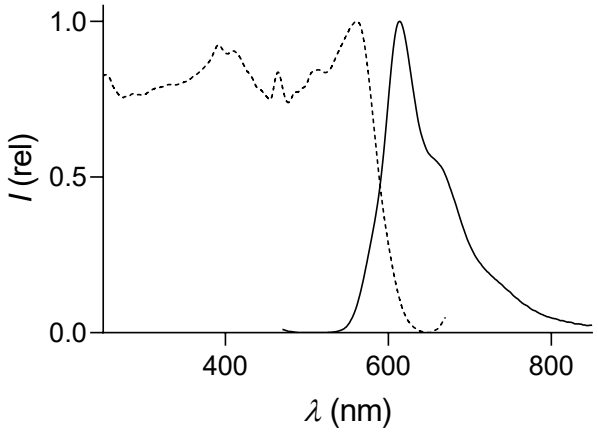

Fig. S53 Excitation (dashed) and fluorescence emission (plain) spectra of **2a** (λ_{ex} = 450 nm, λ_{em} = 700 nm) powder.

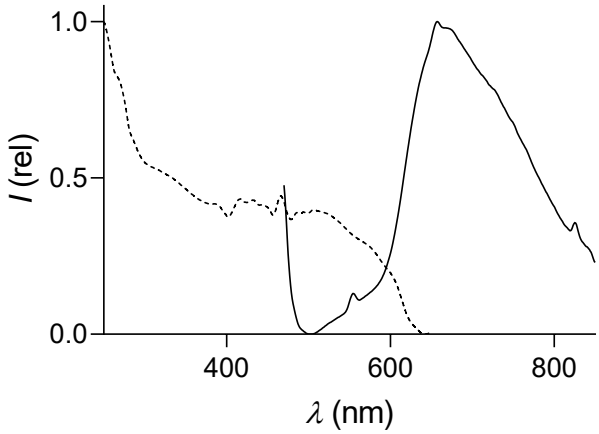

Fig. S54 Excitation (dashed) and fluorescence emission (plain) spectra of **2b** (λ_{ex} = 450 nm, λ_{em} = 700 nm) powder.

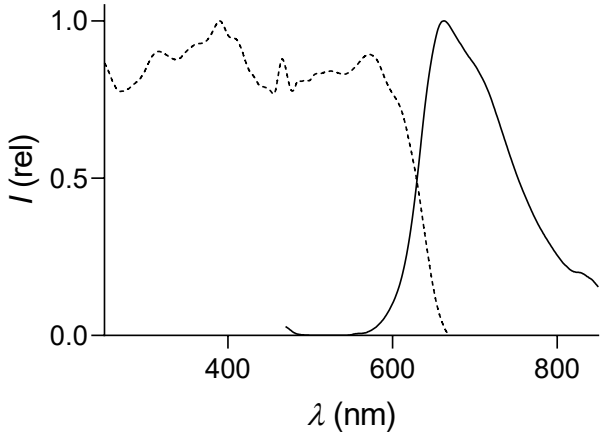

Fig. S55 Excitation (dashed) and fluorescence emission (plain) spectra of **3a** (λ_{ex} = 450 nm, λ_{em} = 700 nm) powder.

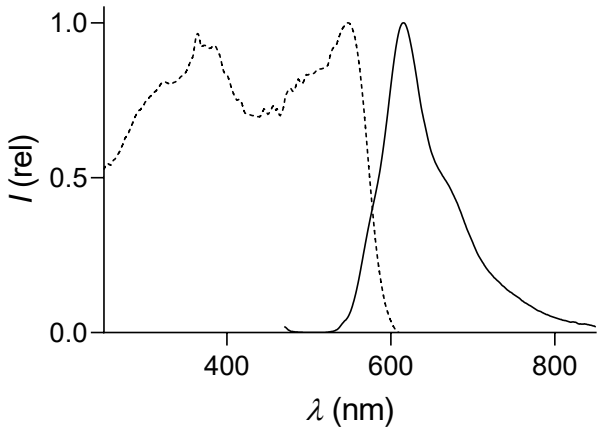

Fig. S56 Excitation (dashed) and fluorescence emission (plain) spectra of **3b** (λ_{ex} = 440 nm, λ_{em} = 650 nm) powder.

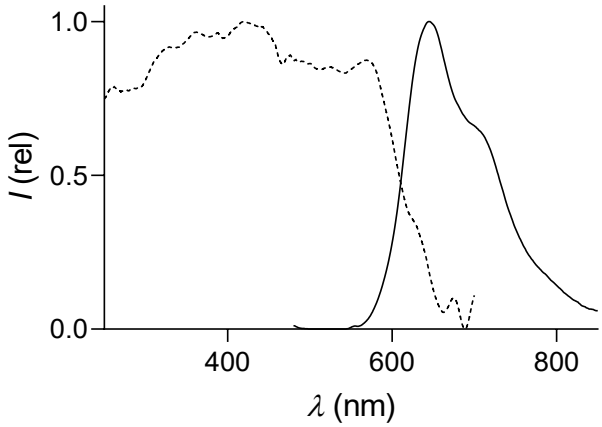

Fig. S57 Excitation (dashed) and fluorescence emission (plain) spectra of **4a** (λ_{ex} = 450 nm, λ_{em} = 730 nm) powder.

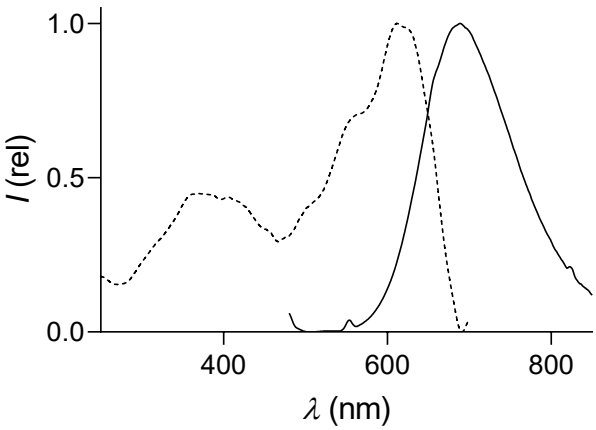

Fig. S58 Excitation (dashed) and fluorescence emission (plain) spectra of **4b** (λ_{ex} = 450 nm, λ_{em} = 725 nm) powder.

7. Single crystal X-ray diffraction

A suitable crystal was selected and placed on a MiTeGen micromount on a XtaLAB Synergy R, HyPix-Arc 100 diffractometer. The crystal was kept at a steady T = 250 K for **4a** and 150 K for **4b** during data collection. The structure was solved with the ShelXT 2018/2 (Sheldrick, 2018) structure solution program using the Intrinsic Phasing solution method and by using **Olex2**[S5] as the graphical interface. The model was refined with version 2018/3 of ShelXL 2018/3 (Sheldrick, 2015) using Least Squares minimization.

7.1.Crystal structure of compound 2a

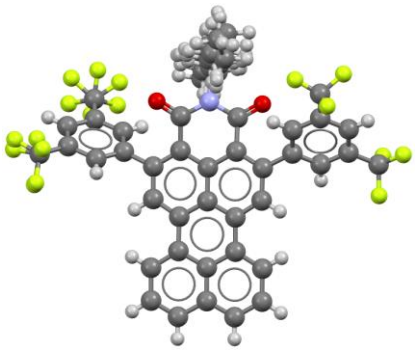

Fig. S59 Representation of the crystal structure resolved for compound **2a,** including rotational freedom in the alkyl chain and the -CF_3 groups.

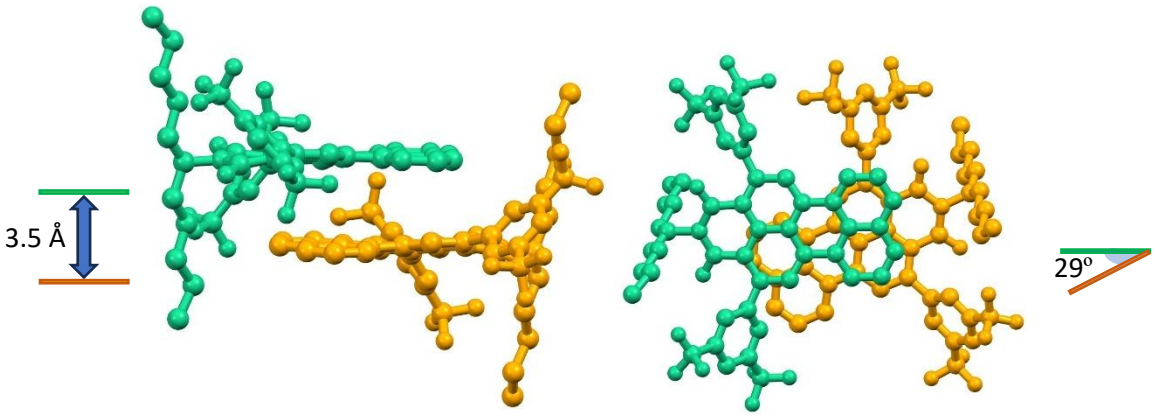

Fig. S60 X-Ray resolved packing structure of two stacked molecules of compound **2a** from two perpendicular points of view, indicating interplanar distances and stacking angle.

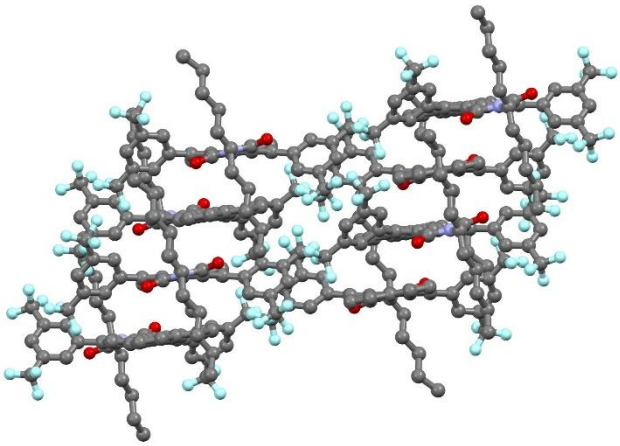

Fig. S61 Single crystal X-ray diffraction structure of **2a**, perpendicular view to the stacking direction, showing homogeneous distance between layers.

Crystal Data. $C_{49}H_{37}F_{12}NO_2$, *Mr* = 1172.08, monoclinic, *P*21/*n* (No. 14), a = 8.0976(3) Å, b = 36.4931(14) Å, c = 28.4083(8) Å, $\alpha = 94.970(3)°$, $\beta = \gamma = 90°$, *V* = 8363.3(5) Å3, *T* = 200.00(10) K, *Z* = 8, *Z'* = 2, μ(Cu K_α) = 1.070, 63448 reflections measured, 15281 unique (R_{int} = 0.0991) which were used in all calculations. The final *wR2* was 0.2763 (all data) and R_1 was 0.0831 (I > 2(I)).

Table S8. Crystalline data of compound **2a**.

Formula	$C_{49}H_{37}F_{12}NO_2$	**Z'**	2
Dcalc./ g·cm^{-3}	1.429	**Wavelength/Å**	1.54184
μ/mm^{-1}	1.070	**Radiation type**	Cu Ka
Formula weight	899.79	**Θ_{min}/°**	1.975

Colour	metallic orange	Θ_{max}/°	68.860
Shape	needle	**Measured refl.**	63448
Size/mm³	0.21×0.02×0.02	**Independent refl.**	15281
T/K	200.00(10)	**Reflections with I > 2(I)**	7098
Crystal system	monoclinic	R_{int}	0.0991
Space group	$P2_1/n$	**Parameters**	1456
***a*/Å**	8.0976(3)	**Restraints**	1484
***b*/Å**	36.4931(14)	**Largest peak**	0.409
***c*/Å**	28.4083(8)	**Deepest hole**	-0.313
***α*/°**	90	**GooF**	1.003
***β*/°**	94.970(3)	wR_2 **(all data)**	0.2763
***γ*/°**	90	wR_2	0.2212
V/Å³	8363.3(5)	R_1 **(all data)**	0.1663
Z	8	R_1	0.0831

Experimental Extended. A metallic orange needle-shaped crystal with dimensions 0.21×0.02×0.02 mm^3 was placed on a MiTeGen micromount. Data were collected using an XtaLAB Synergy R, HyPix-Arc 100 diffractometer operating at T = 200.00(10) K. Data were measured using ω scans of 0.5° per frame for 20.0/50.0 s using Cu K_α radiation. The diffraction pattern was indexed and the total number of runs and images was based on the strategy calculation from the program CrysAlisPro (Rigaku). The maximum resolution that was achieved was Θ = 68.860° (0.83 Å). The unit cell was refined using CrysAlisPro (Rigaku, V1.171.44.116a, 2025) on 10383 reflections, 16% of the observed reflections.

Data reduction, scaling and absorption corrections were performed using CrysAlisPro (Rigaku, V1.171.44.116a, 2025). The final completeness is 99.80 % out to 68.860° in Θ. A cylinder absorption correction was performed using CrysAlisPro 1.171.44.116a (Rigaku Oxford Diffraction, 2025) Numerical absorption correction based on gaussian integration over a multifaceted crystal model. Empirical absorption correction using spherical harmonics, implemented in SCALE3 ABSPACK scaling algorithm. The absorption coefficient μ of this material is 1.070 mm^{-1} at this wavelength (λ = 1.542 Å) and the minimum and maximum transmissions are 0.793 and 1.000.

The structure was solved and the space group $P2_1/n$ (# 14) determined by the ShelXT using Intrinsic Phasing and refined by Least Squares. All non-hydrogen atoms were refined anisotropically. Hydrogen atom positions were calculated geometrically and refined using the riding model. Hydrogen atom positions were calculated geometrically and refined using the riding model.

7.2.Crystal structure of compound 4a

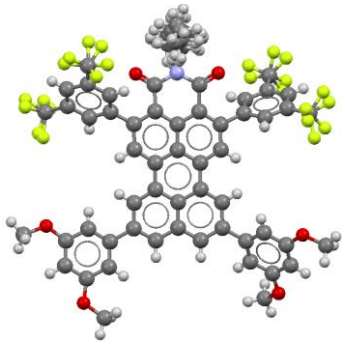

Fig. S62 Representation of the crystal structure resolved for compound **4a** including the possible rotational freedom in the alkyl chain and the -CF_3 groups.

Crystal Data. $C_{65}H_{53}F_{12}NO_6$, *Mr* = 1172.08, triclinic, *P*-1 (No. 2), a = 8.6217(2) Å, b = 18.0300(4) Å, c = 18.8439(3) Å, α = 106.197(2)°, β = 92.734(2)°, γ = 96.796(2)°, *V* = 2783.21(10) Å^3, *T* = 250.00(10) K, *Z* = 2, *Z'* = 1, μ(Cu K_α) = 0.995, 33941 reflections measured, 10206 unique (R_{int} = 0.0350) which were used in all calculations. The final wR_2 was 0.2558 (all data) and R_1 was 0.0822 (I > 2(I)).

Table S9. Crystalline data of compound **4a**.

Formula	$C_{65}H_{53}F_{12}NO_6$	**Z'**	1
Dcalc./ g·cm^{-3}	1.399	**Wavelength/Å**	1.54184
μ/mm^{-1}	0.995	**Radiation type**	Cu Ka
Formula weight	1172.08	**Θ_{min}/°**	2.45
Colour	clear intense red	**Θ_{max}/°**	68.332
Shape	needle	**Measured refl.**	33941
Size/mm^3	0.19×0.05×0.04	**Independent refl.**	10206
T/K	250.00(10)	**Reflections with I > 2(I)**	7546
Crystal system	triclinic	**R_{int}**	0.035
Space group	P-1	**Parameters**	845
***a*/Å**	8.6217(2)	**Restraints**	960
***b*/Å**	18.0300(4)	**Largest peak**	0.623
***c*/Å**	18.8439(3)	**Deepest hole**	-0.656
α/°	106.197(2)	**GooF**	1.052
β/°	92.734(2)	**wR_2 (all data)**	0.2558
γ/°	96.796(2)	**wR_2**	0.237
V/Å^3	2783.21(10)	**R_1 (all data)**	0.1023
Z	2	**R_1**	0.0822

Experimental Extended. A clear intense red needle-shaped crystal with dimensions 0.19×0.05×0.04 mm^3 was placed on a MiTeGen micromount. Data were collected using an XtaLAB Synergy R, HyPix-Arc 100 diffractometer operating at T = 250.00(10) K. Data were measured using ω scans of 0.5° per frame for 0.3 s using CuK_α radiation. The diffraction pattern was indexed and the total number of runs and images was based on the strategy calculation from the program CrysAlisPro (Rigaku) The maximum resolution that was achieved was Θ = 68.332° (0.83 Å). The unit cell was refined using CrysAlisPro (Rigaku, V1.171.43.144a, 2024) on 13119 reflections, 39% of the observed reflections.

Data reduction, scaling and absorption corrections were performed using CrysAlisPro (Rigaku, V1.171.43.144a, 2024). The final completeness is 99.90% out to 68.332° in Θ. Numerical absorption correction based on gaussian integration over a multifaceted crystal. Empirical absorption correction using spherical harmonics was implemented in SCALE3 ABSPACK scaling algorithm. The absorption coefficient μ of this material is 0.995 mm^{-1} at this wavelength (λ = 1.542 Å) and the minimum and maximum transmissions were 0.747 and 1.000.

The structure was solved and the space group P-1 determined by the ShelXT 2018/2 program using Intrinsic Phasing and refined by Least Squares. All non-hydrogen atoms were refined anisotropically. Hydrogen atom positions were calculated geometrically and refined using the riding model.

7.3.Crystal structure of compound 4b

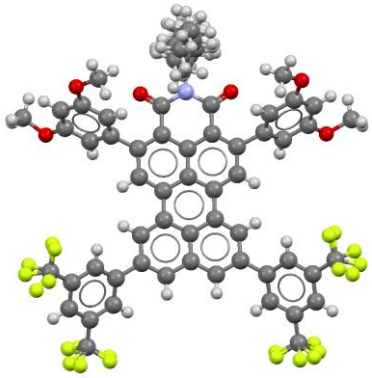

Fig. S63 Representation of the crystal structure resolved for compound **4b** including the possible rotational freedom of the alkyl chain and the -CF_3 groups.

Crystal Data. $C_{64.5}H_{65.75}F_{12}NO_{13.5}$, *Mr* = 1298.93, monoclinic, *P*21/*c* (No. 14), a = 17.5665(16) Å, b = 21.8949(10) Å, c = 17.2854(15) Å, α = 109.319(10)°, $\beta = \gamma = 90°$, *V* = 6273.9(9) Å^3, *T* = 150.00(10) K, *Z* = 4, *Z'* = 1, μ (CuK_α) = 1.026, 53205 reflections measured, 11042 unique (*Rint* = 0.1018) which were used in all calculations. The final wR_2 was 0.3935 (all data) and *R1* was 0.1197 (I > 2(I)).

Table S10. Crystalline data of compound **4b**.

Formula	$C_{64.5}H_{65.75}F_{12}NO_{13.5}$	**Z'**	1
Dcalc./ g·cm^{-3}	1.375	**Wavelength/Å**	1.54184
μ/mm^{-1}	1.026	**Radiation type**	CuK_α
Formula weight	1298.93	**Θ_{min}/°**	2.665
Colour	clear intense orange	**Θ_{max}/°**	66.587
Shape	plate	**Measured refl.**	53205
Size/mm^3	0.14×0.13×0.01	**Independent refl.**	11042
T/K	150.00(10)	**Reflections with I > 2(I)**	5797
Crystal system	monoclinic	**R_{int}**	0.1018
Space group	$P2_1/c$	**Parameters**	875
***a*/Å**	17.5665(16)	**Restraints**	966
***b*/Å**	21.8949(10)	**Largest peak**	0.376
***c*/Å**	17.2854(15)	**Deepest hole**	-0.601
α/°	90	**GooF**	1.087
β/°	109.319 (10)	**wR_2 (all data)**	0.3935
γ/°	90	**wR_2**	0.3452
V/Å^3	6273.9(9)	**R_1 (all data)**	0.01693
Z	4	**R_1**	0.1197

Experimental Extended. A clear intense orange plate-shaped crystal with dimensions 0.14×0.13×0.01 mm^3 was placed on a MiTeGen micromount. Data were collected using an XtaLAB Synergy R, HyPix-Arc 100 diffractometer operating at *T* = 150.00(10) K.

Data were measured using Θ scans of 0.5° per frame for 0.8/11.2 s using CuK_α radiation. The diffraction pattern was indexed and the total number of runs and images was based on the strategy calculation from the program CrysAlisPro (Rigaku) The maximum resolution that was achieved was Θ = 66.587° (0.84 Å) and the unit cell was refined on 7758 reflections, 15% of the observed reflections.

Data reduction, scaling and absorption corrections were performed using CrysAlisPro (Rigaku, V1.171.43.144a, 2024). The final completeness was 99.70 % out to 66.587° in Θ. A gaussian absorption correction was performed using CrysAlisPro 1.171.43.144a (Rigaku Oxford Diffraction, 2024). Numerical absorption correction was performed based on gaussian integration over a

multifaceted crystal model. Empirical absorption correction using spherical harmonics was implemented in SCALE3 ABSPACK scaling algorithm. The absorption coefficient μ of this material was 1.026 mm^{-1} at this wavelength (λ = 1.542 Å) and the minimum and maximum transmissions were 0.845 and 1.000.

The structure was solved and the space group $P2_{1/c}$ determined by the ShelXT 2018/2 program, using Intrinsic Phasing and refined by Least Squares. All non-hydrogen atoms were refined anisotropically. Hydrogen atom positions were calculated geometrically and refined using the riding model. Hydrogen atom positions were calculated geometrically and refined using the riding model.

The structure shows disorder in the -CF_3 groups as well as in the aliphatic chains. They have been modeled in two sets of alternative positions (with relative occupations shown in Table S10). In the case of the C32 and C33 atoms, the disorder is so pronounced that only 75% of the expected electron density for carbons can be located. There are also molecules of very disordered solvent in the interstices that could not be included in the model, a correction has been applied by means of a solvent mask (SQUEEZE, Table S11).

Table S11. Atomic Occupancies for all atoms that are not fully occupied in **4b**.

Atom	Occupancy	Atom	Occupancy	Atom	Occupancy	Atom	Occupancy
F1A	0.491(7)	H27A	0.459(13)	F1B	0.509(7)	H27C	0.541(13)
F2A	0.491(7)	H27B	0.459(13)	F2B	0.509(7)	H27D	0.541(13)
F3A	0.491(7)	C28A	0.459(13)	F3B	0.509(7)	C28B	0.541(13)
F4A	0.298(11)	H28A	0.459(13)	F4B	0.702(11)	H28D	0.541(13)
F5A	0.298(11)	H28B	0.459(13)	F5B	0.702(11)	H28E	0.541(13)
F6A	0.298(11)	H28C	0.459(13)	F6B	0.702(11)	H28F	0.541(13)
F7A	0.490(9)	C29A	0.48(2)	F7B	0.510(9)	C29B	0.52(2)
F8A	0.490(9)	H29A	0.48(2)	F8B	0.510(9)	H29C	0.52(2)
F9A	0.490(9)	H29B	0.48(2)	F9B	0.510(9)	H29D	0.52(2)
F10A	0.42(3)	C30A	0.48(2)	F10B	0.58(3)	C30B	0.52(2)
F11A	0.42(3)	H30A	0.48(2)	F11B	0.58(3)	H30C	0.52(2)
F12A	0.42(3)	H30B	0.48(2)	F12B	0.58(3)	H30D	0.52(2)
C24A	0.459(13)	C31A	0.48(2)	C24B	0.541(13)	C31B	0.52(2)
H24A	0.459(13)	H31A	0.48(2)	H24C	0.541(13)	H31C	0.52(2)
H24B	0.459(13)	H31B	0.48(2)	H24D	0.541(13)	H31D	0.52(2)
C25A	0.459(13)	C32A	0.363(17)	C25B	0.541(13)	C32B	0.387(17)
H25A	0.459(13)	H32A	0.363(17)	H25C	0.541(13)	H32C	0.387(17)
H25B	0.459(13)	H32B	0.363(17)	H25D	0.541(13)	H32D	0.387(17)
C26A	0.459(13)	C33A	0.363(17)	C26B	0.541(13)	C33B	0.387(17)
H26A	0.459(13)	H33A	0.363(17)	H26C	0.541(13)	H33D	0.387(17)
H26B	0.459(13)	H33B	0.363(17)	H26D	0.541(13)	H33E	0.387(17)
C27A	0.459(13)	H33C	0.363(17)	C27B	0.541(13)	H33F	0.387(17)

Table S12. Solvent masking (Olex2) information for **4b**.

Number	x	y	z	V	e	Content
1	0	0	0	506.7	147.4	15H2O
2	0	0.5	0.5	506.7	147.4	15H2O

8. NMR characterization

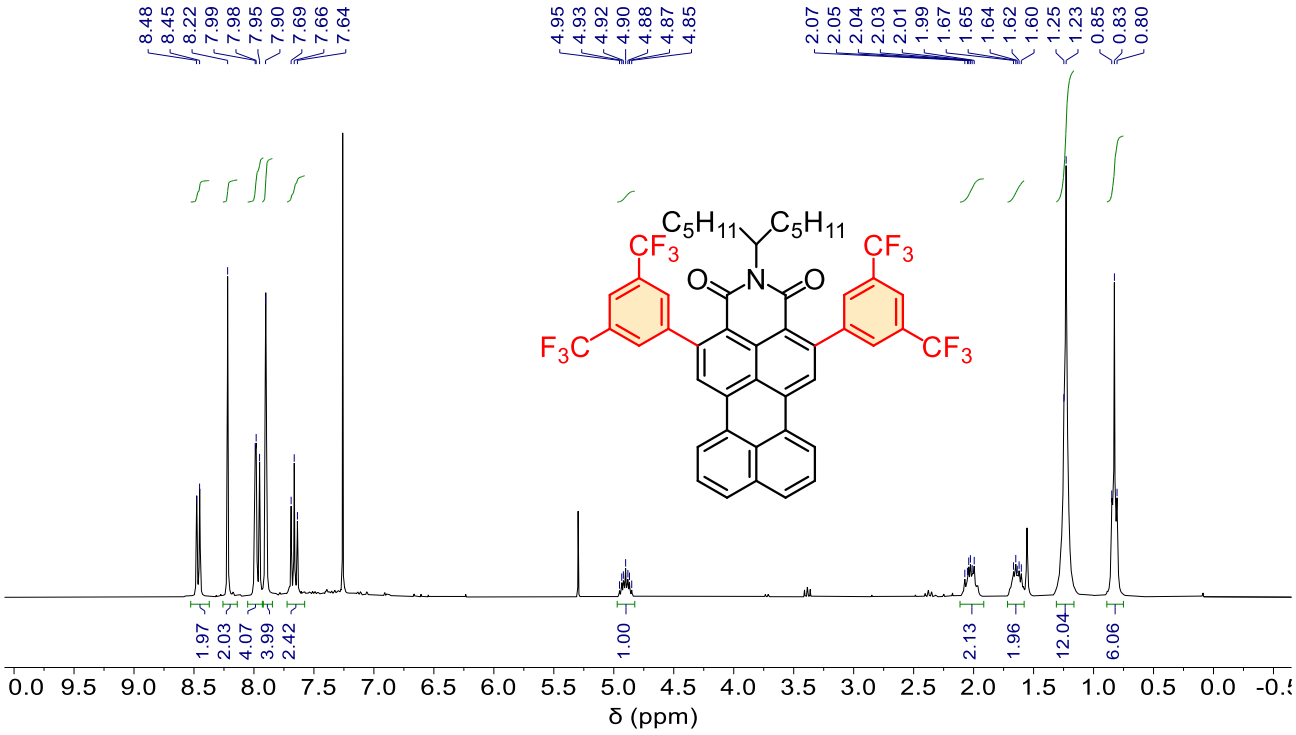

Fig. S64 ^{1}H NMR (300 MHz) spectrum of compound **2a** in $CDCl_3$.

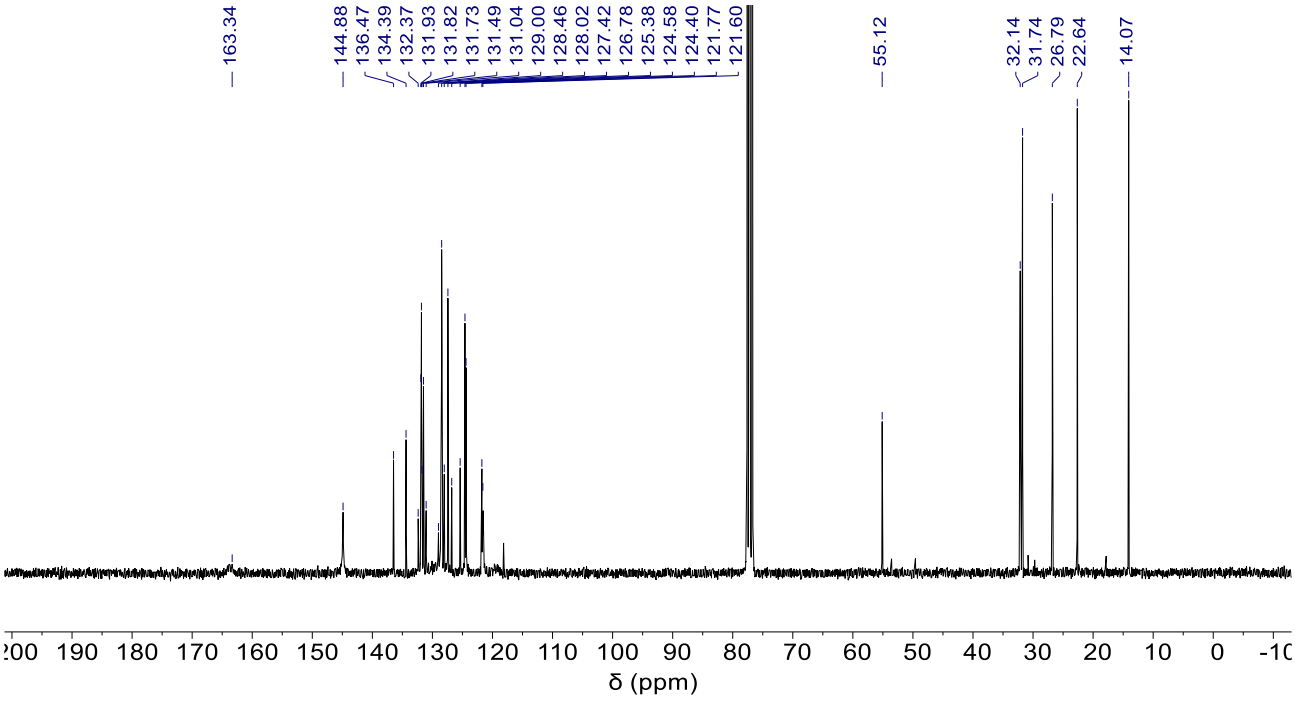

Fig. S65 ^{13}C NMR (75 MHz) spectrum of compound **2a** in $CDCl_3$.

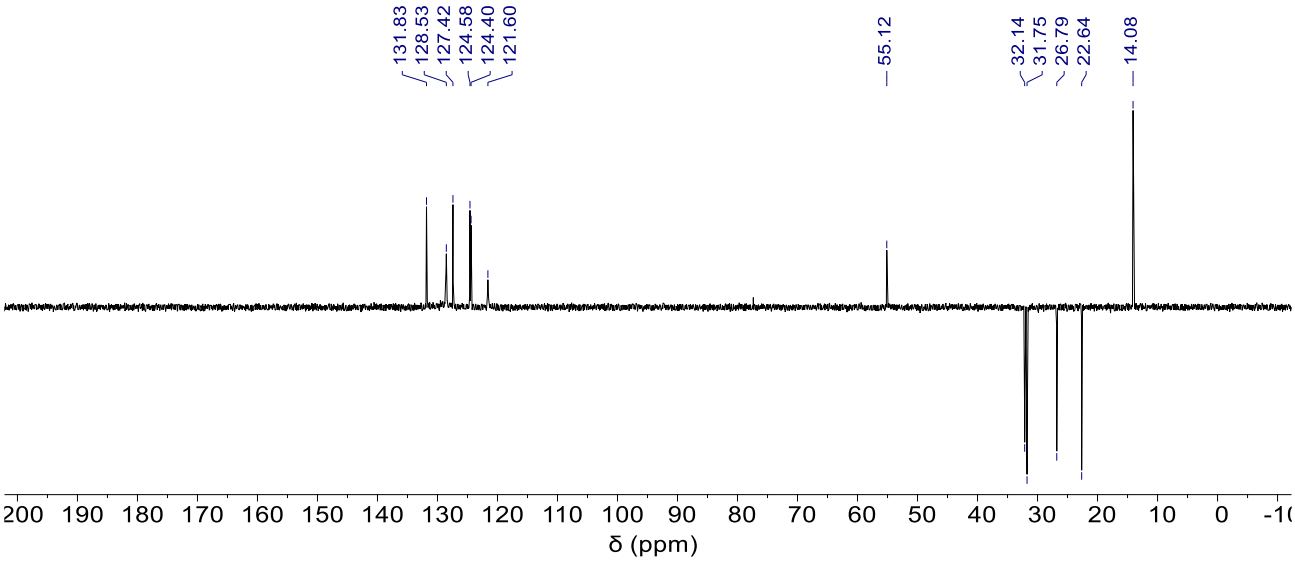

Fig. S66 DEPT NMR (75 MHz) spectrum of compound **2a** in $CDCl_3$.

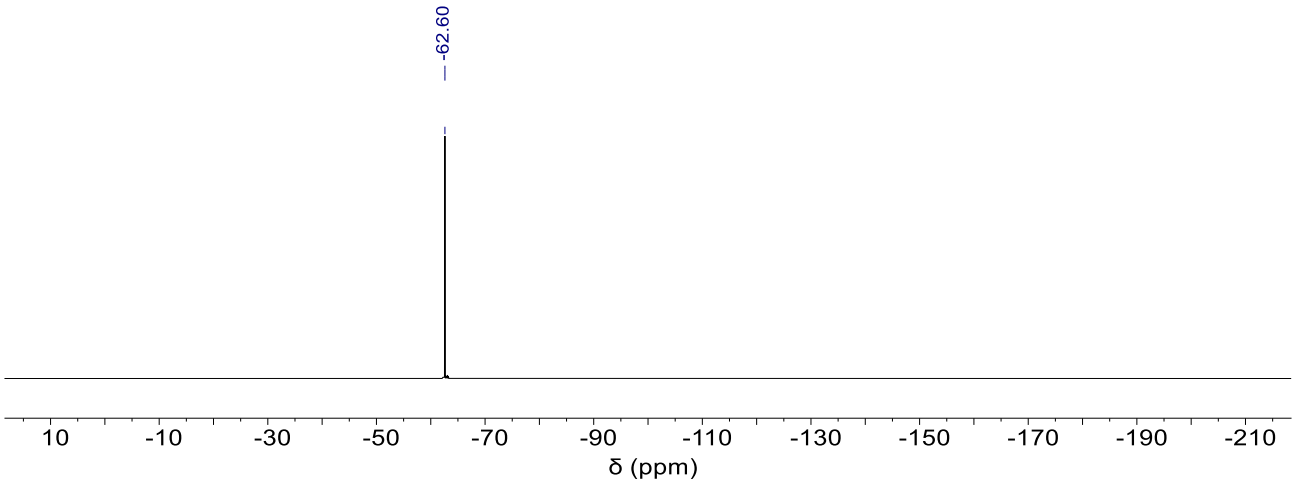

Fig. S67 ^{19}F-NMR (282 MHz) spectrum of compound **2a** in $CDCl_3$.

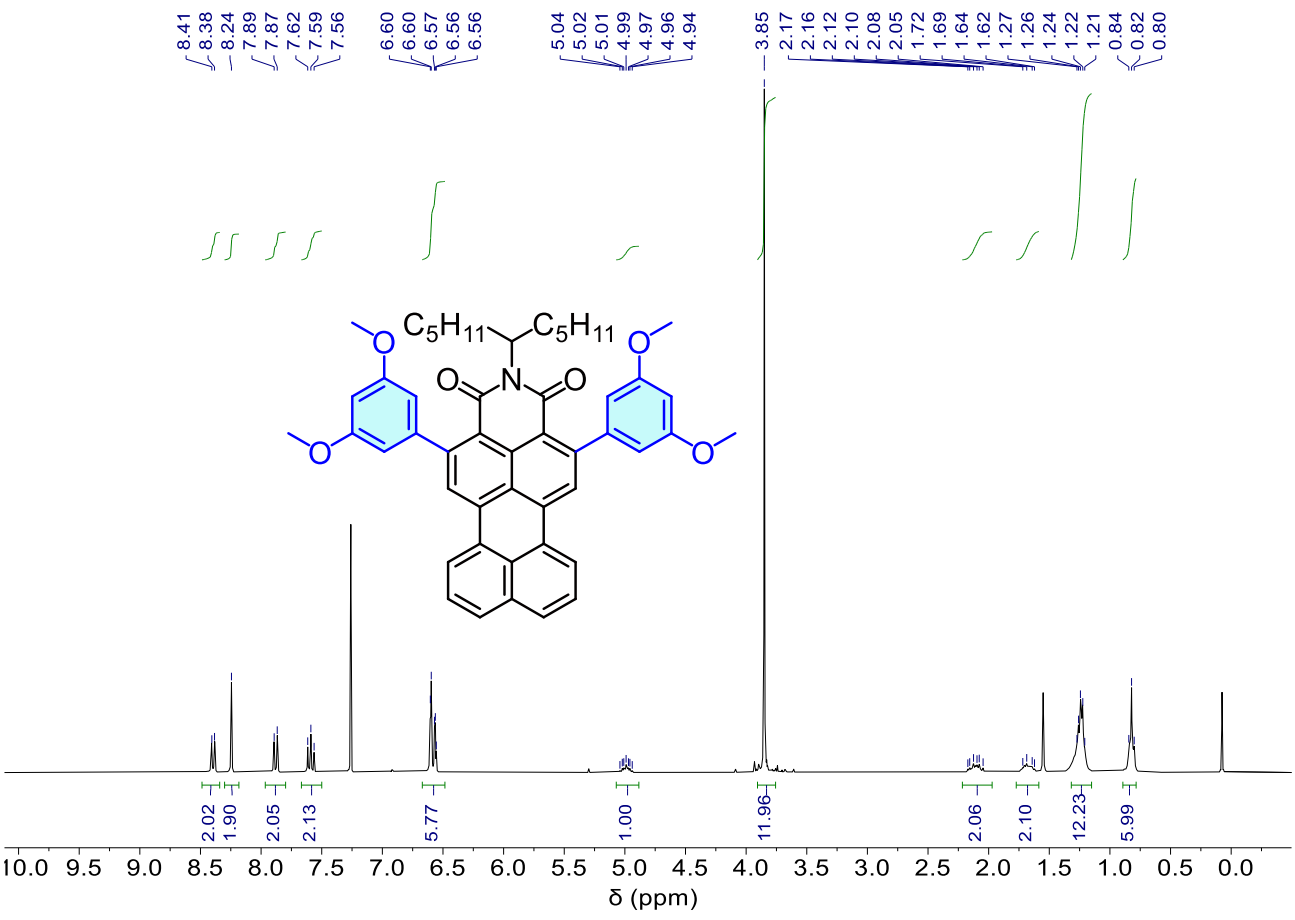

Fig. S68 ^{1}H NMR (300 MHz) spectrum of compound **2b** in $CDCl_3$.

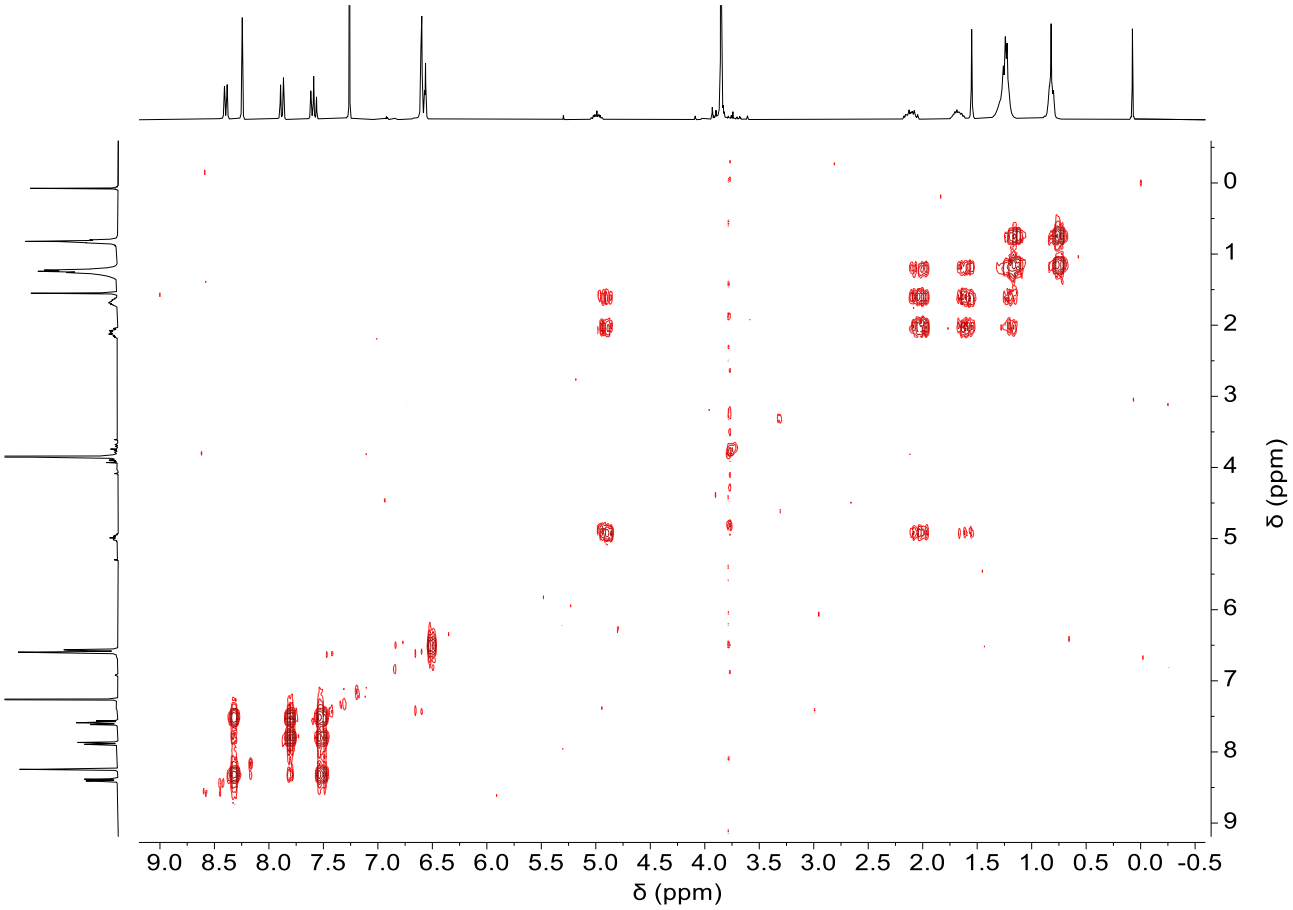

Fig. S69 ^{1}H-^{1}H COSY NMR (300 MHz) spectrum of compound **2b** in $CDCl_3$.

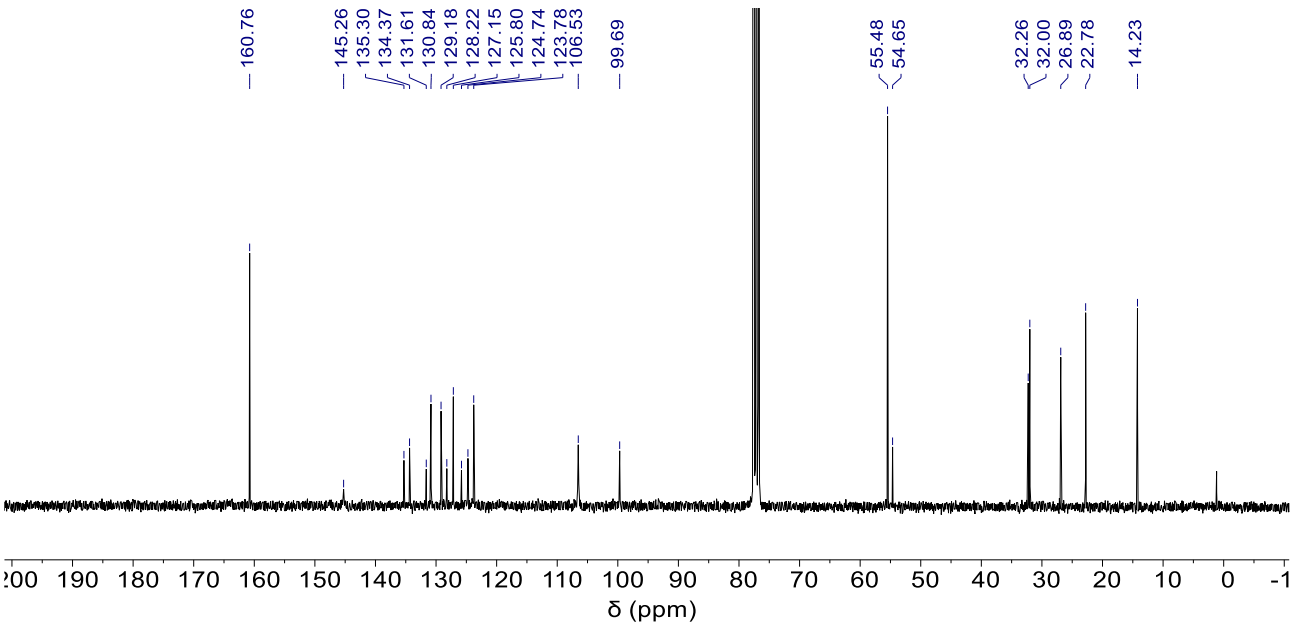

Fig. S70 ^{13}C NMR (75 MHz) spectrum of compound **2b** in $CDCl_3$.

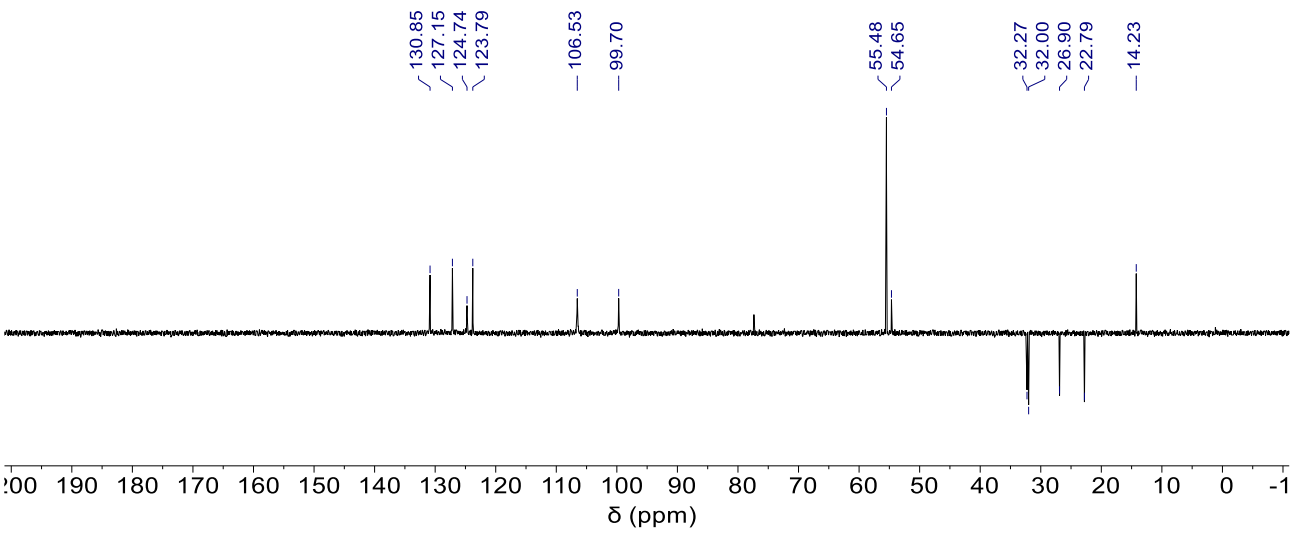

Fig. S71 DEPT (75 MHz) spectrum of compound **2b** in $CDCl_3$.

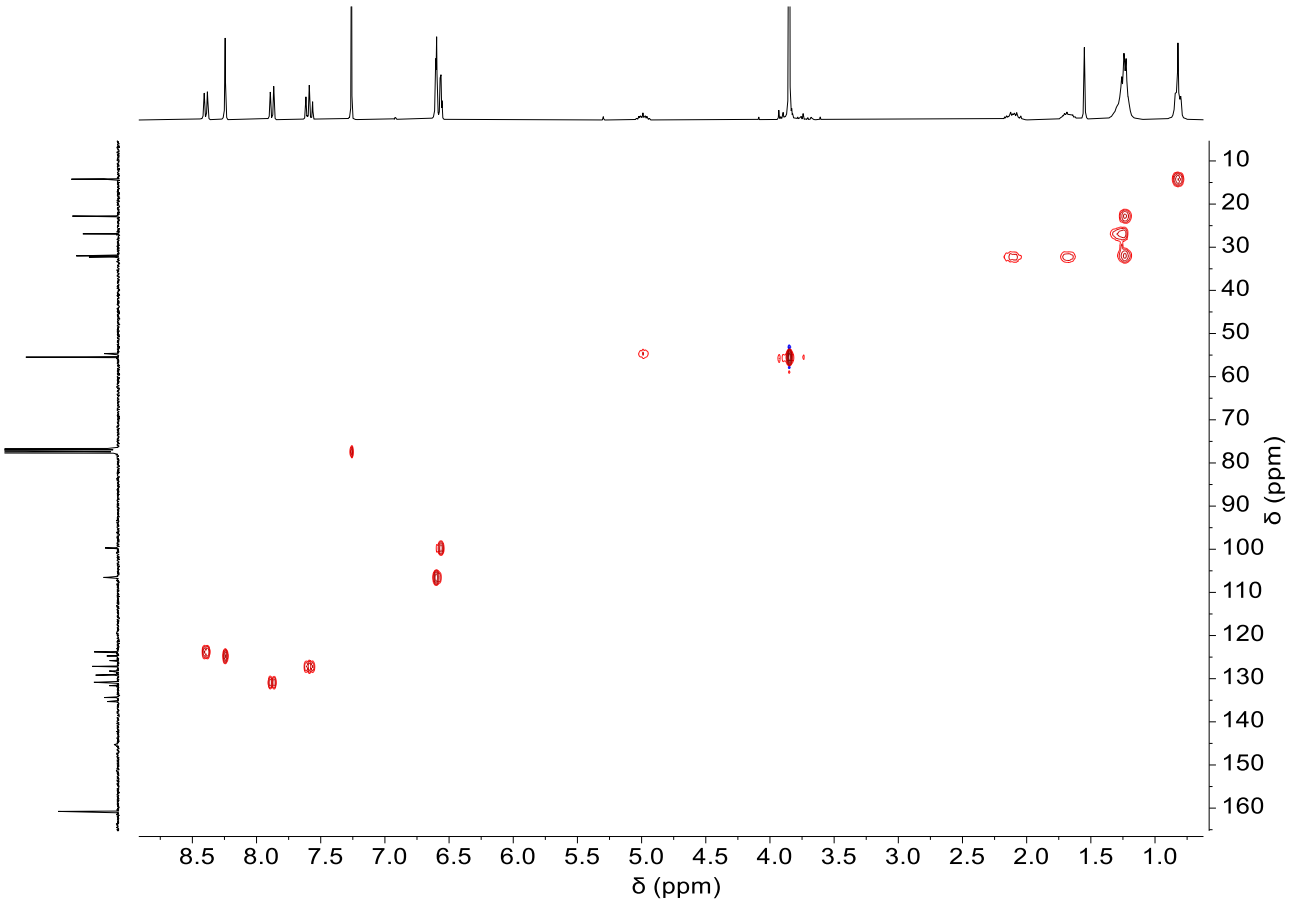

Fig. S72 HMQC (300 MHz) spectrum of compound **2b** in $CDCl_3$.

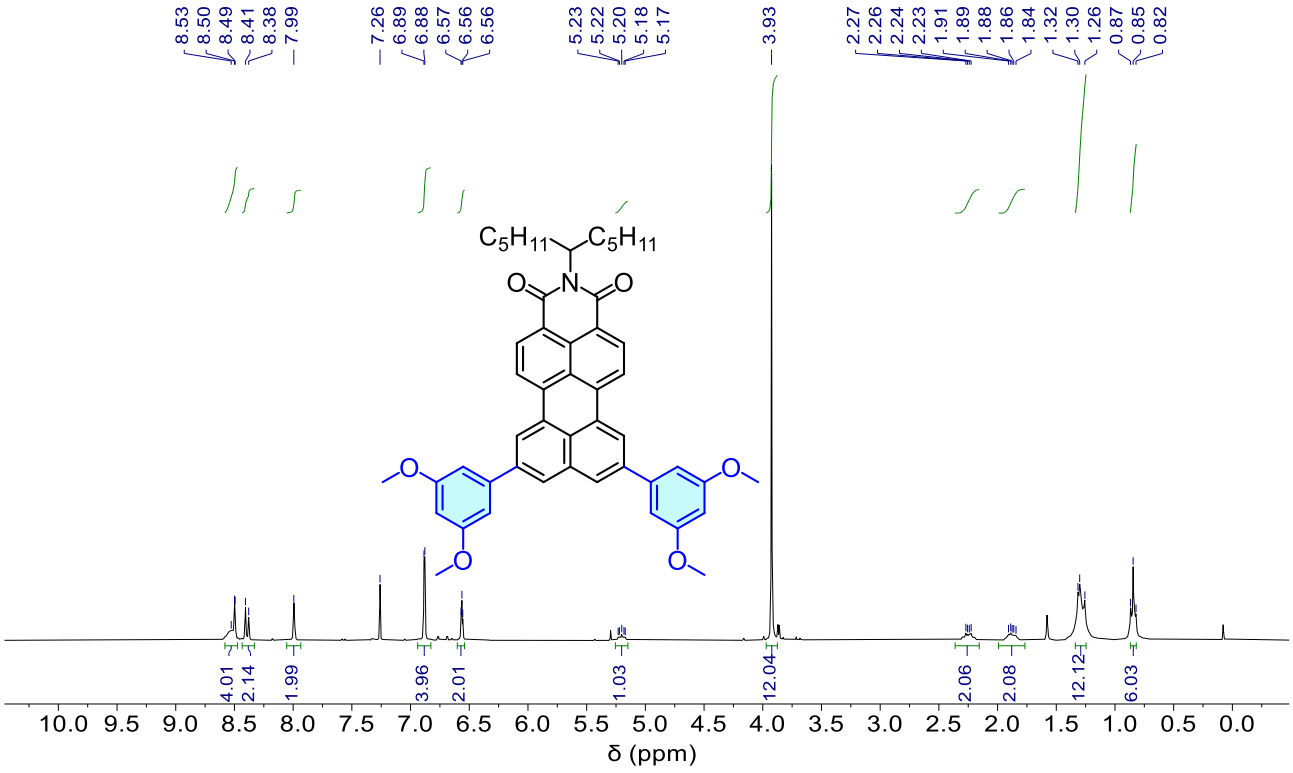

Fig. S73 ^{1}H NMR (300 MHz) spectrum of compound **3a** in $CDCl_3$.

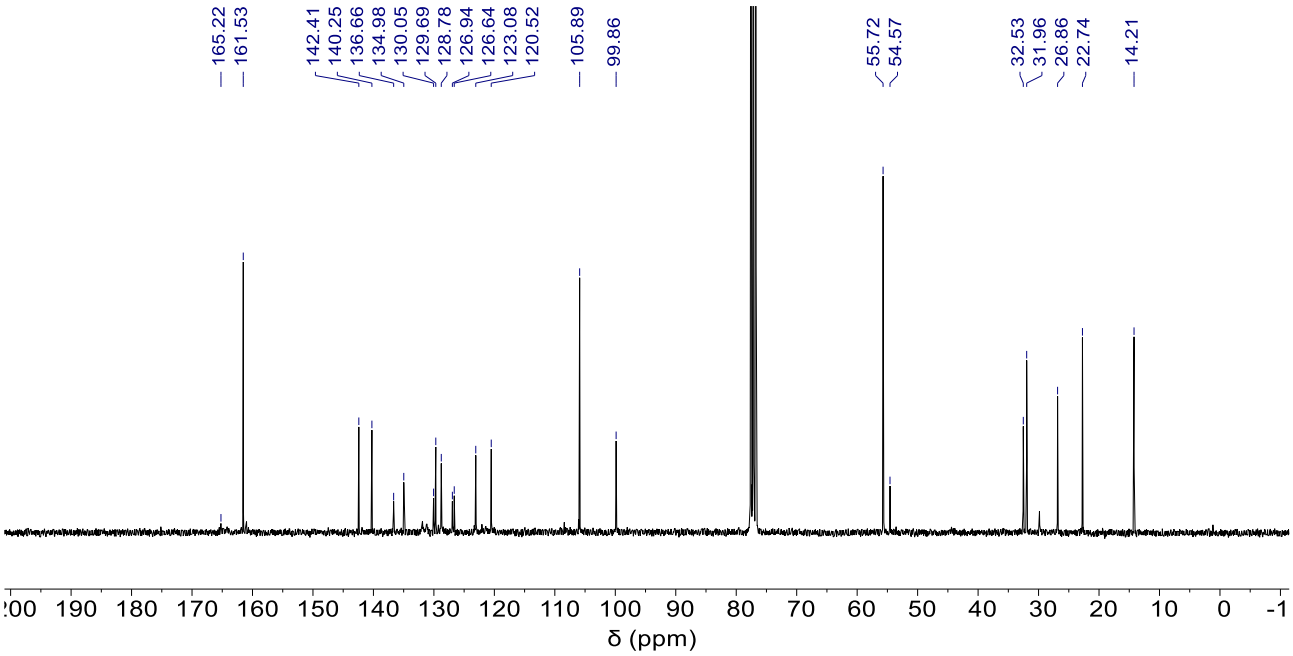

Fig. S74 ^{13}C NMR (75 MHz) spectrum of compound **3a** in $CDCl_3$.

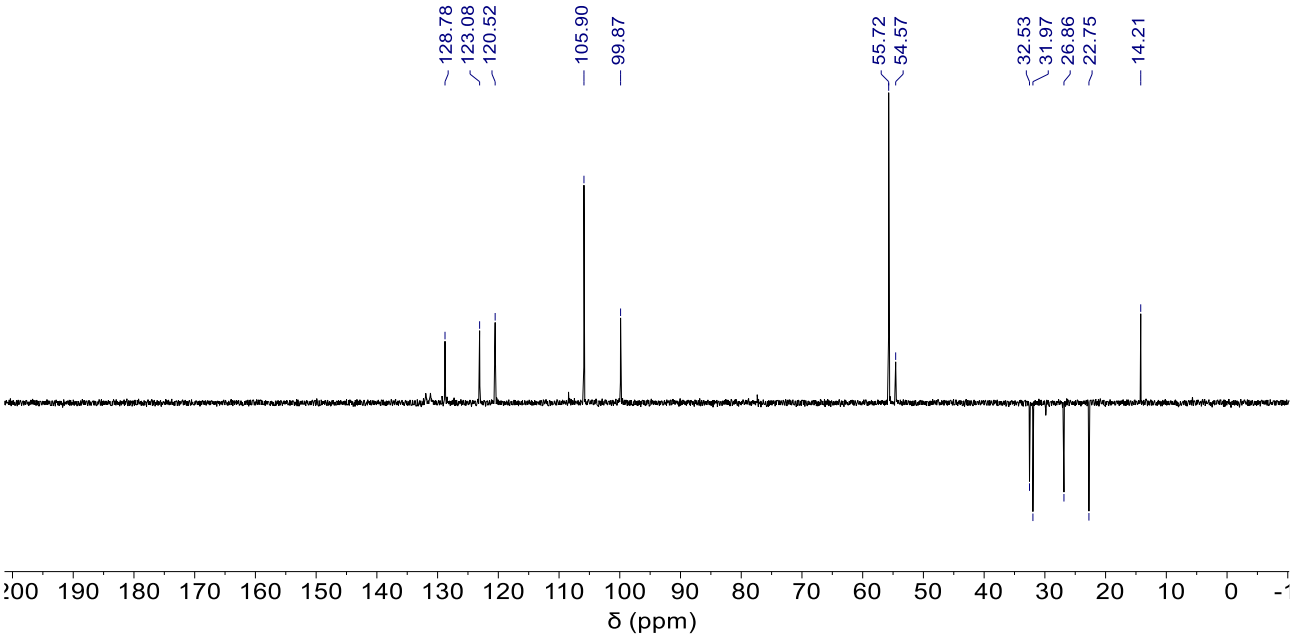

Fig. S75 DEPT NMR (75 MHz) spectrum of compound **3a** in $CDCl_3$.

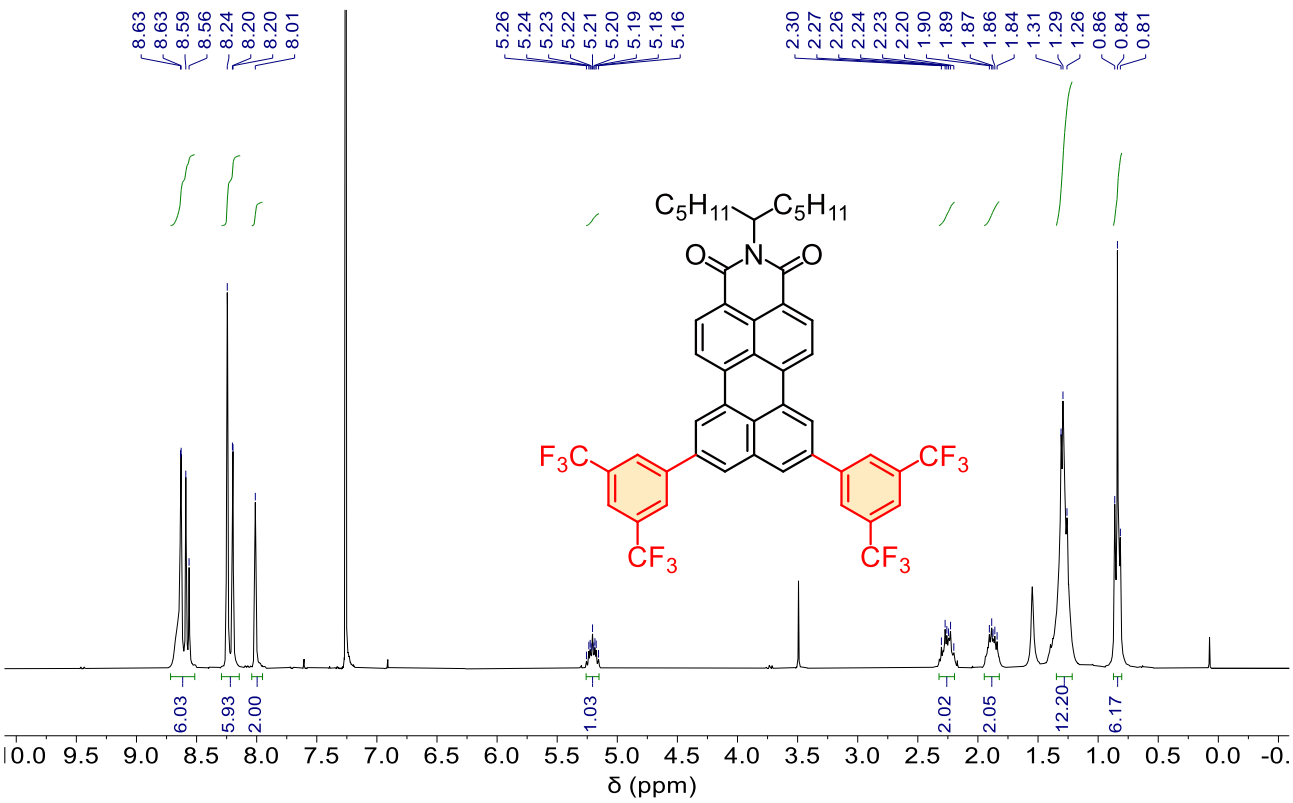

Fig. S76 ^{1}H NMR (300 MHz) spectrum of compound **3b** in $CDCl_3$.

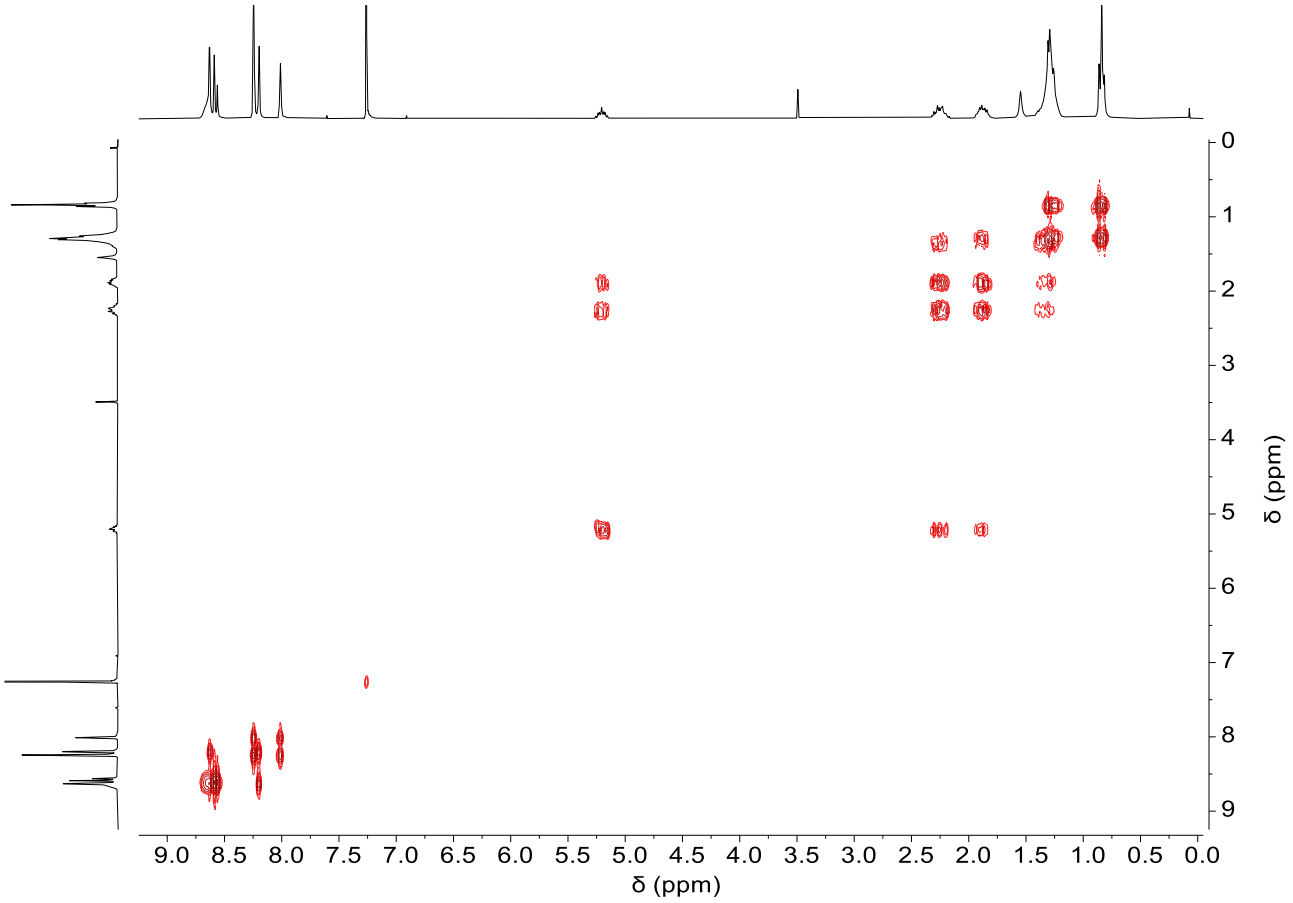

Fig. S77 ^{1}H-^{1}H COSY NMR (300 MHz) spectrum of compound **3b** in $CDCl_3$.

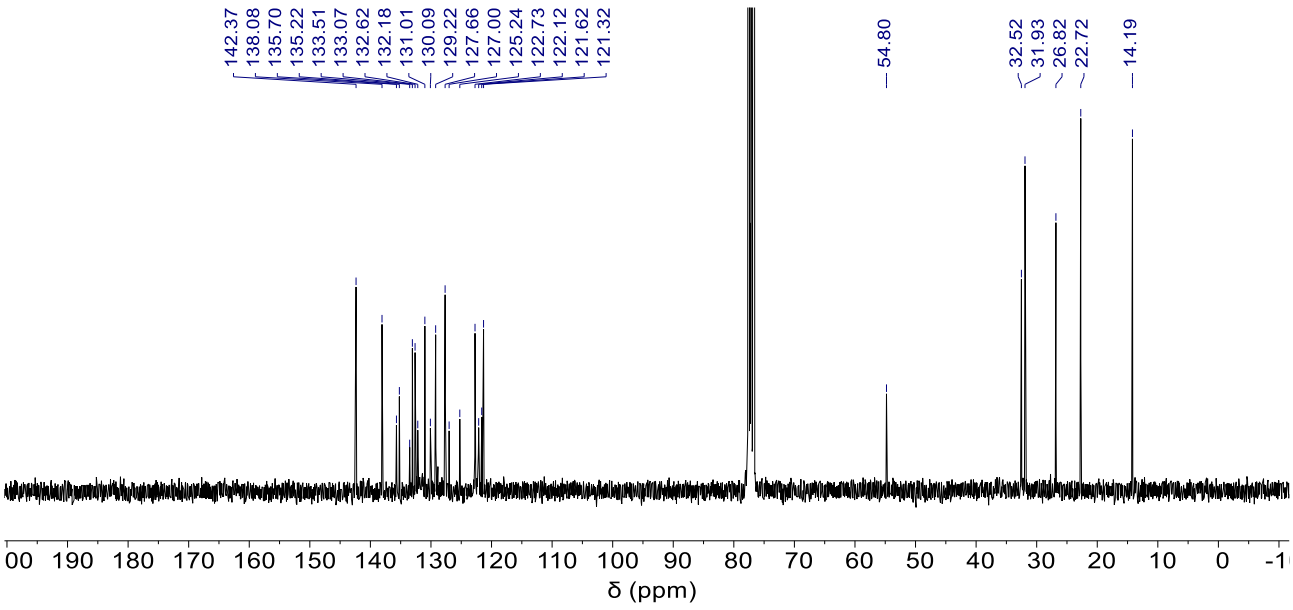

Fig. S78 ^{13}C NMR (75 MHz) spectrum of compound **3b** in $CDCl_3$.

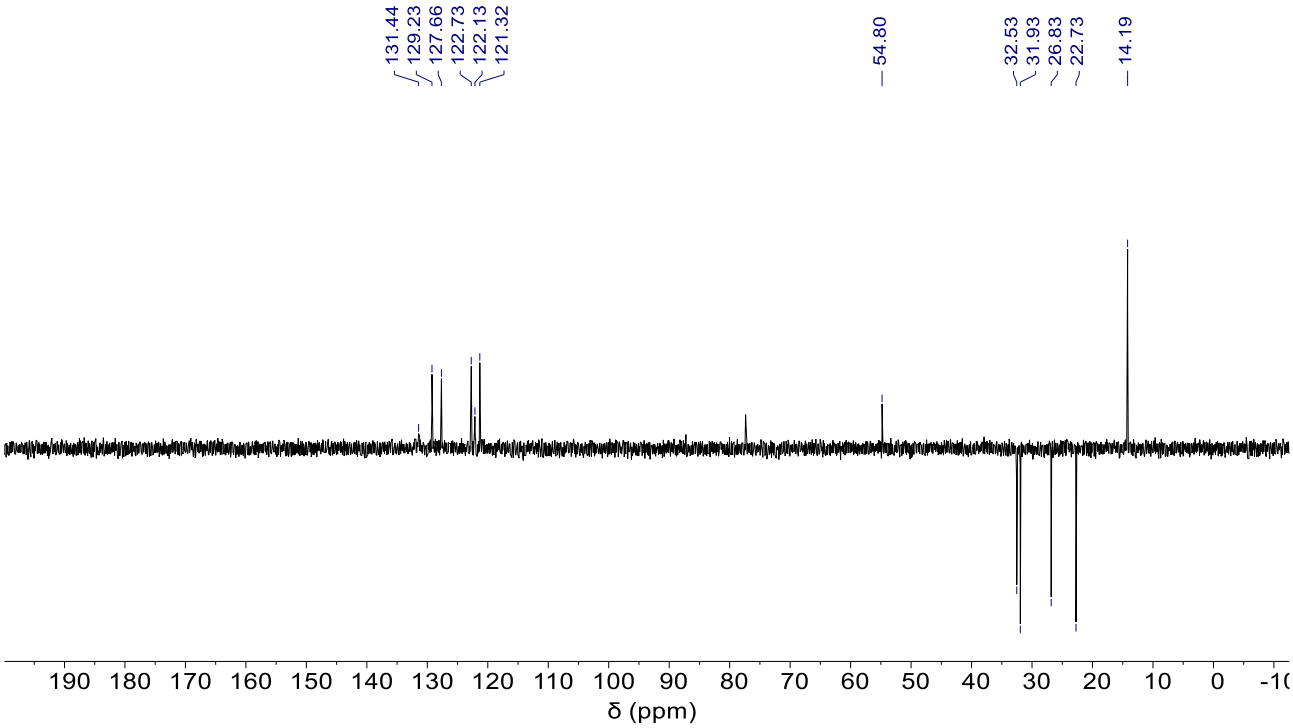

Fig. S79 DEPT (75 MHz) spectrum of compound **3b** in $CDCl_3$.

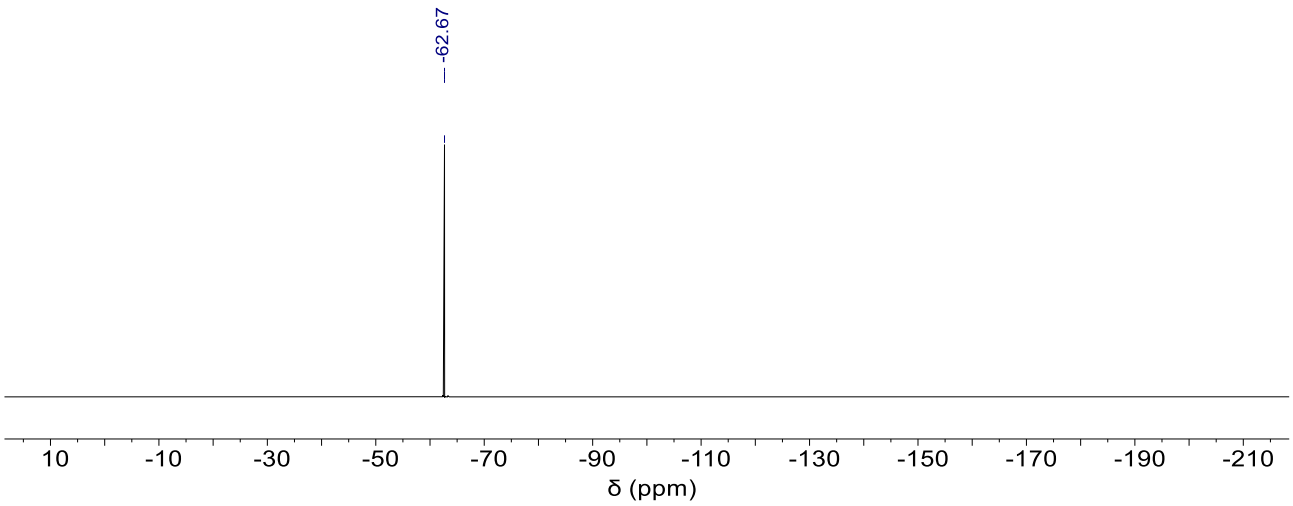

Fig. S80 ^{19}F-NMR (282 MHz) spectrum of compound **3b** in $CDCl_3$.

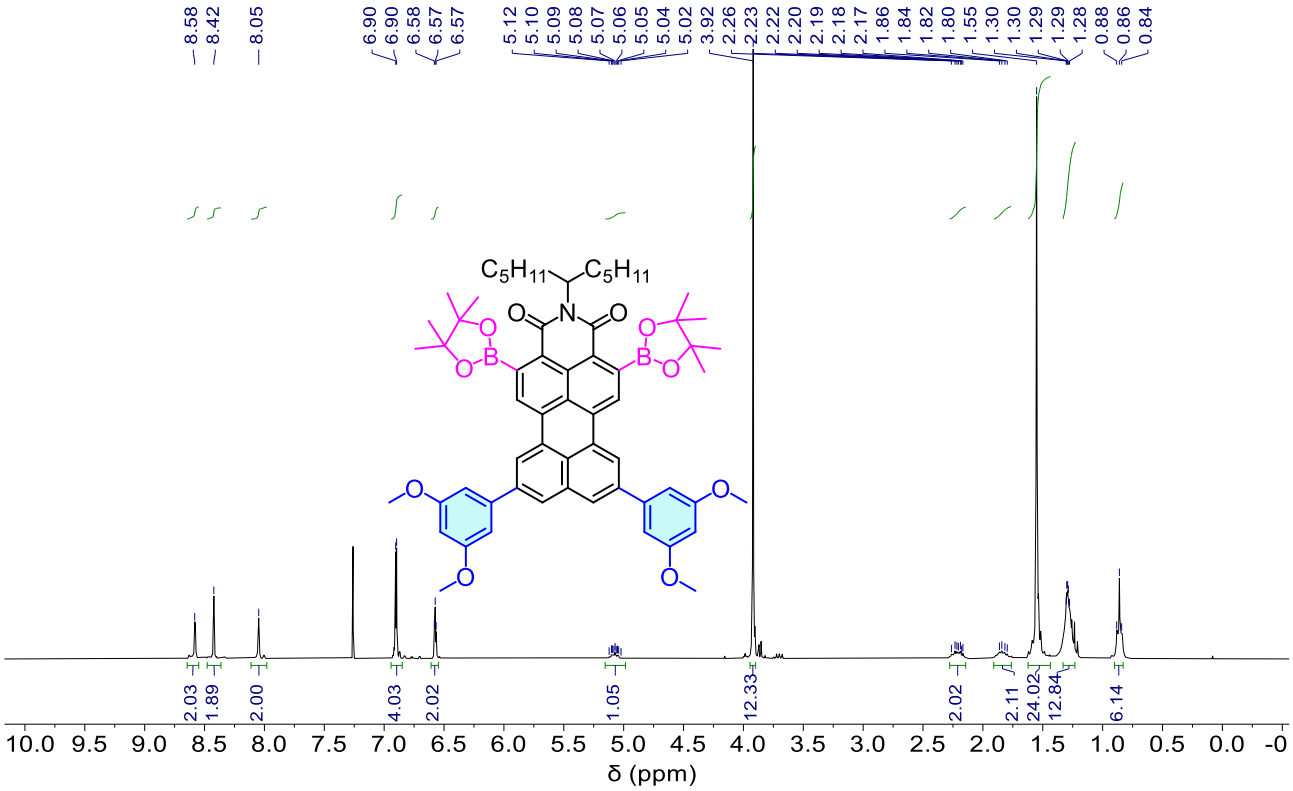

Fig. S81 ^{1}H NMR (300 MHz) spectrum of compound **6a** in $CDCl_3$.

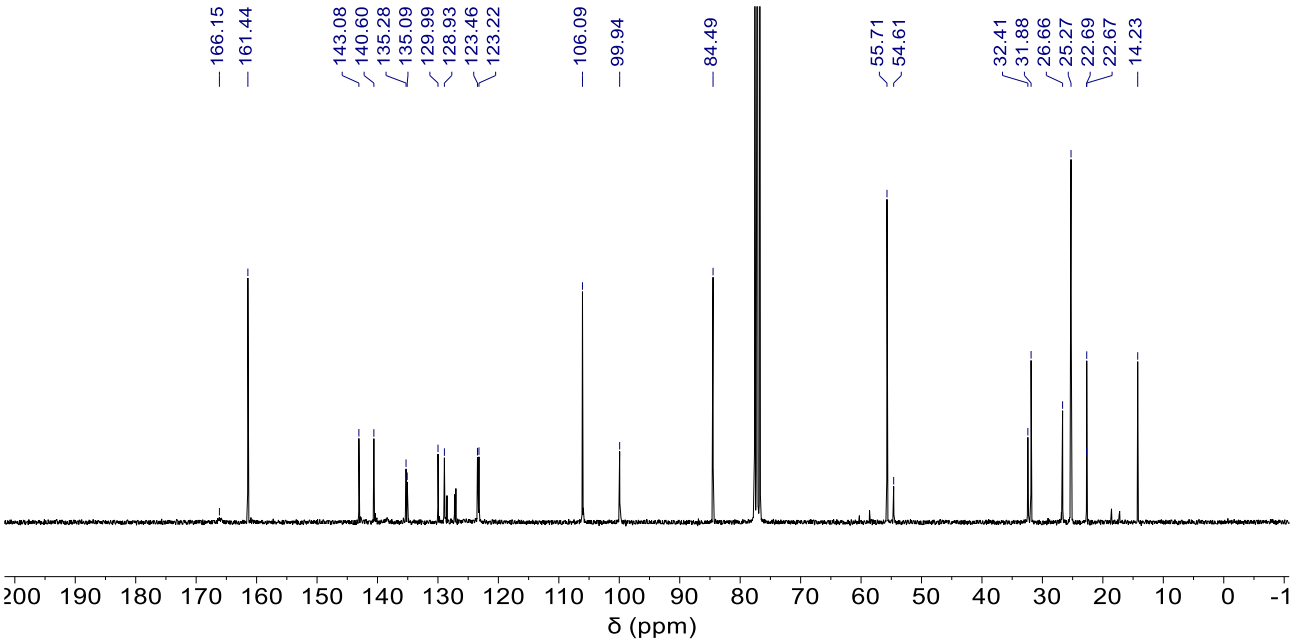

Fig. S82 ^{13}C NMR (75 MHz) spectrum of compound **6a** in $CDCl_3$.

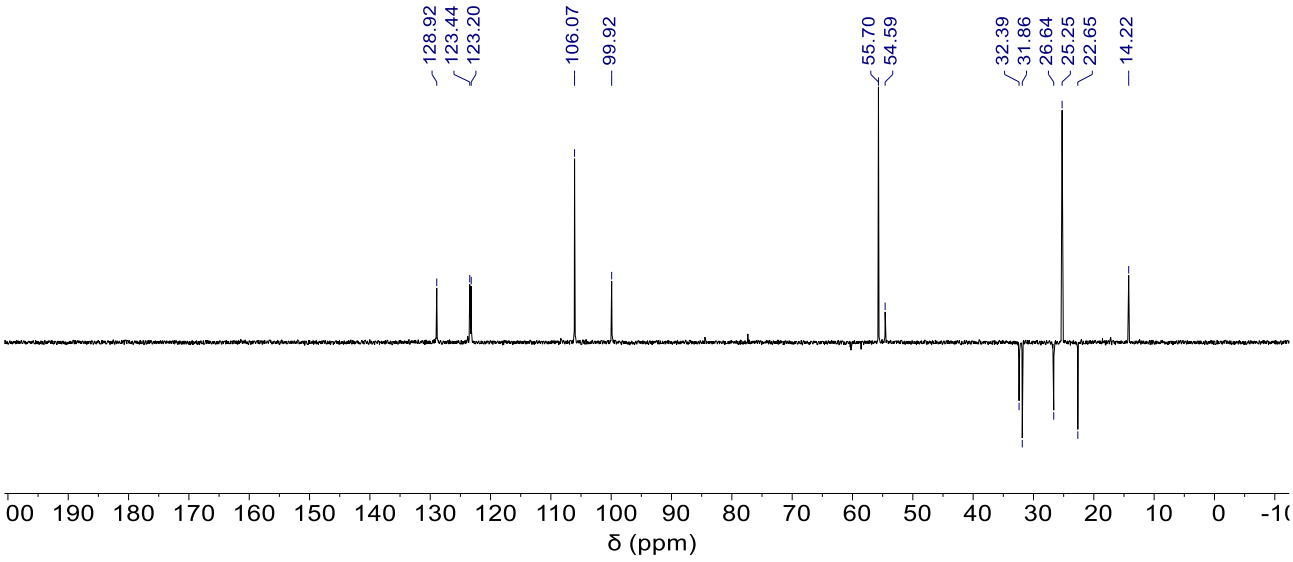

Fig. S83 DEPT NMR (75 MHz) spectrum of compound **6a** in $CDCl_3$.

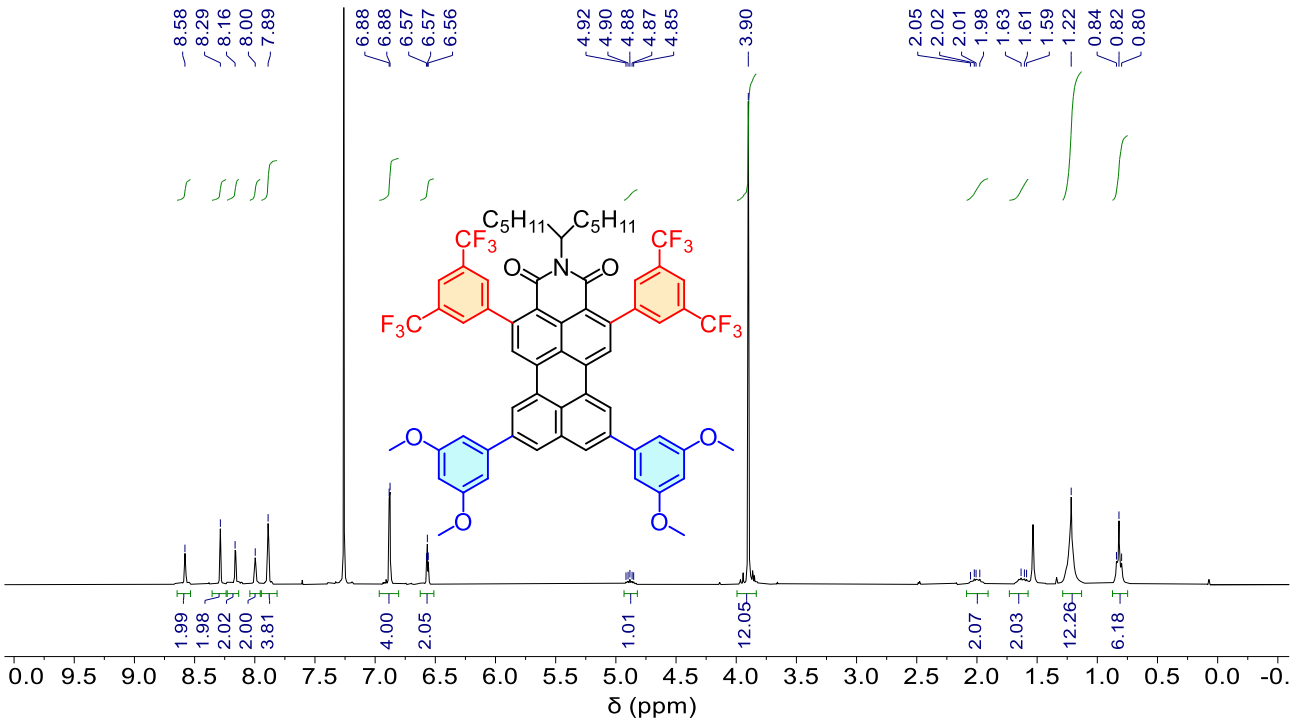

Fig. S84 ^1H NMR (300 MHz) spectrum of compound **4a** in $CDCl_3$.

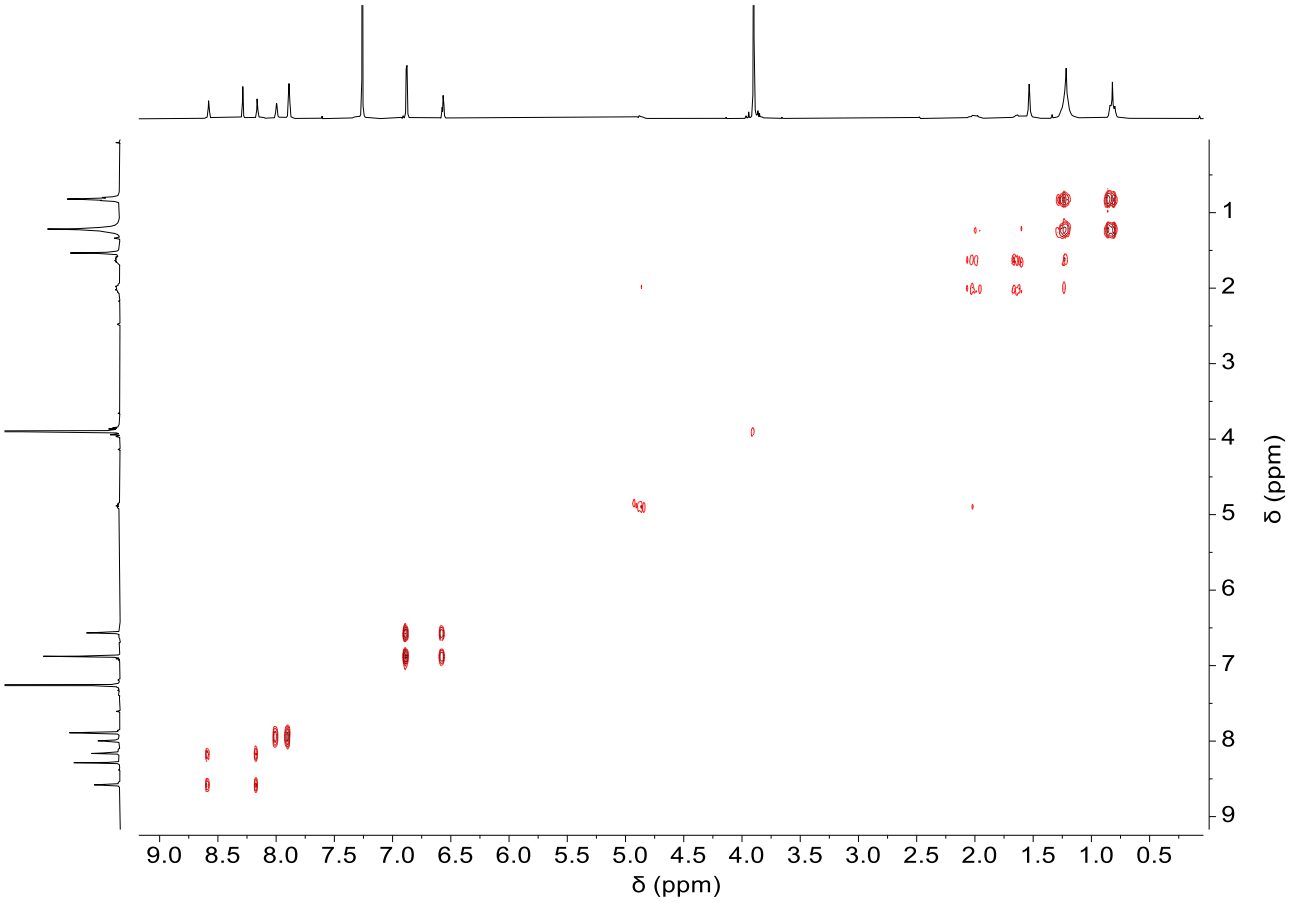

Fig. S85 ^{1}H-^{1}H COSY NMR (300 MHz) spectrum of compound **4a** in $CDCl_3$.

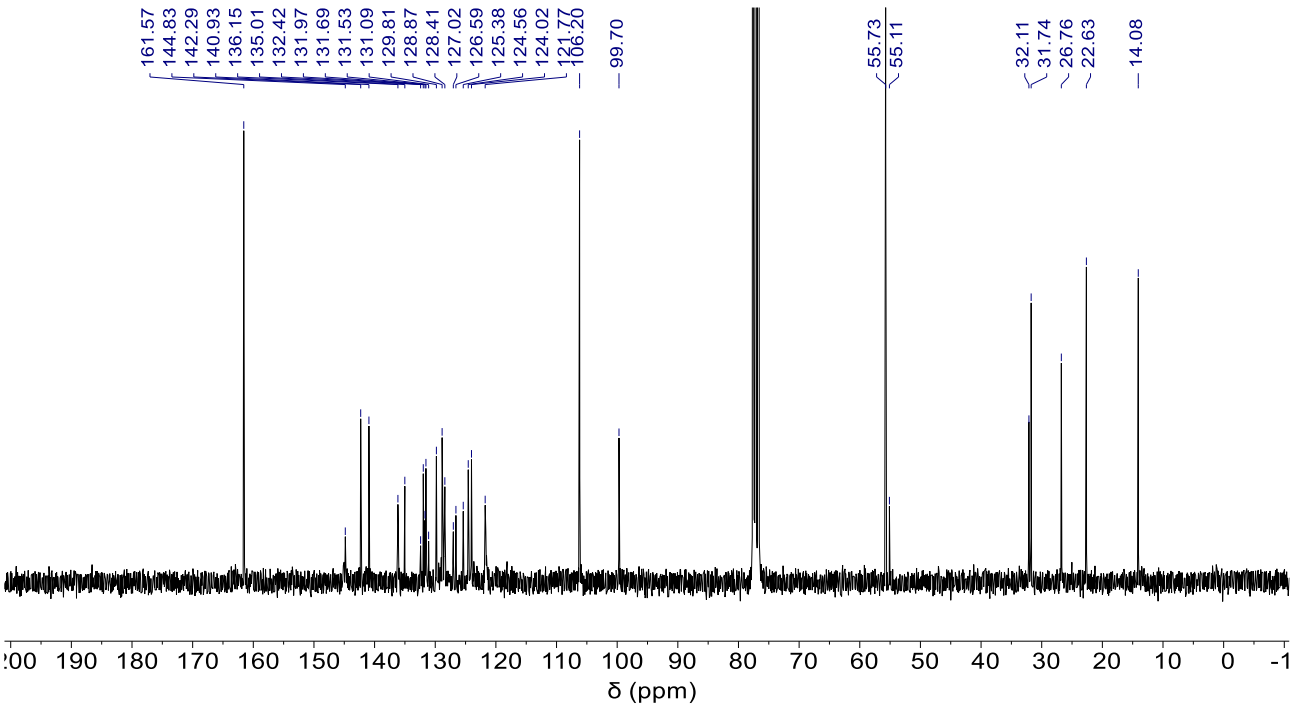

Fig. S86 ^{13}C NMR (75 MHz) spectrum of compound **4a** in $CDCl_3$.

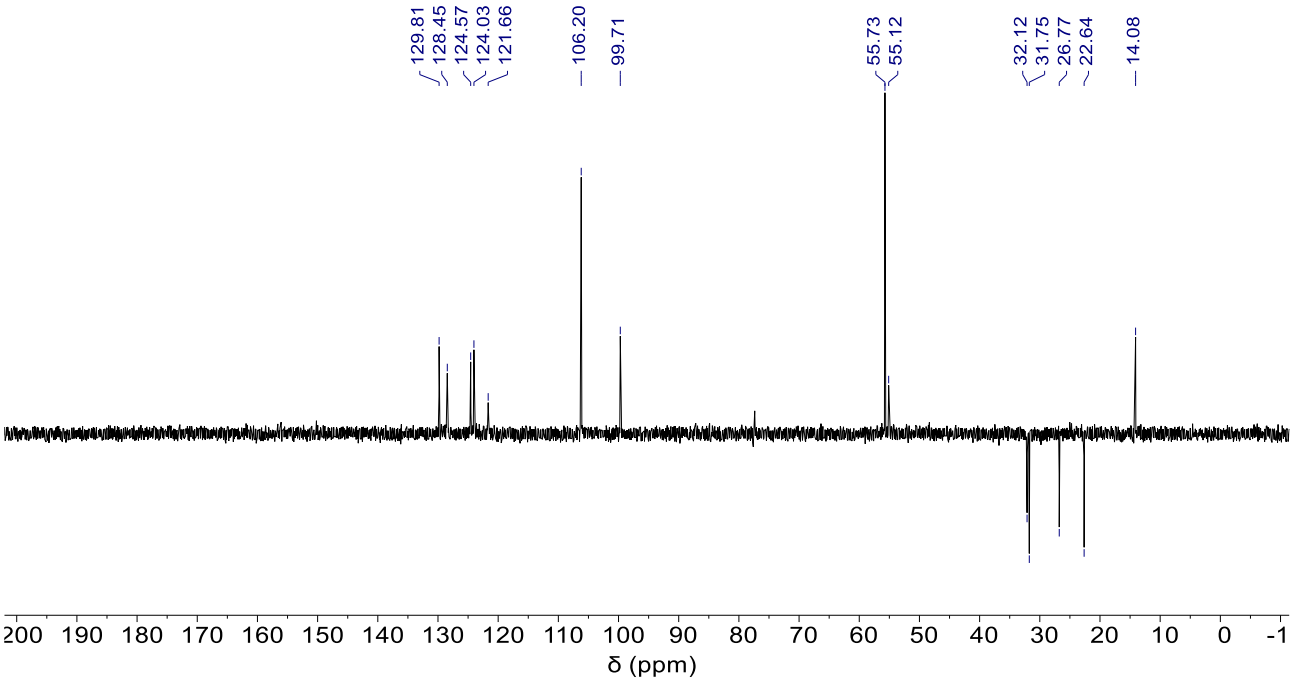

Fig. S87 DEPT NMR (75 MHz) spectrum of compound **4a** in $CDCl_3$.

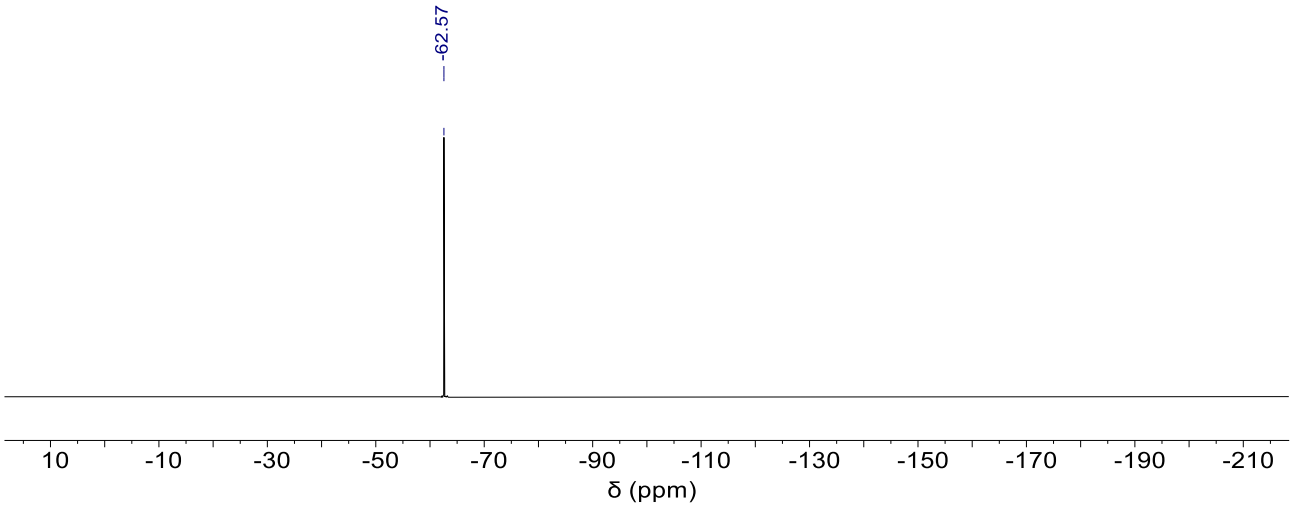

Fig. S88 ^{19}F-NMR (128 MHz) spectrum of compound **4a** in $CDCl_3$.

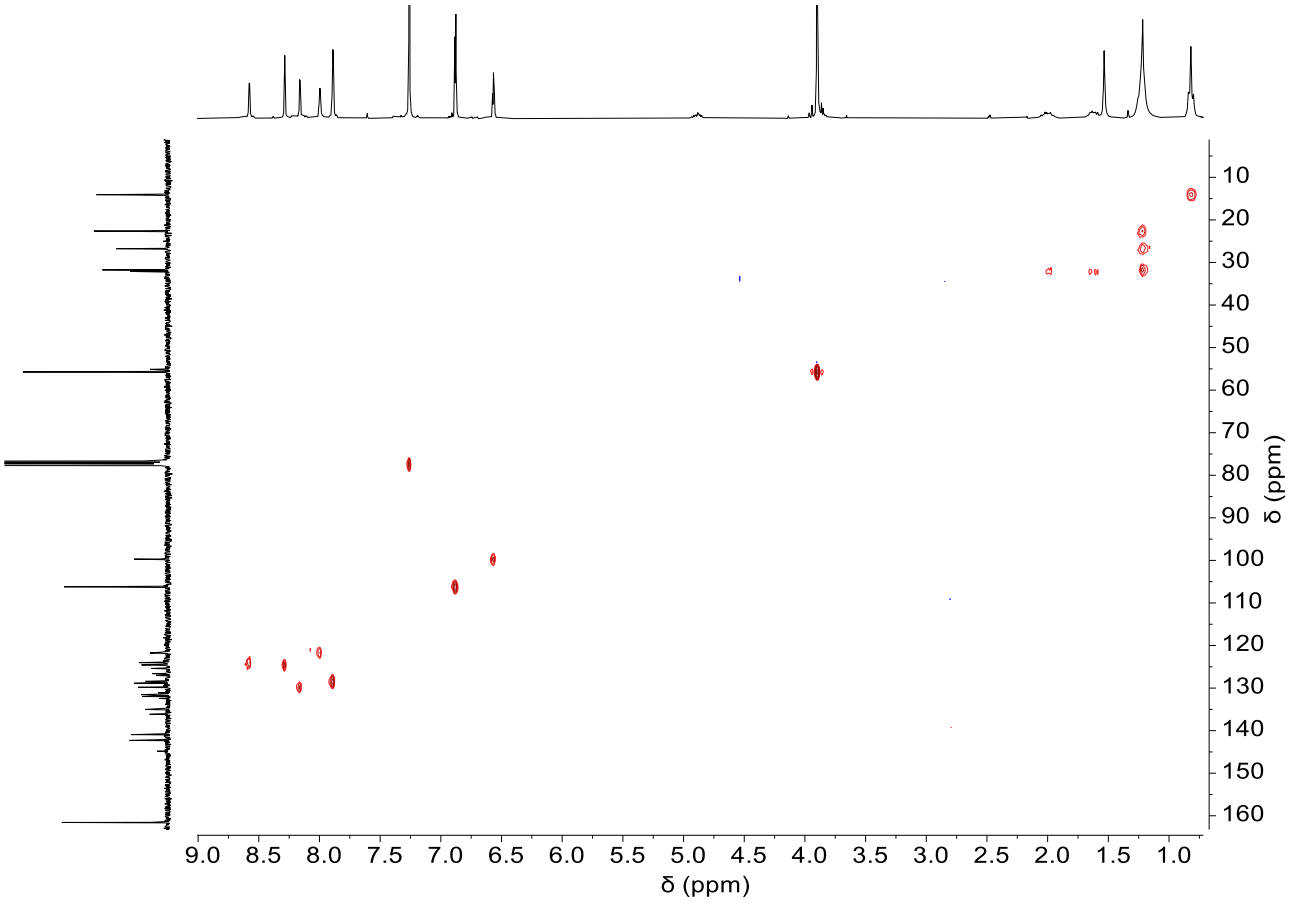

Fig. S89 HMQC (300 MHz) spectrum of compound **4a** in $CDCl_3$.

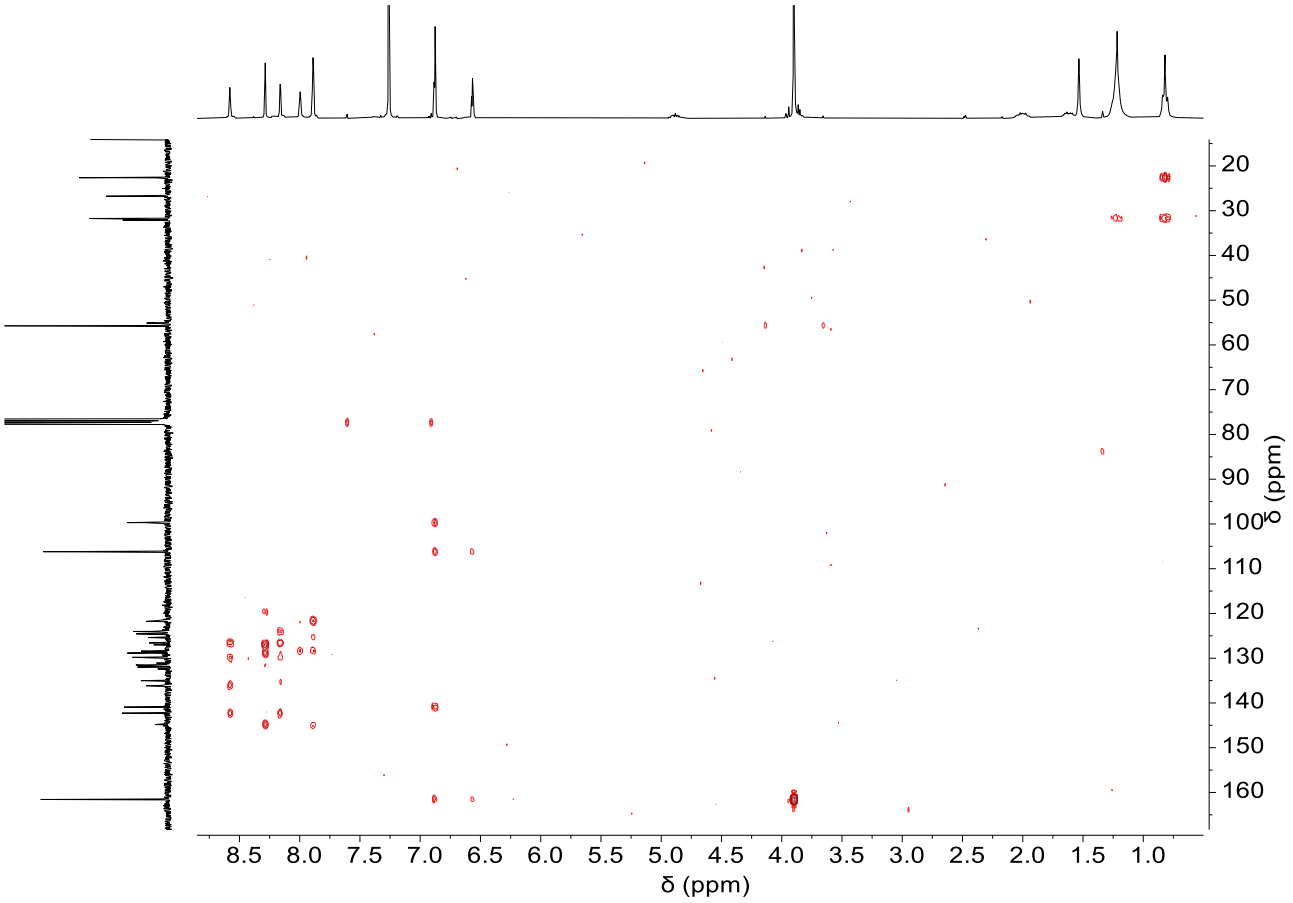

Fig. S90 HMBC (300 MHz) spectrum of compound **4a** in $CDCl_3$.

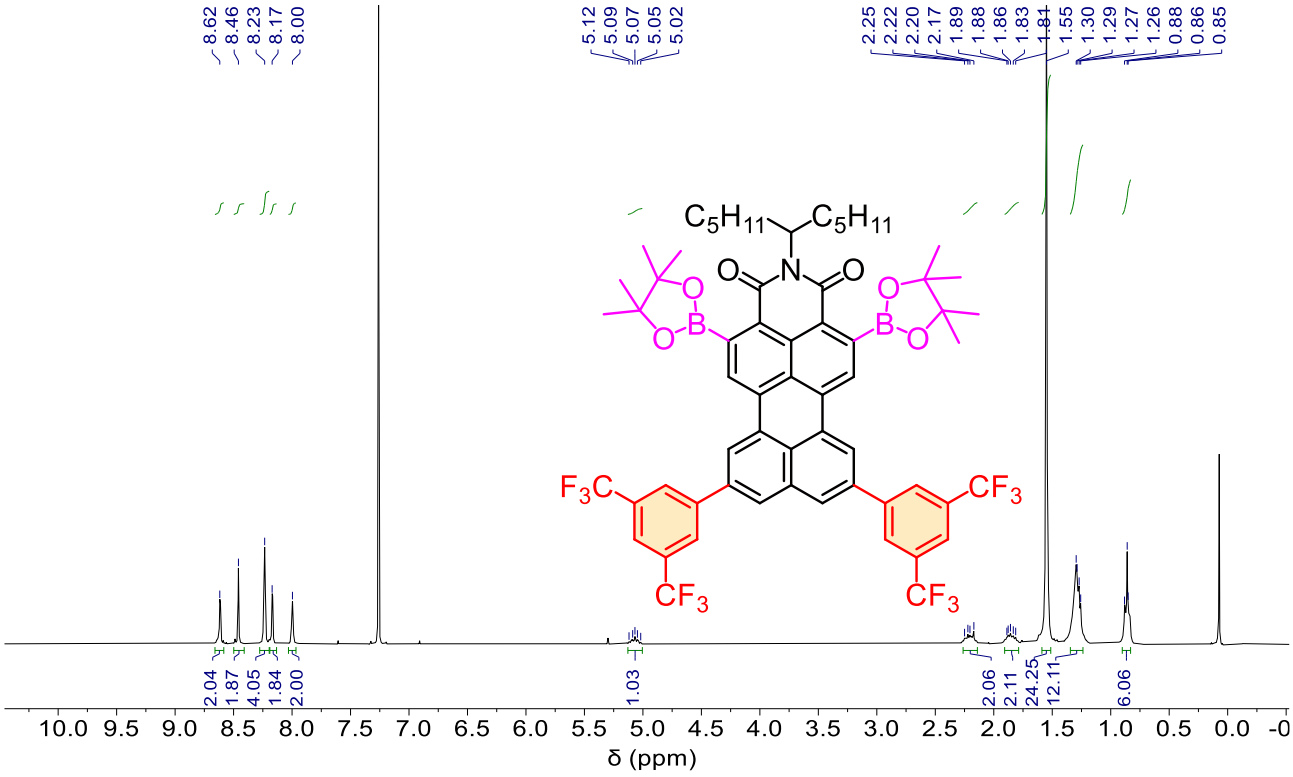

Fig. S91 ^{1}H NMR (300 MHz) spectrum of compound **6b** in $CDCl_3$.

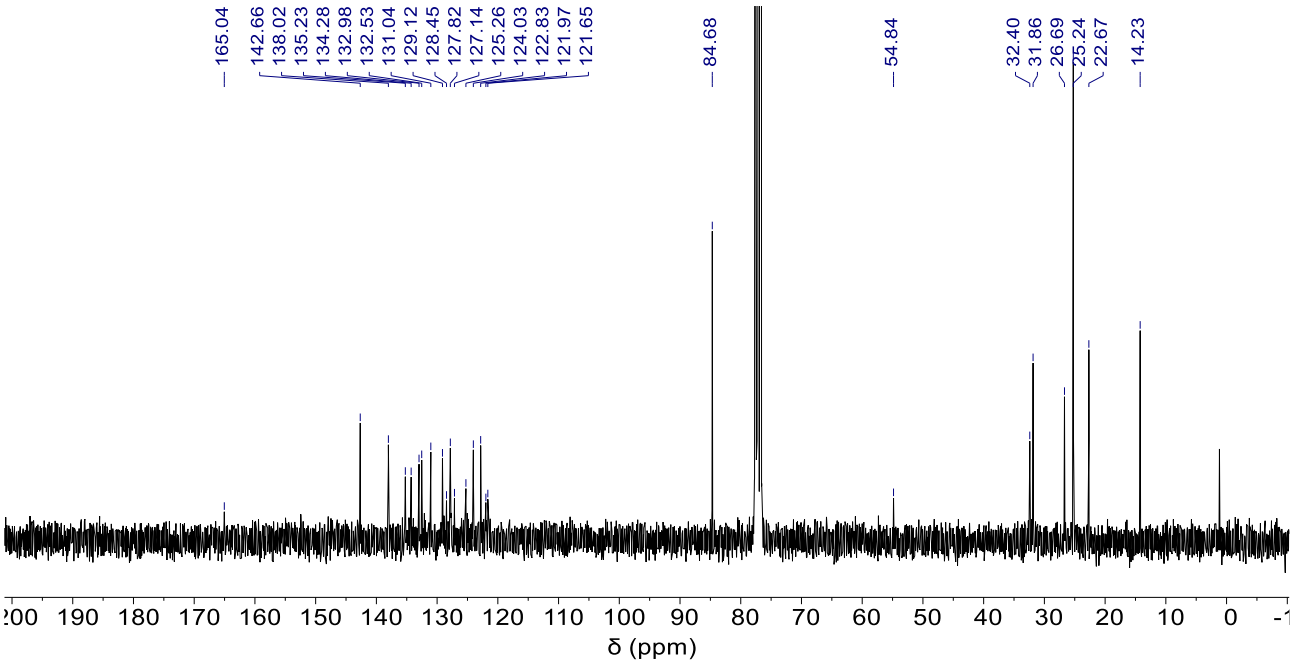

Fig. S92 ^{13}C NMR (75 MHz) spectrum of compound **6b** in $CDCl_3$.

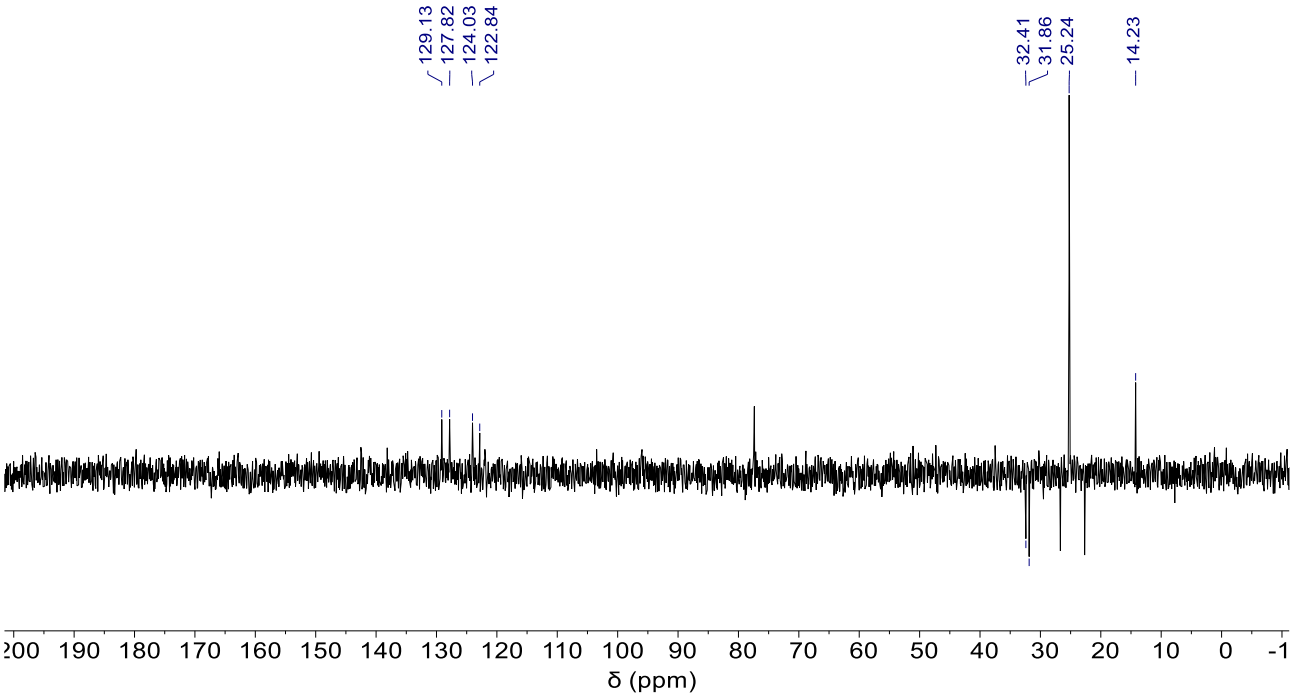

Fig. S93 DEPT (75 MHz) spectrum of compound **6b** in $CDCl_3$.

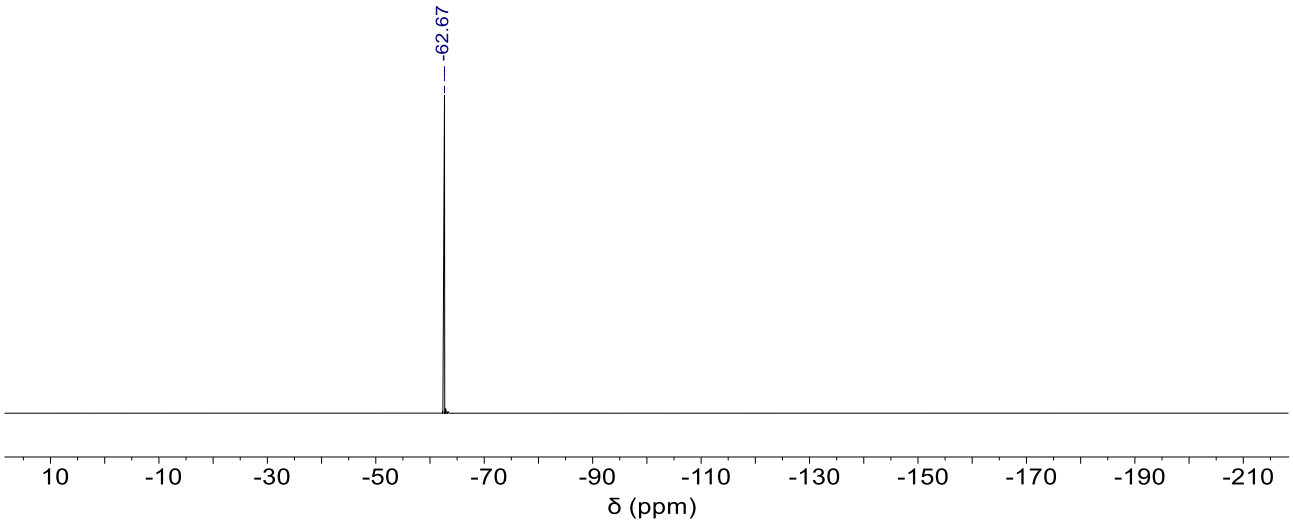

Fig. S94 ^{19}F-NMR (282 MHz) spectrum of compound **6b** in $CDCl_3$.

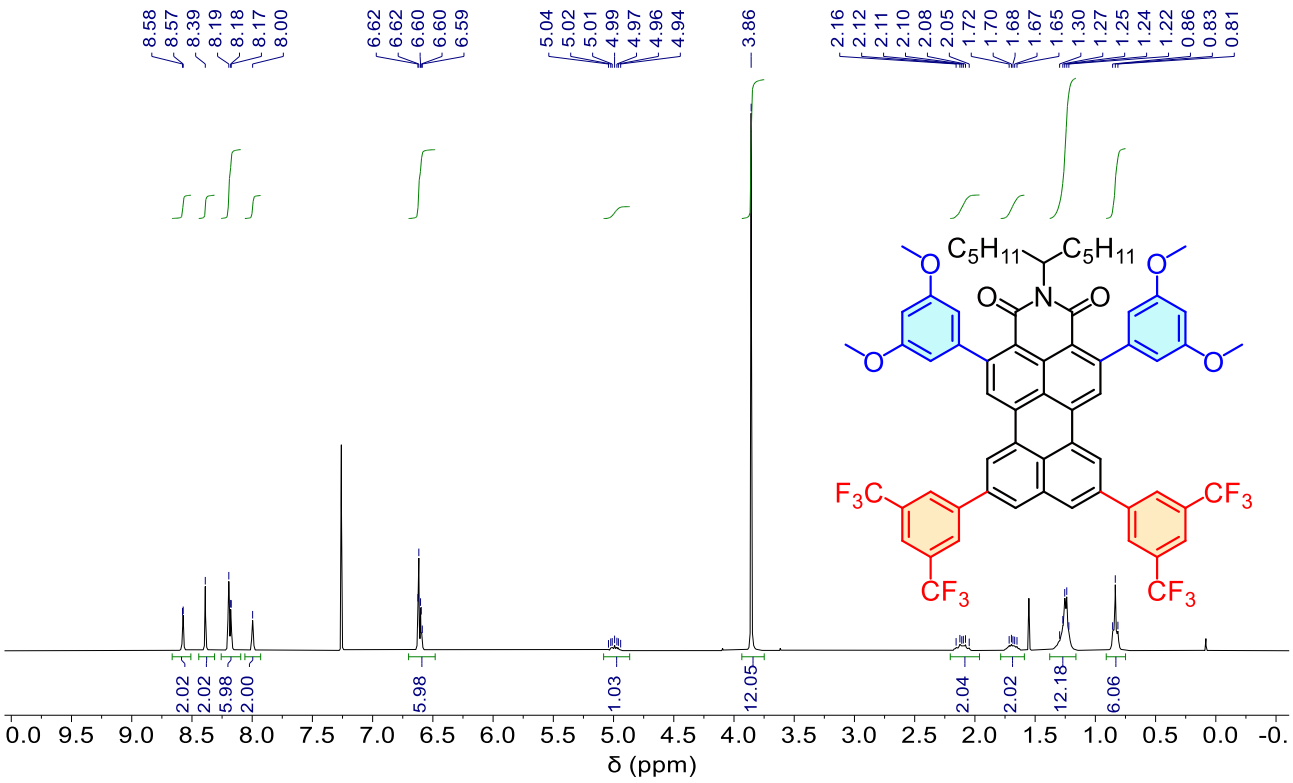

Fig. S95 ^{1}H NMR (300 MHz) spectrum of compound **4b** in $CDCl_3$.

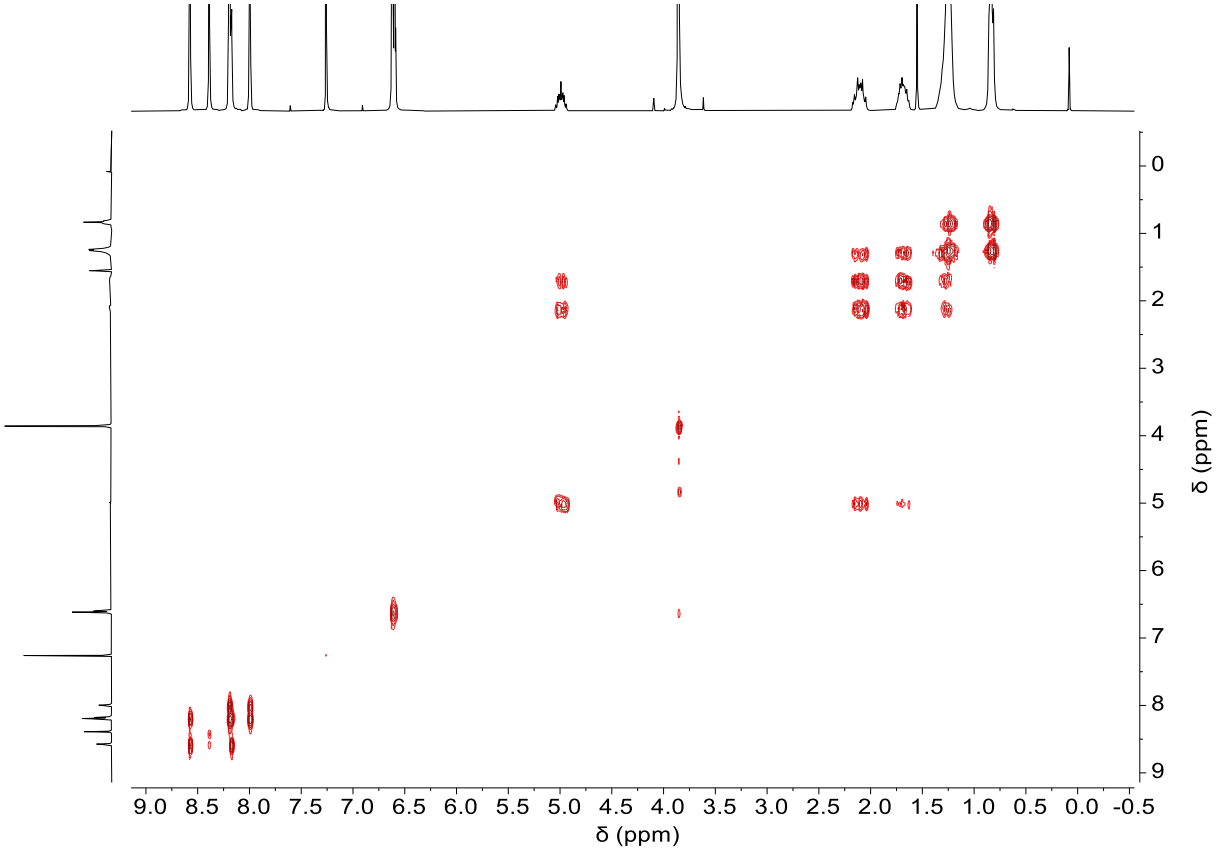

Fig. S96 ^{1}H-^{1}H COSY NMR (300 MHz) spectrum of compound **4b** in $CDCl_3$

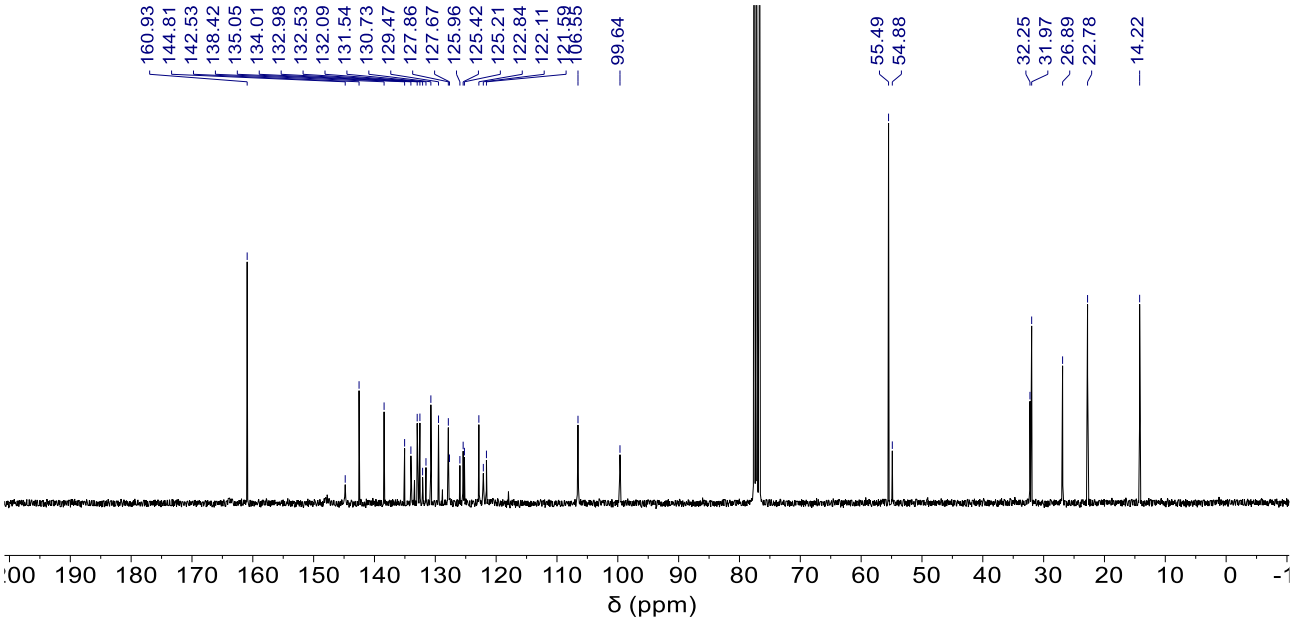

Fig. S97 ^{13}C NMR (75 MHz) spectrum of compound **4b** in $CDCl_3$.

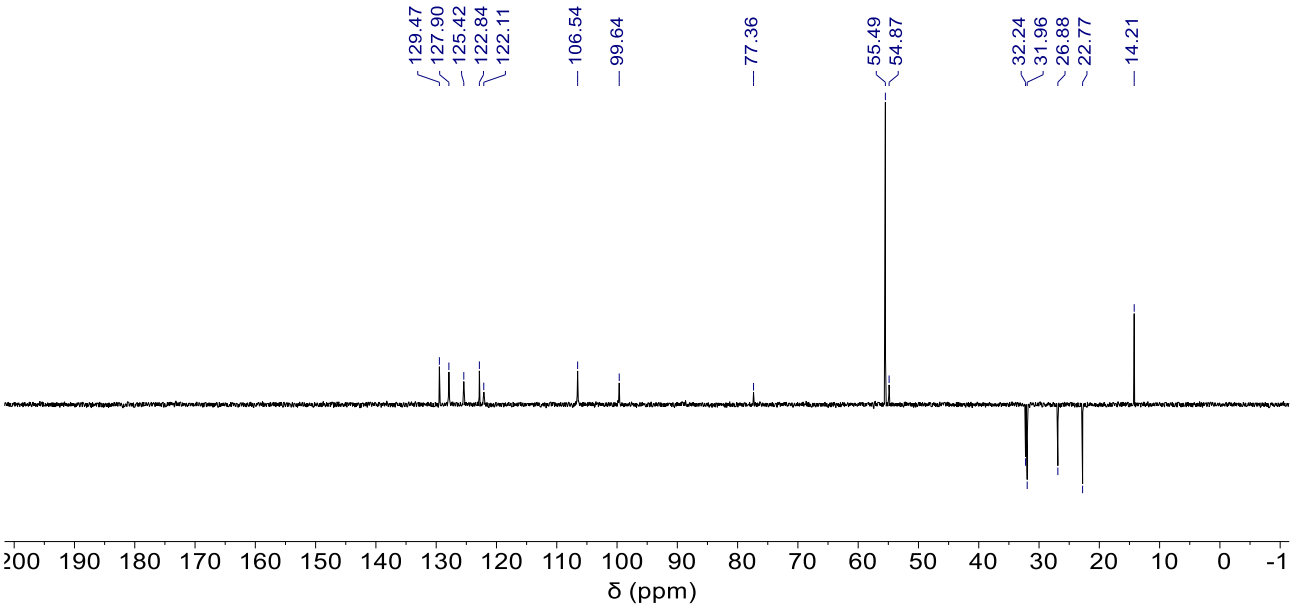

Fig. S98 DEPT (75 MHz) spectrum of compound **4b** in $CDCl_3$.

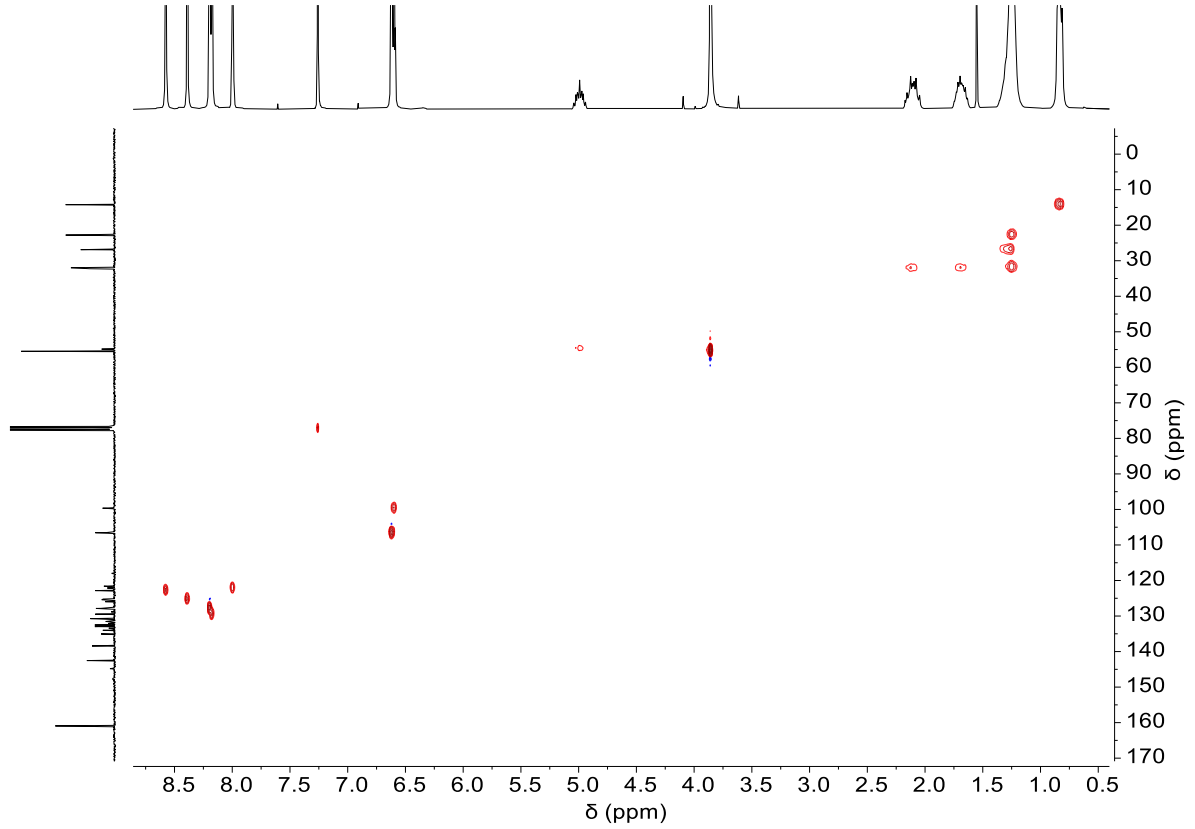

Fig. S99 HMQC (300 MHz) spectrum of compound **4b** in $CDCl_3$.

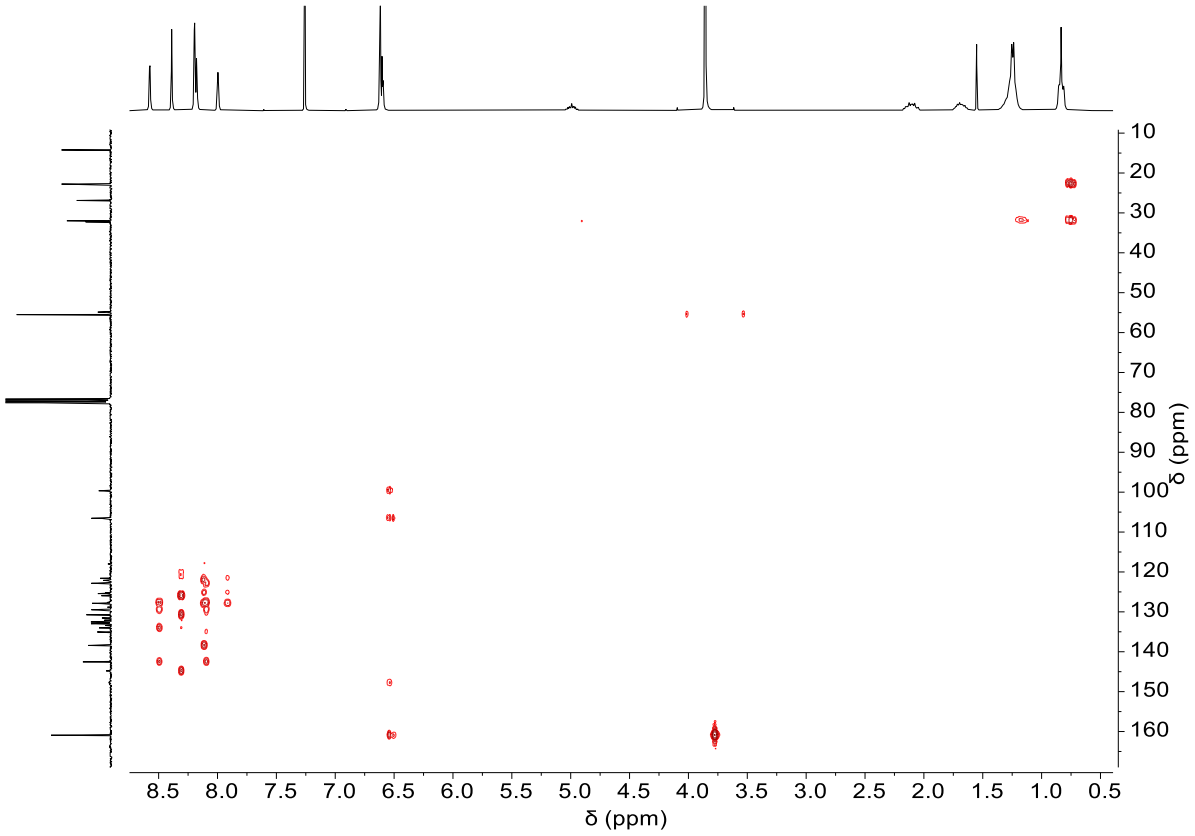

Fig. S100 HMBC (300 MHz) spectrum of compound **4b** in $CDCl_3$.

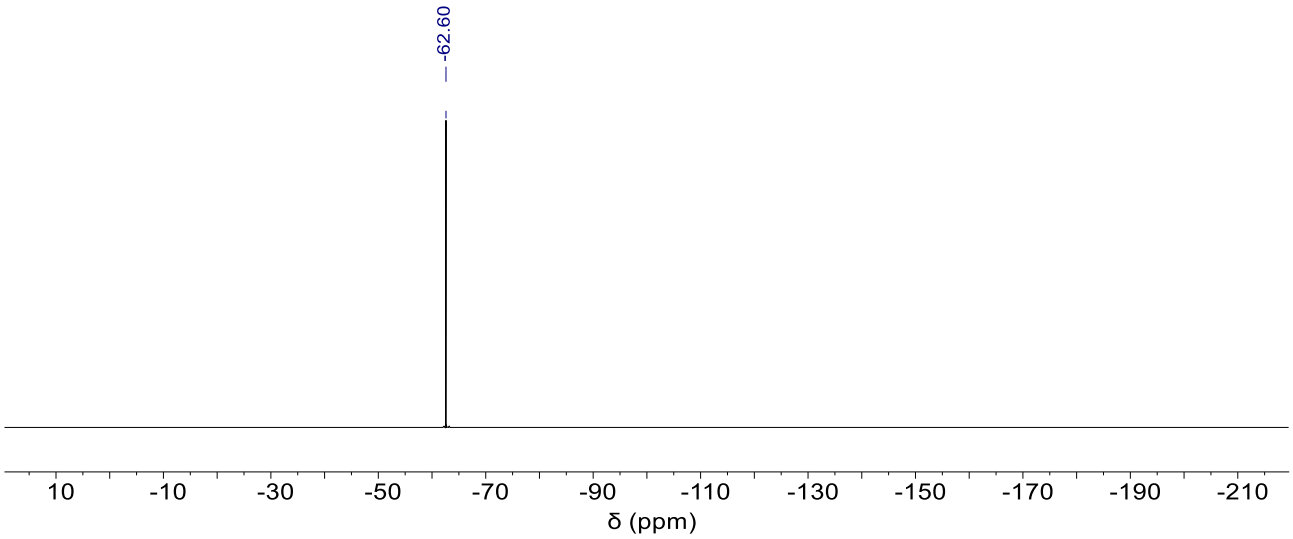

Fig. S101 ^{19}F-NMR (128 MHz) spectrum of compound **4b** in $CDCl_3$.

9. HRMS characterization

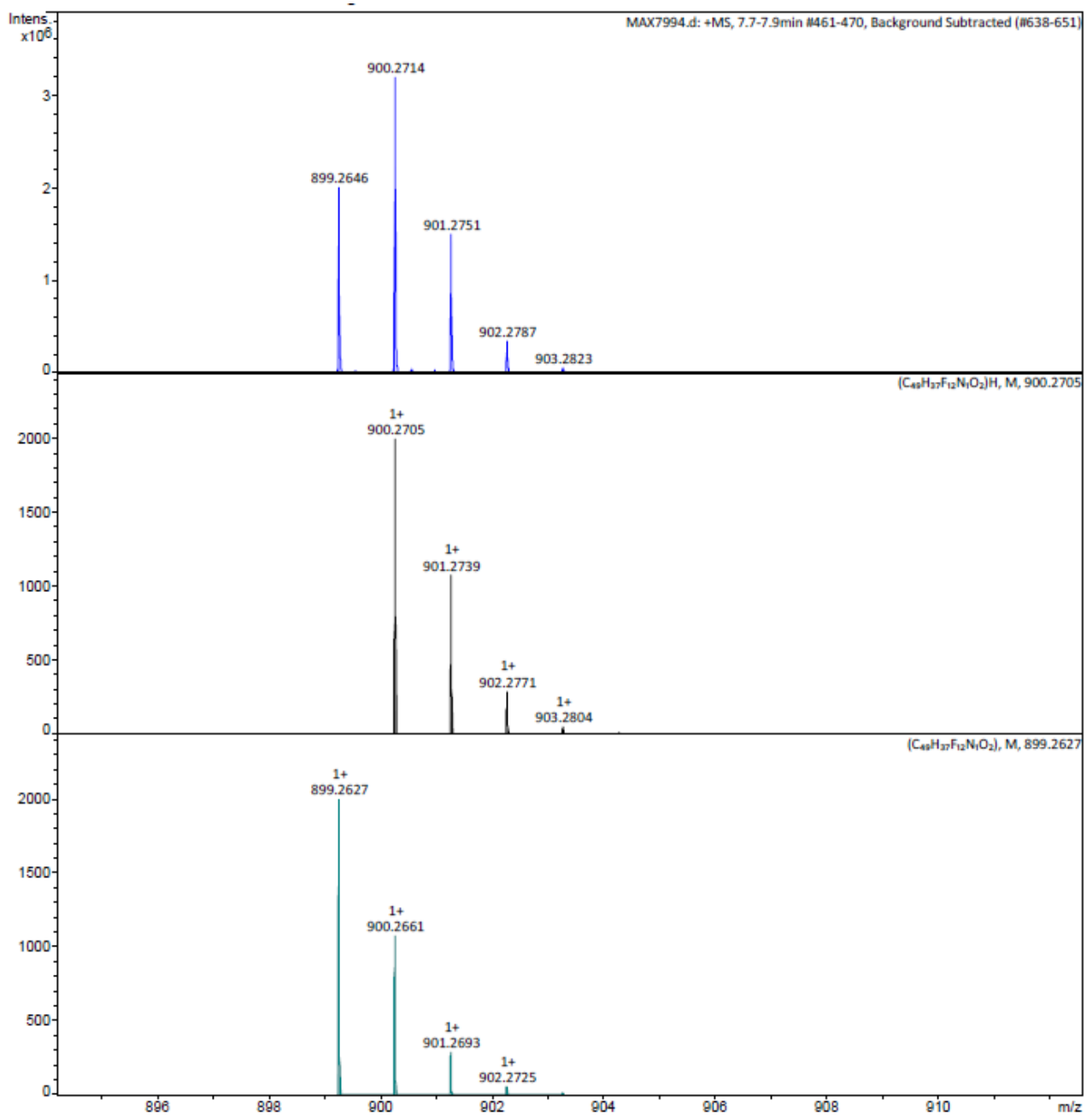

Fig. S102 HRMS (APCI) of compound **2a**, calculated (down) vs measured (up).

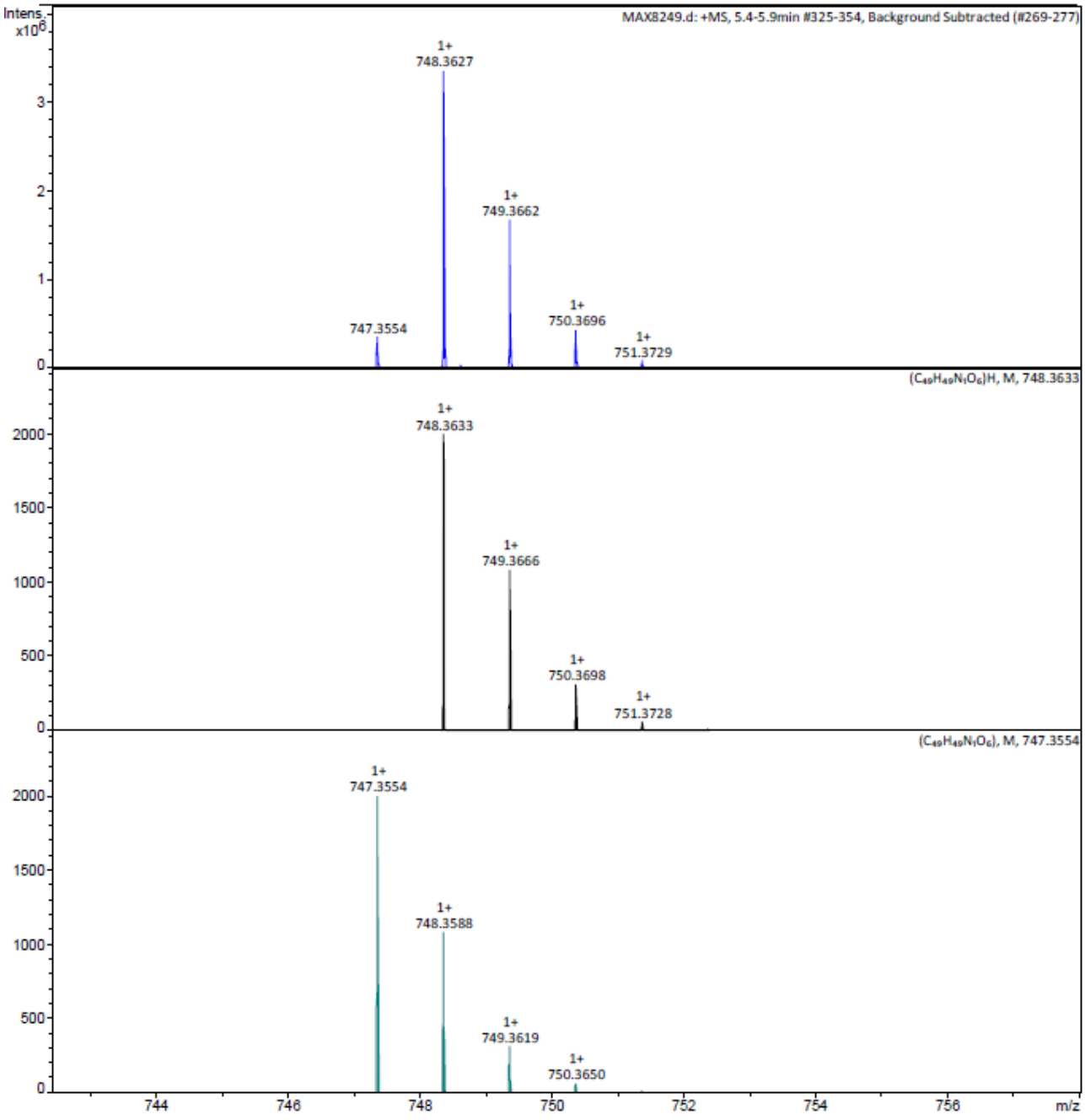

Fig. S103 HRMS (APCI) of compound **2b**, calculated (down) vs measured (up).

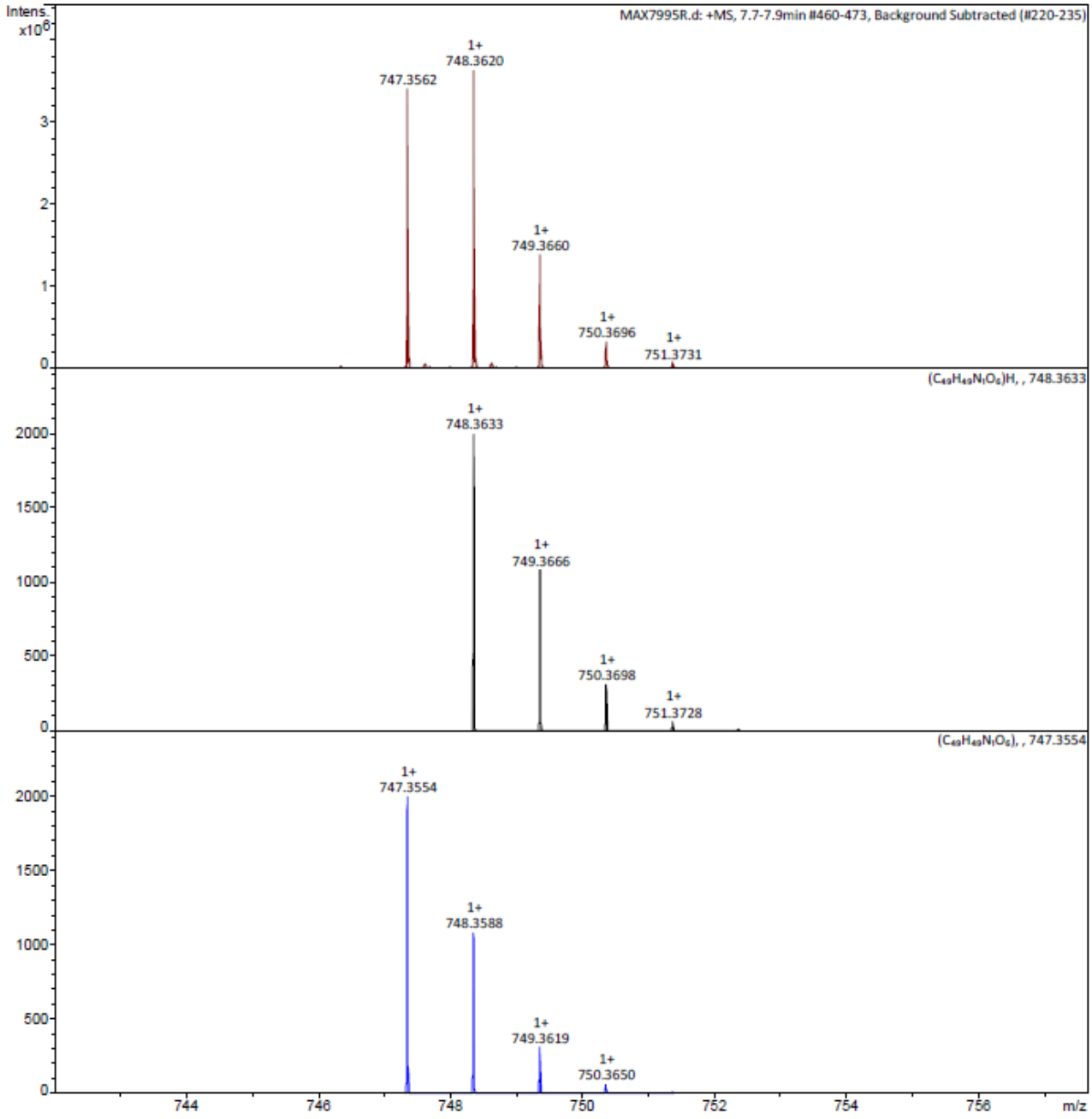

Fig. S104 HRMS (APCI) of compound **3a**, calculated (down) vs measured (up).

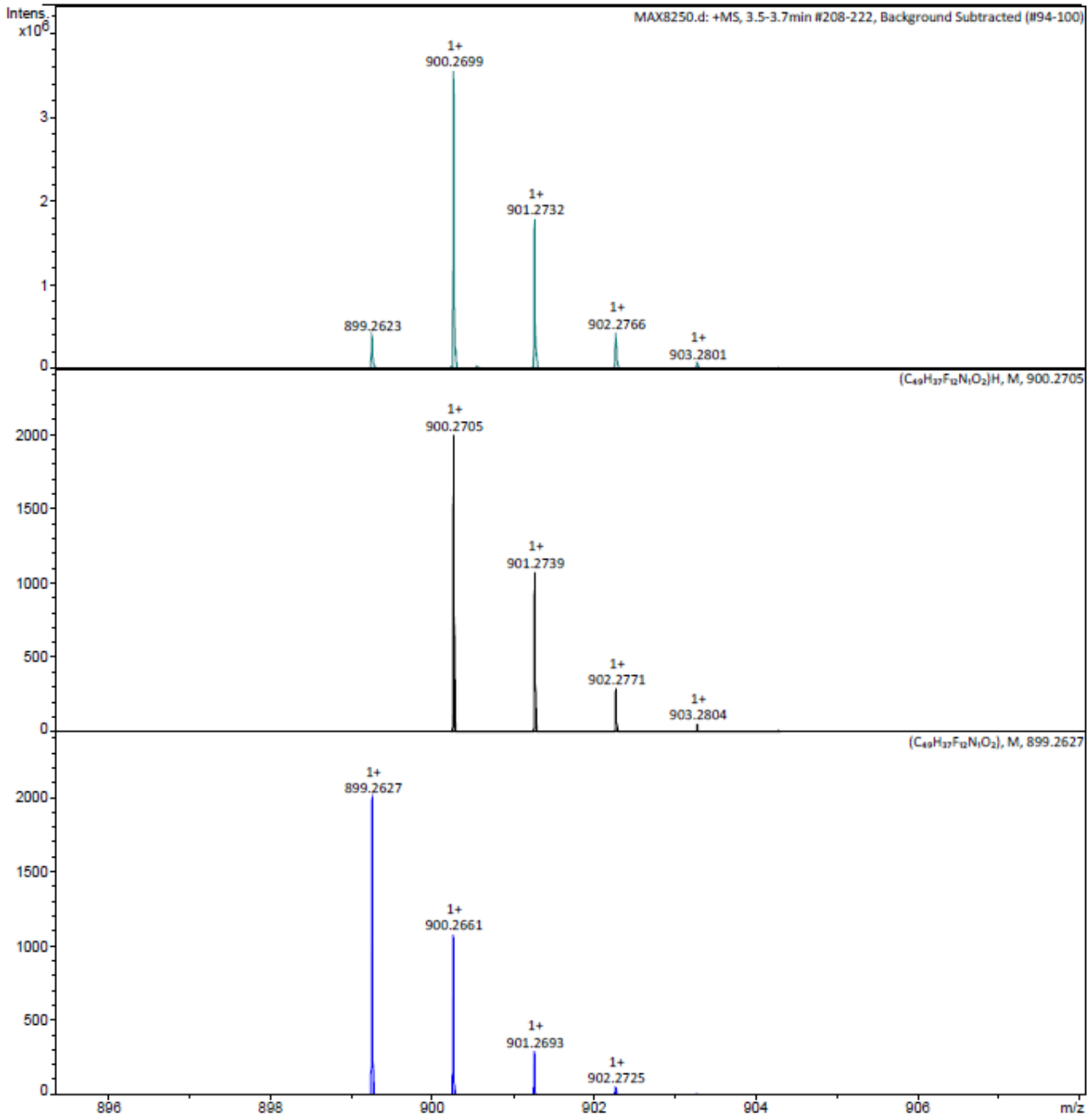

Fig. S105 HRMS (APCI) of compound **3b**, calculated (down) vs measured (up).

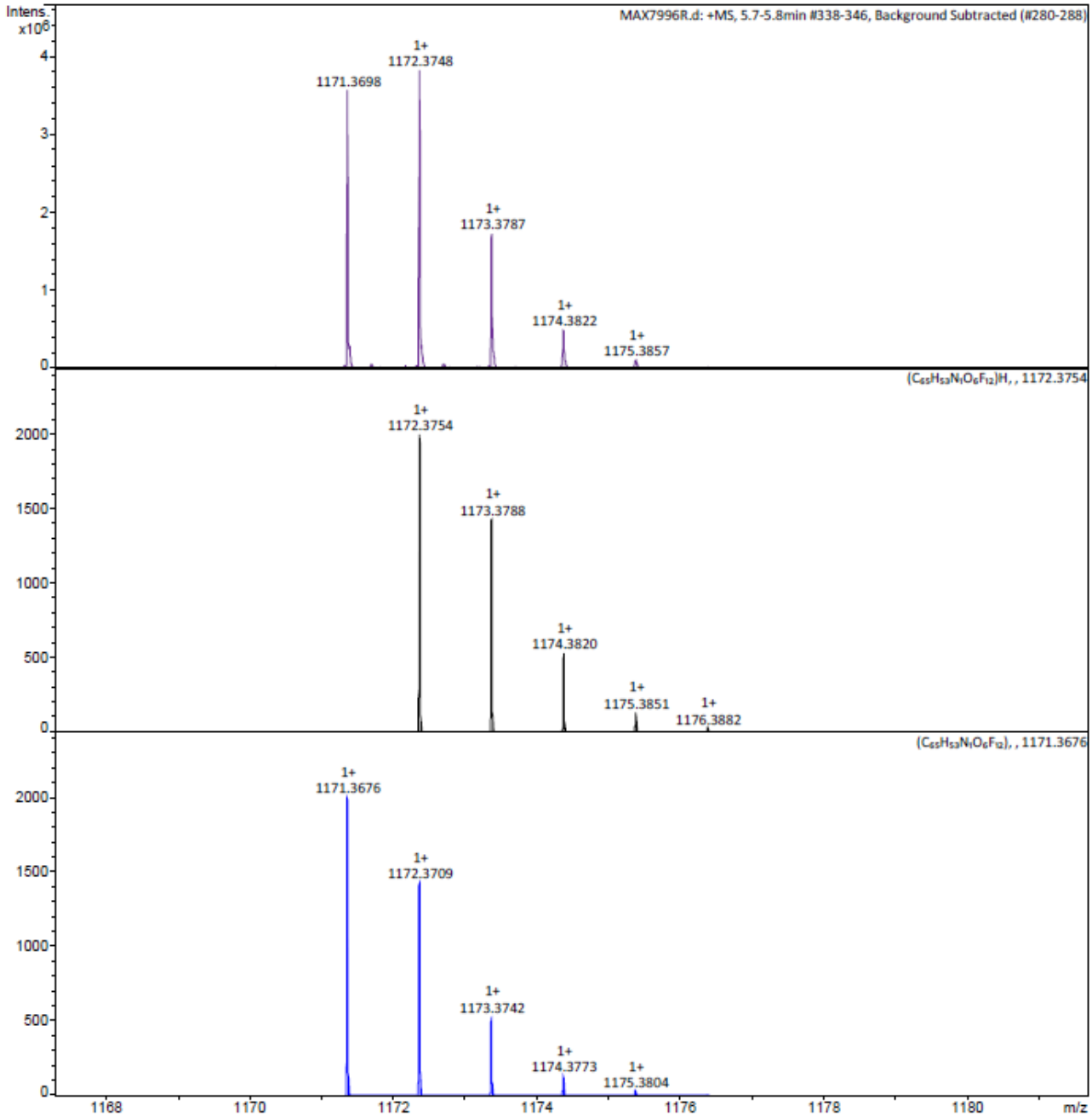

Fig. S106 HRMS (APCI) of compound **4a**, calculated (down) vs measured (up).

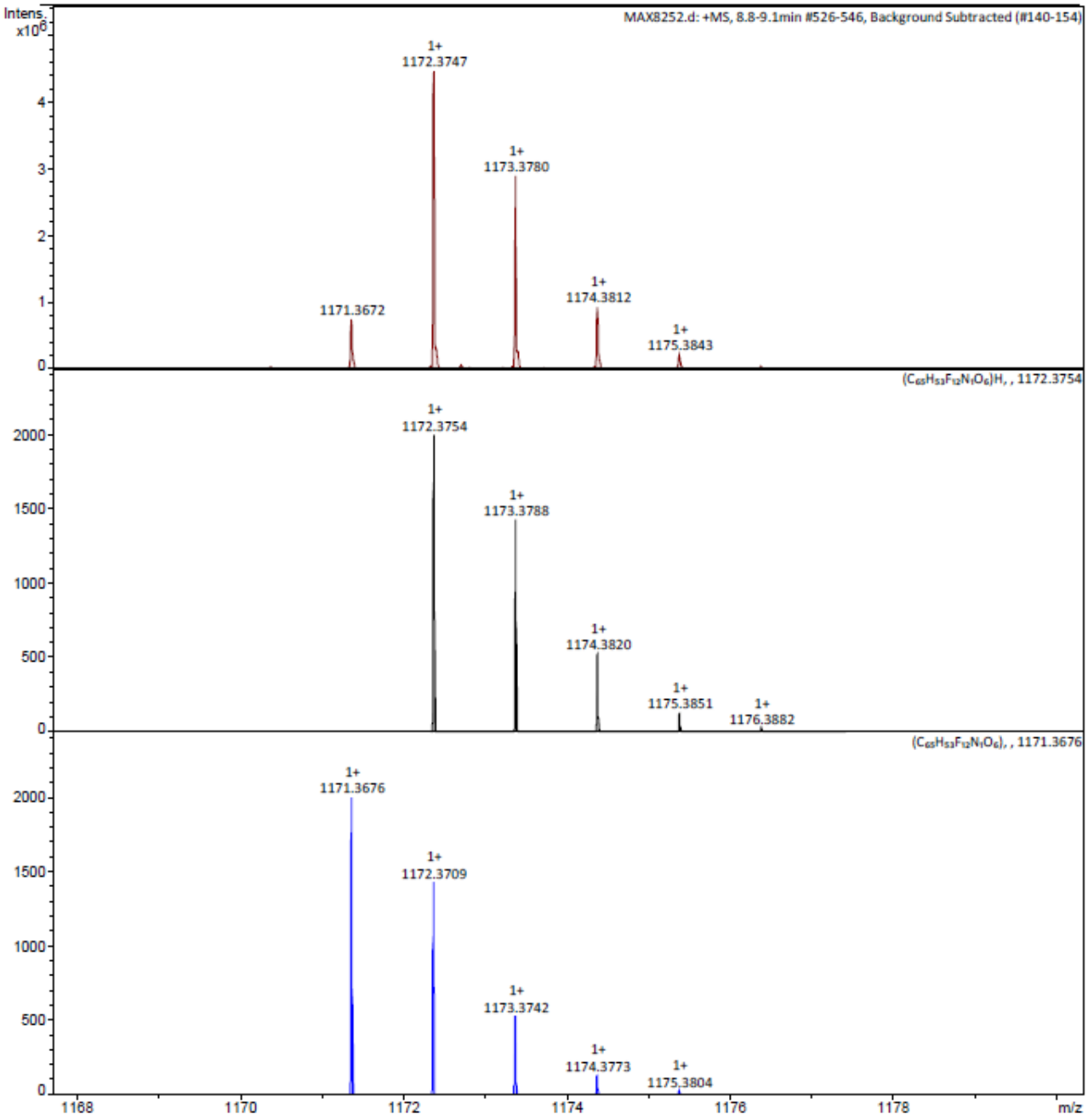

Fig. S107 HRMS (APCI) of compound **4b**, calculated (down) vs measured (up).

10. Supporting references

(S1) D. Sánchez-Fernández, T. Torres and J. García-Calvo, *J. Org. Chem.*, 2025, **90**, 3202–3208.

(S2) C. Lee, W. Yang and R. G. Parr, *Phys. Rev. B*, 1988, **37**, 785–789. b) A. D. Becke, *The Journal of Chemical Physics*, 1993, **98**, 5648–5652. c) W. Kohn, A. D. Becke and R. G. Parr, *J. Phys. Chem.*, 1996, **100**, 12974–12980.

(S3) Gaussian 16, Revision C.01; Frisch, M. J.; Trucks, G. W.; Schlegel, H. B.; Scuseria, G. E.; Robb, M. A.; Cheeseman, J. R.; Scalmani, G.; Barone, V.; Petersson, G. A.; Nakatsuji, H.; Li, X.; Caricato, M.; Marenich, A. V.; Bloino, J.; Janesko, B. G.; Gomperts, R.; Mennucci, B.; Hratchian, H. P.; Ortiz, J. V.; Izmaylov, A. F.; Sonnenberg, J. L.; Williams-Young, D.; Ding, F.; Lipparini, F.; Egidi, F.; Goings, J.; Peng, B.; Petrone, A.; Henderson, T.; Ranasinghe, D.; Zakrzewski, V. G.; Gao, J.; Rega, N.; Zheng, G.; Liang, W.; Hada, M.; Ehara, M.; Toyota, K.; Fukuda, R.; Hasegawa, J.; Ishida, M.; Nakajima, T.; Honda, Y.; Kitao, O.; Nakai, H.; Vreven, T.; Throssell, K.; Montgomery, J. A., Jr.; Peralta, J. E.; Ogliaro, F.; Bearpark, M. J.; Heyd, J. J.; Brothers, E. N.; Kudin, K. N.; Staroverov, V. N.; Keith, T. A.; Kobayashi, R.; Normand, J.; Raghavachari, K.; Rendell, A. P.; Burant, J. C.; Iyengar, S. S.; Tomasi, J.; Cossi, M.; Millam, J. M.; Klene, M.; Adamo, C.; Cammi, R.; Ochterski, J. W.; Martin, R. L.; Morokuma, K.; Farkas, O.; Foresman, J. B.; Fox, D. J. Gaussian, Inc., Wallingford CT, 2016.

(S4) C. M. Cardona, W. Li, A. E. Kaifer, D. Stockdale and G. C. Bazan, *Adv. Mater.*, 2011, **23**, 2367–2371.

(S5) O. V. Dolomanov, L. J. Bourhis, R. J. Gildea, J. A. K. Howard and H. Puschmann, *J Appl Crystallogr*, 2009, **42**, 339–341.